Carbon black: Enhancing phase change materials for direct solar application

H Mey

2016-11-15

Carbon black: Enhancing phase change materials for direct solar application

H Mey

10091484

Department of

Chemical Engineering

University of Pretoria

2016-11-15

Carbon black: Enhancing phase change materials for direct solar application

Synopsis

A solar simulator was used to test whether a carbon black additive could increase the solar absorption of a low temperature organic PCM (consisting of a eutectic mixture of palmitic acid and stearic acid).

Various PCM and carbon black composites (0.01 % to 6 %) were tested, with the 0.06 % carbon black composites showing the fastest temperature increase, reaching 75 ^{0}C much quicker (350 % faster) than the pure PCM. All of the tested PCM composites reached 75 ^{0}C in less than half the time it took the pure PCM. It can therefore be seen that carbon black is very effective at increasing the solar absorption of the PCM.

The carbon black did not have a negative impact on the melting/solidifying onset temperature or the latent heat of the PCM. This proves that at these low concentrations carbon black can help reduce the shortcomings of the PCM without adversely affecting its energy storage properties.

The optimal carbon black concentration changes with the size of the PCM: a shallow PCM layer (2 cm) showed the fastest temperature increase at higher concentrations (between 0.06 % and 0.5 % carbon black), while the deep PCM layer (9 cm) showed the fastest temperature increase at lower concentrations (between 0.01 % and 0.08 % carbon black).

The poor optical properties of the PCM were vastly improved by the carbon black, making the composite an effective direct solar absorber. The carbon black, however, does not provide meaningful thermal conductivity enhancements. Therefore additional heat transfer enhancements (like

graphite) are needed if this novel PCM composite is to be used in a combined system (direct solar absorber, heat transfer fluid and energy storage system).

Keywords: carbon black, solar energy, PCM, stearic acid, concentrated solar power

Contents

Nomenclature

C_p	specific heat	J/(kg·K)
G	solar radiation	W/m^2
H	enthalpy	J/kg
hc	convection heat transfer coefficient	W/(m^2·K)
hk	conduction heat transfer coefficient	W/(m^2·K)
hr	radiation heat transfer coefficient	W/(m^2·K)
k	thermal conductivity	W/(m·K)
M	mass	kg
Nu	Nusselt number	
Pr	Prandtl number	
Ra	Rayleigh number	
S	area	m^2
t	time	s
T	temperature	K
U	wind speed	m/s
X	dimensionless x coordinate	

Greek letters

ε	emissivity	
α	absorptivity	
σ	Stefan-Boltzman's constant	W/(m^2·K^4)
ρ	reflectivity or density	
τ	transmissivity or dimensionless time	
ϕ	dimensionless enthalpy	
λ	latent heat	J/kg
θ	dimensionless temperature	

Subscripts

a	air inside the rig
amb	ambient
b	walls of the container
g1	top glass cover
g2	2nd glass cover
i, j	nodes
m	melting point
pc	phase change node
PCM	phase change material
s	solid

Superscripts

n	new value
o	old value

1. Introduction

The world gets 1,5x10^{18} kWh of solar energy every year. The entire world's energy demands could be met if 0.01 % of this energy could be harnessed.

Concentrated Solar Power (CSP) plants can produce lower cost electricity than Photovoltaic (PV) power plants; they can produce electricity during the night and store the thermal energy more economical and environmentally friendly.

Latent heat storage has a much higher storage density and keeps the temperature more constant. Latent heat storage uses phase change materials (PCMs), but these PCMs usually have very low thermal conductivities and low solar radiation absorption.

Carbon black absorbs energy from all wavelengths of sunlight; this is what gives it its black colour. Carbon black and water mixtures have been used to improve the rate at which water heats up; this enhanced solar absorption could lead to potential applications with PCMs.

Creating novel composites is one of the best ways to improve specific properties of the PCM without adding undesirable side effects like high cost, increased size or a change in the energy storage capacity of the PCM.

Phase change materials have not been extensively studied with regards to its use as the combined direct solar absorber, heat transfer fluid and thermal energy storage (TES) system.

The purpose of this investigation was to see if a PCM with a carbon black additive could be used as the direct solar absorber, with the long term goal of using it in an integrated system with the PCM acting as the direct solar

absorber, heat transfer fluid and the thermal energy storage material. The objectives of this study were therefore:

- to determine whether the solar absorption of the PCM could be increased using a carbon black additive
- to see how stable the PCM/carbon black composite was
- to test the effect of a carbon black additives on various other properties of the PCM (latent heat, melting/solidifying onset temperature, charge/discharge rate)
- to research and test if the PCM composite could potentially be used in an integrated system, with a focus on what thermal conductivity enhancements and direct solar absorber systems are used in the literature.

The use of a carbon black additives in a stearic/palmitic acid eutectic mixture was determined experimentally, first in a small scale laboratory experiment followed by a larger scale laboratory experiment, both using a compact quarts metal halide lamp as a solar simulator.

2. Literature review

2.1. Solar power

The surface of the sun emits electromagnetic waves as a continuous span of wavelengths (from x-rays to deep infrared photons), called solar radiation.

The solar constant is the solar power per unit area that falls on the earth's atmosphere and has a value of 1.367 kW/m^2. This constant can vary slightly in relation to the distance from the earth to the sun and due to solar cycles (Crawley, 2013: 166).

The problem is that this solar energy cannot be used directly and needs to be captured and converted into useful forms of energy (usually electricity or heat). Solar energy has a low average energy density (around 170 W/m^2) and its intermittence means that it is more convenient that the solar energy conversion process include concentration and storage (Desideri & Campana, 2014).

Hour average solar data for Pretoria from January to February 2016 between 10 am and 11 am was obtained from The Southern African Universities Radiometric Network (SAURAN). The direct normal irradiance in W/m^2 is given in Figure 2-1. The top values between 800 W/m^2 and 1000 W/m^2 are for clear sky days and are similar to the values used for the solar simulator experiment.

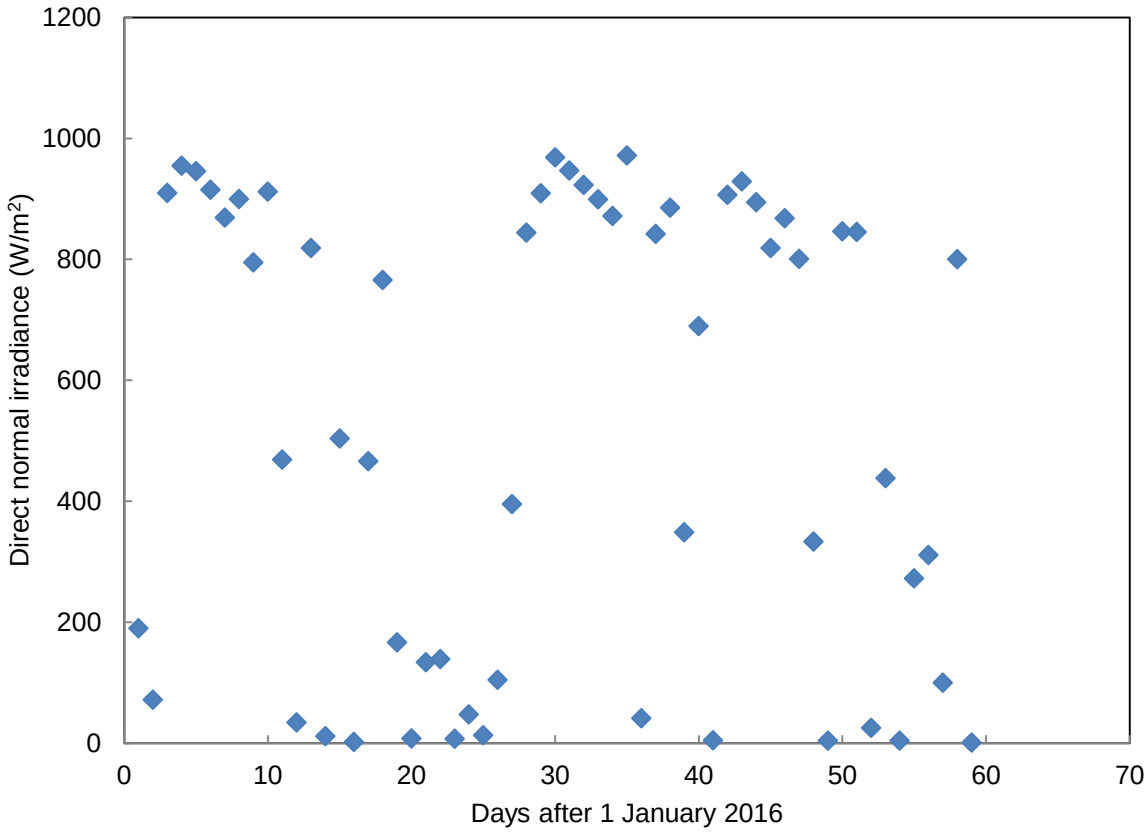

Figure 2-1: Solar data for Pretoria from January to February 2016 at 10 am (Brooks *et al*, 2015).

The solar radiation also changes over the course of the year, as seen in Figure 2-2.

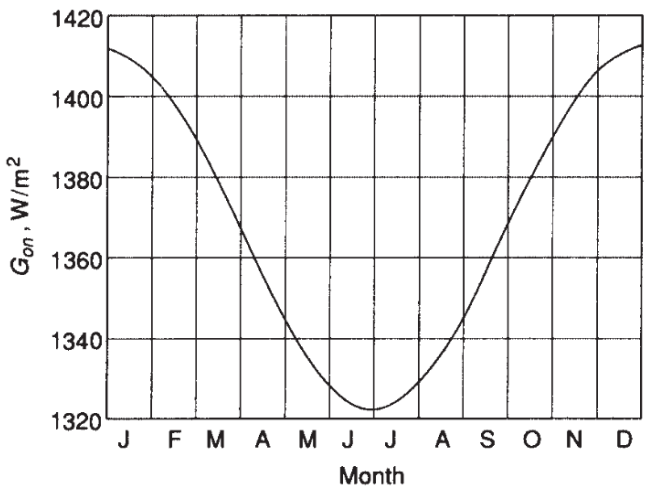

Figure 2-2: Extra-terrestrial solar radiation change over the course of a year (Duffie & Beckman, 2013: 9).

The direct normal irradiation average for the Earth is given in Figure 2-3. South Africa receives a high amount of solar radiation, making it a promising place for solar energy applications.

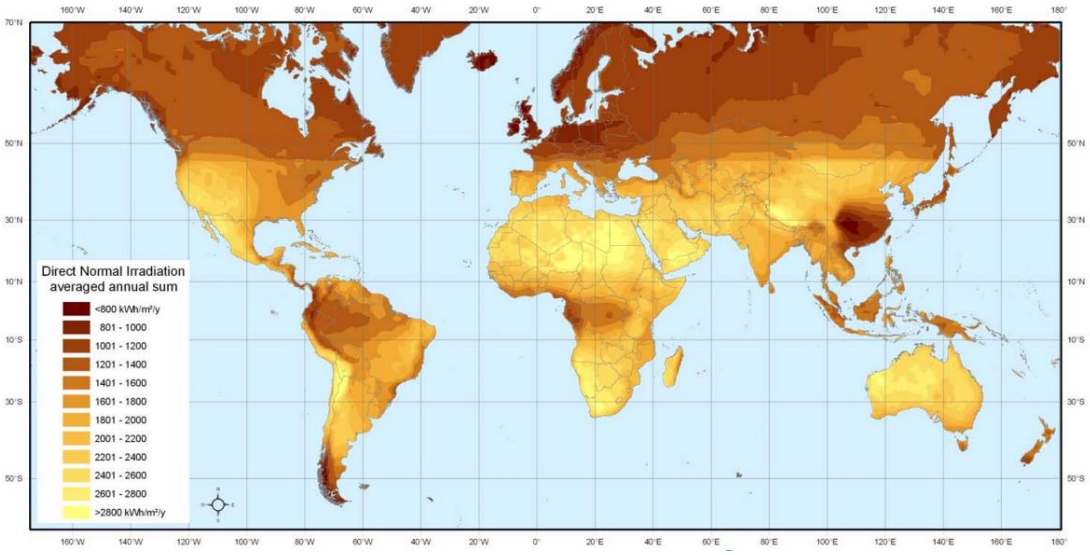

Figure 2-3: The direct normal irradiation average for a year with the lighter areas having a higher amount of annual radiation (Trieb *et al*, 2009).

The average direct normal irradiation of South Africa is given in Figure 2-4. The Northern Cape receives the most solar irradiation, making it a prime place for solar energy applications in South Africa.

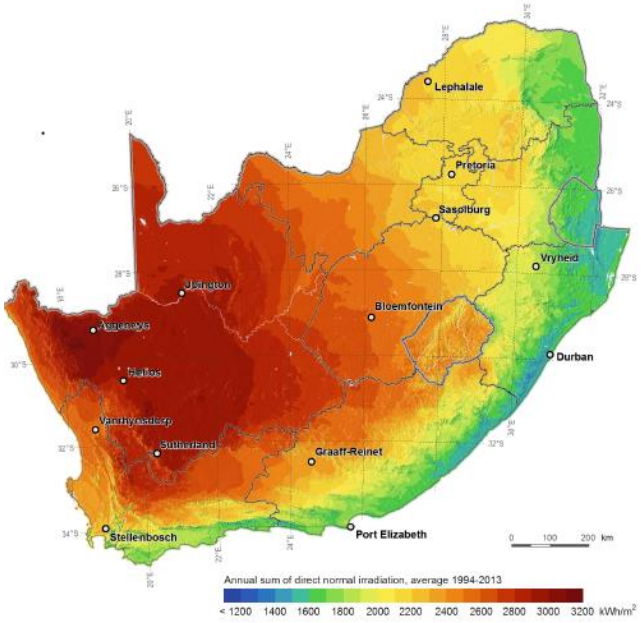

Figure 2-4: The direct normal irradiation average for a year, with the darker areas having a higher amount of annual radiation (Suri *et al*, 2015).

2.2. Direct solar absorption

The efficiency of direct solar collectors is limited by the absorption properties of the working fluids. The working fluids usually used in solar collectors have bad absorption properties. On the other hand volumetric absorbers using nanofluids have better thermal transfer and excellent optical properties (Saidur *et al*, 2012).

In normal solar thermal collectors solar energy is absorbed by a layer of material on plates or tubes, this energy (in the form of heat) is then carried away by working fluids. Direct solar collectors on the other hand absorb the solar energy directly into the working fluid and this working fluid also carries out the generated heat.

In the past the working fluid was black liquids which contained millimetre to micrometre-sized particles. These liquids had very good photo thermal properties but they caused extreme abrasion, sedimentation and plug

problems. Using nanofluids as the working fluid solves these problems while keeping the advantageous properties of the liquids (Han *et al*, 2011) .

The most important properties of nanofluids for solar absorption as discussed by Han *et al* (2011) are:

- Photo thermal property: affects the solar absorption ability of the nanofluid
- Viscosity and rheological behaviours: affects the stability and flow behaviours as well as the heat transfer
- Thermal conductivity: affects the heat transfer efficiency

The optical properties of the nanofluid depend on the optical properties of the materials that it is made of, and the size and shape of the particles.

Carbon nanohorns are nanomaterials with many cavities and a large surface area. These carbon-based nanostructured materials can improve the optical properties of direct solar absorbers (Saidur *et al*, 2012).

According to Saidur *et al* (2012) the thermal conductivity of nanofluids are improved by nanoparticles because of:

- The dispersion of nanoparticles
- Intensification of turbulence
- Brownian motion
- Thermophoresis

The efficiency of nanofluid solar collectors increased when nanoparticles were added to the working fluid, showing very high efficiencies even at low volume fraction nanoparticles. The increase is due to the attenuation of the sunlight which goes through the collector. The efficiency stayed constant after 2 % volume fraction nanoparticles were added. The efficiency of the collector could increase or decrease when the size of the nanoparticles were increased (depending on the nanoparticles) (Mahian *et al*, 2013).

Mahian *et al* (2013) also states that some of the challenges regarding the use of nanofluids are:

- They are expensive
- They can be unstable and may form agglomerates
- Difficulty pumping
- Potential erosion/corrosion

The efficiency of direct solar absorbers depends on the effectiveness of which the solar radiation is absorbed and the heat transfer from the absorber to the working fluid. Nanofluids help increase the conversion of concentrated sunlight into thermal energy and function as the working fluid, solving these problems (Saidur *et al*, 2012).

There are many other nanofluids which are used as direct solar absorbers and some are discussed later.

2.3. Concentrated solar power (CSP)

Central receiver system:

These systems focus on large-scale energy conversion with an output scale in the megawatt range. CSP plants need to collect energy from a large area, many heliostats focus radiation on a central receiver, thereby using optical rather than thermal means.

According to Duffie & Beckman (2013) a CSP plants consist of:

- a heliostat field
- the heliostat controls
- the receiver
- a storage system
- a heat engine to drive the generator.

The heliostats are on fixed on mounts that can move around two axes, tracking the sun and focusing the radiation on the central receiver (Duffie & Beckman, 2013: 628).

The heliostats need to provide the radiation to the receiver at the desired flux density while keeping the cost as low as possible.

The solar collector makes up the biggest cost in the system (Duffie & Beckman, 2013: 629). Improving the efficiency of the solar collector can therefore have a very big impact on the total cost of the system.

How does a CSP work:

Reflectors are used to concentrate the solar radiation onto a receiver, this heats up the heat-transfer fluid (HTF) that circulates in the receiver. The HTF gets heated to a high temperature and is then used in a thermodynamic cycle (usually a Rankine cycle) to generate power.

There are two steps involved in converting the solar energy to electricity. The sunlight is first converted into thermal energy then this thermal energy is converted to electricity in a normal power cycle. This means that there is a primary system which captures, converts and stores the solar energy, and a secondary system which produces the electricity in a similar fashion as conventional power stations.

The solar radiation which hits the collector heats the HTF to temperatures between 290 ºC and 1000 ºC. This temperature depends on the properties of the HTF and the concentration methods. This HTF is then used to generate steam (Desideri & Campana, 2014).

2.3.1. Heat transfer fluids (HTF)

Most CSP plants use synthetic oil that can reach temperatures of about 390 ºC as the HTF. This synthetic oil has a high cost and is therefore only

used in the solar field and requires another fluid to use in the storage system. The synthetic oils used are also highly flammable and polluting. Molten salts are usually used in the storage system; this two fluid system requires a second heat exchanger. The molten salts are usually a mixture of sodium nitrates and potassium nitrates. They are low cost, less flammable, less polluting and can reach higher temperatures with higher efficiencies compared to the synthetic oils. The problem with these molten salts is that they solidify at around 220 ºC and require extra systems to keep them circulating and heated (Desideri & Campana, 2014).

2.3.2. Solar One and Solar Two power plants

Solar One and Solar Two are two of the most well-known CSP plants.

Solar One was a CSP plant with a capacity of more than 10 MWe. It can be seen in Figure 2-5 and consisted of the following:

The heliostat field:

- The heliostat field had 1818 reflectors, with a total array area of 71100 m^2
- Back-silvered glass was used as the reflecting material.

The receiver:

- Cylindrical single-pass superheat boiler
- 90 m above the ground
- 24 panels (0.9 m wide and 13.7 m long)
- The panels are made out of alloy tubes welded together and coated with a nonselective flat back paint with an absorptance of 0.96 after two coats.
- The maximum temperature of the absorbing surface is 620 ^{0}C

Figure 2-5: The heliostat field and receiver tower of Solar One (Duffie & Beckman, 2013: 630).

Power generation system:

- Heat exchangers separate the TES from the steam cycle
- Excess steam is used to heat oil before being transferred to a bed of sand, oil and gravel
- Contains the turbine generator, its auxiliaries and the cooling system

(Duffie & Beckman, 2013: 632)

Problems with the receiver:

Temperature gradients formed in the panels due to the disproportionate spread of the incoming radiation, this lead to the panels warping. The warping caused gaps in the panels where the radiation could pass through and hit the support structure. This could have potentially lead to an increase in the amount of leaks in the tubes. The absorptance of the black paint on the receiver also reduced by around 0.02 per year (Duffie & Beckman, 2013: 632).

Differences between Solar One and Solar Two:

Solar One stopped operation in 1988 and was replaced by Solar Two in 1996; an important finding from Solar One was that the storage system was not sufficient to run the turbine at peak efficiency. Solar two therefore replaced the oil-rock thermocline storage unit with a more modern molten salt storage system (Duffie & Beckman, 2013: 633).

Adding an energy storage unit to a CSP plant increases the cost from $0.08 - $0.15 to $0.15 - $0.20 per kilowatt-hour (Chen, 2011: 245). A novel PCM composite could help reduce this added cost while still providing the benefit of a TES system.

2.3.3. CSP vs. photovoltaic cells

A photovoltaic cell uses the photovoltaic effect to turn solar radiation into electrical energy. It has no thermal or mechanical cycles and undergoes no chemical reactions (Crawley, 2013: 169).

Photovoltaic cells contain semiconductor materials (usually silicon). The photons hit the cell and separate negative and positive charge carriers which in turn creates an electrical voltage and the electrical current is created (Quaschning & Muriel, 2002).

CSP plants store the sun’s energy as thermal energy while PV applications store electrical energy in batteries. Batteries are not economical or environmentally friendly for large-scale power plants.

The higher and more uniform the solar radiation is, the higher the efficiency of a CSP plant will be, some locations are therefore more suited for CSP plants than others.

The storage system in CSP plants guarantees the continuous electricity production even when there is no solar radiation; this causes the CSP to produce more electricity than PV plants.

The CSP plants produce lower cost electricity than PV plants in all the cases that were considered because electricity can be produced during the night.

CSP plants use only direct sunlight that hit the collectors (the direct normal irradiation). Photovoltaic technology can use the direct sunlight and also the light that is scattered by water vapor, clouds and particles in the atmosphere as well as the reflected light due to the albedo effect. Despite this advantage CSP plants can store the thermal energy more economical and environmentally friendly. Depending on the size of the thermal energy storage (TES) system, CSP plants can partially or totally solve the problem of discontinuous electricity generation due to cloudy days or night time. This is a key feature to ensure that solar thermal power plants become a mature energy production technology (Desideri & Campana, 2014).

2.4. Fresnel Lens

Fresnel Lens is an emerging technology in CSP, even though they were already invented in 1822. They work based on the law of refraction: light travels in a straight line but when it goes through the interface of a transparent medium with a different density its path changes. The Fresnel lens differs from a normal lens in that undesirable material of the lens is removed, reducing the absorption losses while keeping the contour profile of the lens (Kumar, Shrivastava & Untawale, 2015).

Some of the advantages of Fresnel-CSP as discussed by (Kumar *et al*, 2015) are:

- Extremely high temperatures can be produced
- High thermal efficiency
- Lower investment cost, shorter payback period and smaller plant sizes

- The concentrator does not require maintenance

The disadvantages of Fresnel-CSP are also discussed by (Kumar *et al*, 2015):

- Difficult to create sharp edged Fresnel lenses due to the production method
- Ultraviolet degradation occurs
- The dust that accumulates in the grooves needs to be frequently cleaned
- Usually requires a tracking system
- The high operating temperatures requires special heat transfer fluids
- Only works with DNI

Despite the challenges of Fresnel Lenses they are gaining popularity, especially over normal parabolic concentrators and could have large future applications.

2.5. Thermal energy storage (TES)

Energy demand has increased while nonrenewable fossil fuels are being depleted. This has led to an increase in the gap between the energy demand and its supply and one way to help stop this is by storing excess energy (Sharma *et al*, 2015). The large gap between energy supply/demand at can be exacerbated when renewable energy sources are used (solar energy requires sunshine, wind energy requires wind, etc.).

This is where TES plays a big part to save expensive fuels and reduce the waste of energy and capital. PCMs are very effective because they store solar energy during sunshine days for use at night or during days with less sunshine. This storage of energy helps counteract the shortcomings of large scale direct solar radiation as a source of energy (Sharma *et al*, 2015).

TES corrects the difference in the supply and demand of energy. There are two main types of TES systems:

1.) Sensible storage systems: When the temperature of a substance is increased, its energy is also increased. The energy that the substance releases or absorbs as its temperature changes is called its sensible heat.

2.) Latent storage systems: The energy that is needed to change the phase of a material (solid to liquid or liquid to gas) is called the heat of vaporization or the heat of fusion depending on the phase change, this is called the latent heat.

Any latent heat TES system needs the following three components:

1.) A substance which can store the heat: undergoing a solid to liquid transition in the operating temperature range, so that most of the heat is stored as latent heat.

2.) Something to hold the substance in 1.)

3. A heat exchanger surface to transfer the heat to and from the PCM (Hasnain, 1998).

In energy storage there needs to be a minimum of three steps: charging, storing and discharging, and these steps should preferably be able to happen multiple times.

According to Desideri & Campana (2014) the most important requirements for a TES system are:

- High energy density in the storage material (storage capacity)
- Good heat transfer between the HTF and the storage medium (efficiency)
- Mechanical and chemical stability (must support many cycles)

- Compatibility between heat exchanger, HTF and the storage medium (safety)
- Complete reversibility of a number of charging and discharging cycles (lifetime)
- Low thermal losses
- Ease of control
- Operation strategy, maximum load, nominal temperature and specific enthalpy drop in load and integration into the power plant

In latent heat storage the thermal energy is stored isothermally, usually the solid-liquid transition is used and these substances are called phase change materials (PCM). The usage of PCMs reduces the size of the heating systems but the heat transfer design and selection is harder. The performance of these materials can also degrade after some number of freeze-melt cycles. The large amount of energy that can be stored in a small volume of PCMs results in one of the lowest costs for any storage concept.

Solar TES systems need to have a high heat capacity and thermal conductivity and must be useable at high temperatures. PCMs can fulfil this role: PCMs have a large latent heat capacity, low cost and very little super cooling. One big drawback of most PCMs in solar TES however is their low thermal conductivity, but nanoparticles can be added to PCMs to help increase the heat transfer in latent heat TES systems (Mahian *et al*, 2013).

2.5.1. High temperature TES

High temperatures in this context are when the storage is performed at temperatures between 120 ºC and 600 ºC.

2.5.1.1. Active systems

Forced convection heat transfer is used to transfer the heat into the storage material. The storage medium goes through the solar receiver or steam generator.

In direct storage the HTF is also the storage material and it should therefore have good heat transfer and good storage material characteristics. When molten salts or steam is used there is no need for expensive heat exchangers and allows the plant to be operated at high temperatures and leads to a big reduction in costs.

In an indirect system there is a separate medium which stores the heat.

2.5.1.2. Passive systems

In passives systems the HTF carries the energy from the energy source to the separate storage medium to charge it and gets energy from the storage medium when it is discharging. The HTF's temperature decreases while discharging because the storage material cools down and the heat transfer is low.

The development of new and better TES systems is very important (but is less developed than other solar power aspects) for the future of concentrated solar power and while only sensible heat TES systems have been used on real solar power plants, latent heat storage, with higher storage density and almost constant temperature is a promising alternative (Gil *et al*, 2010).

2.5.2. Other TES devices

Solar ponds are a simple and cheap way of storing solar energy as low temperature thermal energy. The dark bottom of the salt pond absorbs the solar radiation which increases the temperature of the water. A density

gradient is created where the salt concentration increases with depth. The thermal energy stored in the lower layers is then removed without disturbing the upper layers.

Solar energy can also be stored using solid media like rocks, pebbles, metals, concrete, sand, etc. and can be used for either low or high temperatures since they will not freeze or boil (Desideri & Campana, 2014).

2.6. Phase change materials

Normally a large volume of storage materials were needed to store energy in the form of sensible heat, but this can be significantly reduced by using latent heat storage.

TES and therefore PCMs allow for the efficient use of the fluctuating energy sources by matching the supply and demand of energy. PCM are efficient at storing thermal energy because of their high storage density and small temperature variations during charging and discharging (Nkwetta & Haghighat, 2014).

2.6.1. Latent heat storage

Latent heat storage requires much smaller weight and volume material to store the same amount of energy. For example, you need 80 times the amount of energy to melt 1 kg of ice compared to raising the temperature of 1 kg of water by 18 ºC.

Liquid-gas PCMs can have high heats of transformations but their accompanying volume change is too high for practical applications and therefore solid-liquid PCMs are normally used (Hasnain, 1998).

Latent heat thermal energy storage (LHTES), which uses PCMs is preferred for TES because PCMs have a high storage density and the temperature does not vary much between storage and retrieval.

A good TES system can eliminate the difference between the energy supply and demand and is critical in energy systems to increase its performance, reliability and applicability (Sarı & Karaipekli, 2007).

2.6.2. How do PCMs work

The PCMs are put in long thin tubes inside a container and the solar heat is sent through the small spaces between the tubes which melts the PCMs. The heat is therefore stored as a bit of sensible heat as well as latent heat due to the heat of fusion. When discharging low temperature air is circulated between the spaces and picks up the stored heat from the PCMs and transports it.

PCMs can be classified into:

- Inorganic compounds: salt hydrates, salts, metals, alloys
- Organic compounds
- Eutectics of inorganic and/or organic compounds: mixture of two or more salts

(Hasnain, 1998)

Some common PCMs are listed in Table 2-1.

Table 2-1: Summary of latent heat storage materials (Hasnain, 1998)

Temperature Range (°C)	Material	Transition Temperature (°C)	Heat of Fusion (kJ/kg)
0-100	Water	0	335
	Paraffin	20-60	140-280
	Salt hydrate	30-50	170-270
100-400	$AlCl_3$	192	280
	$LiNO_3$	250	370
	Na_2O_2	360	314
400-800	50LiOH/50LiF	427	512
	$KClO_4$	527	1253
	LiH	699	2678
800-1500	LiF	868	932
	NaF	993	750
	MgF_2	1271	936
	Si	1415	1654

2.6.3. PCM vs. sensible heat storage using water

The most widely used energy storage system is the sensible heating of water. Water is cheap, widely available and has good heat transfer properties but has a low energy storage capacity and big temperature variation when used as a storage medium. Water also has a high vapour pressure which requires additional safety measures when used at high temperatures.

PCMs have a high energy storage capacity (250 kJ/kg for Glauber salt, 170 kJ/kg for calcium chloride hexahydrate and 200 kJ/kg for paraffin waxes). The energy is also given over a smaller temperature range, this is especially helpful with solar-assisted heat pumps which will work at steady-state conditions and will have a better performance coefficient (Sari & Kaygusuz, 2001).

2.6.4. Organic PCMs

Organic PCMs are well suited for solar energy storage because of their small freezing and melting temperature range, and their congruent melting (Sharma *et al*, 2015). Most organic PCMs are also readily available, relatively cheap and nontoxic. Organic PCMs have been widely studied in solar energy storage, but not as combined energy storage and radiation absorption media.

A eutectic mixture is one in which two or more components (organic-organic, organic-inorganic, inorganic-inorganic) form a composition which melts and freezes at a single temperature, this temperature is lower than the melting points of each separate component. These mixtures usually melt and freeze congruently and the components do not separate out (Sharma *et al*, 2015).

Saturated fatty acids are given by the formula $CH_3(CH_2)_nCOOH$ and divided into categories depending on the length of the chain:

1. Capric acid (n=8)
2. Lauric acid (n=10)
3. Myristic acid (n=12)
4. Palmitic acid (n=14)
5. Stearic acid (n=16)

These saturated fatty acids (consisting of only single bonds between the carbon atoms) are made from a nonpolluting supply of vegetable and animal sources (Sharma *et al*, 2015).

The different categories of fatty acids each have their own characteristics, unlike paraffin's which show much bigger similarities. These fatty acids have better phase change properties than paraffin's but are more expensive (Sharma *et al*, 2015).

Sharma *et al* (2015) lists the superior properties of fatty acids as:

1. Congruent melting
2. Good thermal and chemical stability
3. Nontoxic
4. Biodegradable
5. Good melting range
6. Capable of thousands of melting/freezing cycles without notable degradation in thermal properties.

Sarı, Sarı & Önal (2004) studied the thermal properties of lauric acid, stearic acid, myristic acid, palmitic acid, and palmitic acid/stearic acid eutectic mixtures over 360 repeated melt/freeze cycles. They found that the thermal reliability of these PCMs were good for a one year period.

Baran & Sari (2003) tested a palmitic acid-stearic acid eutectic mixture by surrounding a heat transfer pipe with the solid PCM. They found that a thin liquid layer was quickly formed between the solid PCM and the pipe. They found that natural convection (enhanced by the buoyance effect) was the main heat transfer factor controlling the melting front. Baran & Sari (2003) also concluded that a palmitic acid-stearic acid eutectic mixture can be used in TES applications because of its good heat transfer and phase change characteristics.

However the low melting points of organic PCMs mean that they have not been looked at for high temperature applications like power plants (Sharma *et al*, 2015).

Stearic acid is a fatty acid and a useful PCM:

- Has a very good melting temperature range
- High latent heat capacity
- Very little or no supercooling during phase change

- Congruent melting (liquid and solid have the same composition)
- Not toxic
- Vapour pressure is low
- Does not corrode metal containers
- Has good thermal and chemical stability

(Karaipekli, Sarı & Kaygusuz, 2007)

Stearic acid is therefore a suitable material for TES and its physical properties are listed in Table 2-2.

Table 2-2: Thermophysical properties of stearic acid (Sari & Kaygusuz, 2001)

Property	**Value**
Chemical formula	$CH_3(CH_2)_{16}COOH$
Melting point (°C)	54–56
Density (g/cm^3)	
Solid	1,08
Liquid	1,15
Latent heat (kJ/kg)	186,50
Thermal conductivity (W/m°C)	0,18
Specific heat, C_p (kJ/kg°C)	
Solid	2,83
Liquid	2,38
Physical properties given by the Merck Company	
Merck Catalog number	100671
Total assay (GC)	
Stearic and palmitic acid	>90%
Stearic acid (GC)	>40%
Palmitic acid (GC)	>40%
Melting point (°C)	54–56
Acid number	200–210
Heavy metal (as Pb)	<0.001%
Iodine number	3
Sulfated ash	<0.050%

Stearic acid has one major drawback: its thermal conductivity is only 0.2 W/(m·K) to 0.3 W/(m·K). This low thermal conductivity means that the rate at which it stores and releases heat while it is melting or crystallizing is very low.

This thermal conductivity can be increased with the use of nanoparticles. Karaipekli *et al* (2007) tested exfoliated graphite (EG) and carbon fibre (CF) additives together with stearic acid. The mass fraction EG and CF additives added to the stearic acid showed an almost linear relationship with the thermal conductivity of the composite material. The thermal conductivity of stearic acid increased by 266.6 % when 10 % mass fraction EG was added.

The time it took the PCMs to melt was also greatly reduced with the addition of the EG or CF. This shows that EG and CF is a good method to increase the thermal conductivity of stearic acid without lowering its latent heat storage capacity (Karaipekli *et al*, 2007).

This low thermal conductivity of PCM causes them to need improved heat transfer techniques to increase the charging/discharging rates. To develop a good TES system you therefore need an understanding of PCMs, heat exchangers and PCM container materials.

2.6.5. Improving thermal properties of PCMs

The very low thermal conductivity of PCMs causes their charging and discharging rates to be slow, PCMs therefore require some kind of heat transfer enhancements (Agyenim *et al*, 2010). In this section these heat transfer enhancements are discussed in more detail.

2.6.5.1. PCMs + carbon nanofillers

Carbon nanofillers can be used to increase the thermal conductivity and energy storage properties of PCMs. The presence of nanofillers decreases

the phase change enthalpies slightly and has a negligible influence on the phase change temperature. It was found that the thermal conductivity increased with an increase in the nanofiller loading. Thermal conductivity enhancements also greatly depend on the geometry of the carbon nanofillers. Graphite nanoparticles showed the biggest relative enhancement (164 % at a loading of 5 wt.%) (Fan *et al*, 2013).

Motahar *et al* (2014) added mesoporous silica ($MPSiO_2$) nanoparticles in n-octadecane at 1 wt.%, 3 wt.% and 5 wt.% and an increase in the thermal conductivity of 5 % for 3 % load and 6 % increase for a 5 % load was found. The viscosity of the liquid PCM with a 5 % $MPSiO_2$ load was found to be 60 % higher than the pure PCM.

Li, Chen & Wu (2014a) tested phase change microcapsules of carbon nanotubes grafted with stearyl alcohol and found that the thermal conductivity of the microPCMs with 4 % CNTs increased by 79.2 %. The microPCMs still showed good durability and thermal stability after 100 heating and cooling cycles.

2.6.5.2. PCMs + Expanded Graphite (EG)

When paraffin is used as the PCM with 0, 2, 4, 7 and 10 weight % EG the thermal conductivity of the composites are 0.22 W/(m·K), 0.40 W/(m·K), 0.52 W/(m·K), 0.68 W/(m·K) and 0.82 W/(m·K) respectively. This increase in thermal conductivity caused the PCM to melt at a much faster rate. It was found that the melting temperature and latent heat capacities of the PCM composites did not change significantly. The PCM with 10 % EG has good potential for LHTES applications because of its:

1. High thermal conductivity
2. Form stability
3. Direct usability (no extra container)
4. Good melting temperature

5. Good latent heat storage capacity

(Sarı & Karaipekli, 2007)

It was also found that the melting time of the PCM composite with 4 wt. % EG and 10 wt. % EG decreased by 16 % and 32 % respectively (when compared to pure paraffin). This decrease in melting time was due to the increased heat transfer caused by the thermal conductivity increase (Sarı & Karaipekli, 2007).

Mills *et al* (2006) found that the thermal conductivity of paraffin wax can be increased by two orders of magnitude with the use of a porous graphite matrix. They found that this composite matrix had a thermal conductivity 20-130 times bigger than the pure PCM.

2.6.5.3. PCM + graphite

Graphite has only been tried as a thermal conductivity enhancer for low temperatures (below 150 ºC), but this is too low for many CSP technologies and its stability, storage capacity and thermal conductivity should be tested at higher temperatures.

The thermal conductivity of PCMs can be increased by a factor of up to 14 with the use of graphite. The graphite component did however decrease the thermal conductivity of the PCM as the temperature increased (2,25 % decrease per ºC) (Pincemin *et al*, 2008).

Zhang & Fang (2006) prepared a paraffin/expanded graphite composite PCM which had a large thermal storage capacity with a better thermal conductivity and no liquid leakage during its phase change.

Li *et al* (2014b) tested stearic acid with carbon additives (multi-walled carbon nanotubes, graphene and graphite) and found that the melting onset temperature of the nanocomposties were lower than that of the

stearic acid. The carbon additives successfully improved the heat conduction but weakened the natural convection in the liquid state. A 5% graphite addition improved the PCM's charging rate by 37 % and the discharge rate by 320 %. Graphite had the lowest thermal conductivity of the additives but proved to be the most effective at improving the heat transfer of the PCM (Li *et al*, 2014b).

Fan *et al* (2013) investigated the thermal conductivity and energy storage properties of paraffin based PCMs with carbon nanofillers (short and long multi walled carbon nanotubes, carbon nanofibers and graphene nanoplatelets). Carbon nanofillers were used in weight concentrations of 1 wt.% to 5 wt.%. The nanofillers slightly decreased the phase change enthalpies and had no significant effect on the phase change temperatures. The thermal conductivity increased as the amount of nanofiller was increased, but the relative increase were dependent on the size and shape of the nanofiller. Graphene nanoplatelets (GNP) were the most effective with a 164 % enhancement at a 5 % load. Fan *et al* (2013) attributed the GNP effectiveness to their two-dimensional planar structure that reduces the filler/matrix thermal interface resistance.

Li (2013) also found that the thermal conductivity increased when carbon nanoparticles were added to paraffin. The thermal conductivity was 2.89 times higher for a 1 % nano-graphite load and 7.41 times higher at a 10 % nano-graphite load.

Organic PCMs have low thermal conductivities which lead to a slow thermal response when they are used in high power applications. Şahan, Fois & Paksoy (2015) studied paraffin-nanomagnetite (Fe_3O_4) composites at 10 % and 20 % mass fractions. They found that the latent heat storage capacity was 8 % higher than that of pure paraffin. The thermal conductivity of the PCM was also increased by 48 % and 60 % for the 10 % and 20 % composites respectively.

There are currently two ways to try and increase the paraffin wax's thermal conductivity: insertion of a metal matrix into the wax or creating the TES system with fins for the storage tubes. However these metal matrixes increase the weight and volume of the system. To solve this it is important to create a novel composite PCM which has good heat conductivity and without liquid leakage during its phase change (Zhang & Fang, 2006).

It is clear that various fillers can be used to increase the thermal conductivity of organic PCMs but they must be kept as low as possible so that the high energy density of the PCM can be preserved (Sharma *et al*, 2015).

2.6.5.4. Other heat transfer enhancements

There are many more ways to improve the heat transfer of PCMs, some of the main types of heat transfer enhancements are shown in Table 2-3.

Table 2-3: Summary of heat transfer enhancement techniques

Heat transfer technique	Example
Finned tubes	Al-Abidi *et al* (2013) tested internal fins, external fins and a combination of internal/external fins in a triplex-tube heat exchanger (TTHX) and found that there was no significant difference between the three techniques, but that the fins did reduce the melting time by 43.3 % compared to that without fins. Sciacovelli, Guelpa & Verda (2014) tested tree shaped fins under transient conditions. They found that the discharge efficiency increased by 24 % when fins with two bifurcation are used. They also note that the optimal fins depend on the operating time of the latent heat thermal energy storage system, with y-shaped fins with wide angles being better for short operating times while smaller angles are better for longer operating times. This strengthened the idea that the transient behaviour of the system plays a very important part in its optimization. Al-Abidi *et al* (2013) used a numerical model to study the heat transfer of PCMs in a TTHX. They found that the fin length, fin thickness, number of fins, TTHX materials,

	Stefan number and the PCM unit geometry all had a significant influence on the PCM melting speed. They found that the number of fins and the fin length had a much bigger effect compared to the fin thickness. They found a maximum decrease of 34.7 % in the melting time for their most optimal configuration. They verified their model with experimental data and found it to be in good agreement. Velraj *et al* (1997) found the heat transfer enhancement with fins was several fold and showed promise for solar thermal storage applications.
Metal matrix	Baby & Balaji (2013) tested the use of copper as well as an aluminum porous matrix filled with a PCM. They found that the operation time for a heat sink with this matrix was 7.5 times that of a heat sink without the matrix, at 10 W. They also found that the orientation of the heat sink did not have a significant effect on the performance of the PCM filled matrix. Trelles & Dufly (2003) found that using an aluminum matrix considerably improved the performance of the system. They found a porosity of 0.8 (80 % PCM, 20 % aluminum) to be the most effective, increasing the aluminum reduces its thermal energy storage capacity while decreasing the amount of aluminum increases the thermal resistance of the system.
High conductivity additives	Kibria *et al* (2015) reviewed thermal conductivity from various sources. They found that graphite nano composites showed 12 times higher thermal conductivity compared to pure stearic acid. The carbon additive improves the conduction but reduces the natural convection in the liquid state. They found that adding nano-particles to PCMs could have negative effects on latent heat, viscosity, specific heat and dispersion stability. The nano particles can also act as a nucleant agent. The use of TiO_2 nanoparticles in a $BaCl_2$-H_2O nano fluid PCM reduced the melting and freezing time by 100 minutes and 109 minutes respectively. The addition of nano particles in a Al_2O_3-H_2O nano fluid PCM decreased the freezing time by 20.5 %. After a certain concentration nanoparticles are added to a PCM it can start to have a negative effect on the other PCM properties, which causes a limitation to allowable amount of dispersed nano

	particles. TES systems require PCMs with high thermal conductivities to improve the efficiency of the crystallization during the discharge process. The heat transfer rate was improved by 3.35 times for graphite at 5 vol.%. Choi *et al* (2014) also found that graphite showed the most promise out of the tested carbon additives.
Encapsulation	Salunkhe & Shembekar (2012) reviewed the use of encapsulation and found that encapsulation size, shell material, shell thickness and the encapsulation geometry are all important encapsulation parameters. The encapsulation of organic PCMs is harder than that of inorganic PCMs because of the organic PCM's similar structure to that of their plastic container. They also found that a very big drawback in encapsulation for commercialization is the high cost. Using silica encapsulation the thermal conductivity of a PCM was increased from 0.1505 W/(m·K) to 0.6213 W/(m·K). The solidification time was measured for copper, stainless steel, Teflon and PVC encapsulation with copper and stainless steel giving the shortest solidification time while PVC had the longest solidification time. Similarly they found the melting time for certain encapsulation materials were: copper (7 hours), aluminum (7 hours), polyethylene (8 hours), acrylic (9 hours) and PVC (9.3 hours).
Multitubes	Agyenim (2016) tested PCM melting with added circular fins, longitudinal fins and multitube systems. They found that the multitube system had the shortest melt time (275 minutes) followed by the longitudinal fins (430 minutes) and lastly the circular fins (8 hours). They note that the multitube system underwent subcooling during discharge while the longitudinal finned system showed no subcooling and performed the best during discharge. They recommend a combination of a multitube system and a longitudinal finned system for optimal charge and discharge performance. Esapour *et al* (2016) tested PCMs in a multitube heat exchanger. They found that an increase in the inlet temperature increased the melting rate and decreased the total melting time, while a similar mass flow rate did not

	increase the melting rate to the same extent. They found that increasing the amount of tubes from 1 to 4 lead to a 29 % reduction in melting time, this is because the melt region became larger and the including vortices strengthens which increased the convective heat transfer.

The thermal conductivity change can be complex as described by Kibria *et al* (2015), who reviewed various studies where paraffin wax and multi-walled carbon nanotubes were investigated. They found that the thermal conductivity of the PCM had a sudden increase near the melting point, followed by a sharp decrease in the liquid phase. The increase in the more orderly solid, around the melting point, is explained by the accelerated molecular vibrations in the matrix. The decrease when the PCM turns into a liquid is explained by the disorderly structure of the liquid compared to the solid.

The cost of nano/micro-particles can vary widely based on their size/structure/purity, but an example of their prices from Sigma-Aldrich (2017) are given in Table 2-4.

Table 2-4: Cost analysis of different nano/micro-particles (Sigma-Aldrich, 2017)

Particle	**R/g**
SWCNT	12000.00
MWCNT	667.00-2000.00
Graphene nanoplatelets	9460.00
Mesoporous silica ($MPSiO_2$) nanoparticles	227.00
Fe_3O_4 (50-100 nm)	20.10
TiO_2 nanoparticles (21 nm)	22.10

Baby & Balaji (2013) calls the use of heat transfer enhancement techniques “inevitable” to improve the thermal performance of the low thermal conductivity PCMs. The thermal conductivity of the PCM is therefore very important to consider for solar applications.

2.7. Carbon black

Carbon black is an aggregate of graphite microcrystals that can have large differences in size, because of this carbon black can be seen as polycrystalline graphite (Pierson, 1993: 47).

Long, Nascarella & Valberg (2013) on the other hand refers to carbon black as a fine powder of a quasigraphitic form of almost pure elemental carbon. Specific grades of carbon black can be produced by varying the conditions under which it is made. This allows carbon black with a certain surface area, particle size, structure, conductivity or colour to be made for specific applications. It can be seen that the term carbon black encompasses various substances that can have slightly different properties based on their structure.

2.7.1. Carbon black manufacturing

Carbon black is usually made by the burning of hydrocarbons in an insufficient amount of air. The graphite crystallites that make up the carbon black particles can usually not be detected by diffraction techniques because of their small size (Pierson, 1993: 288). The carbon blacks produced by different methods have different properties and are sometimes referred to by different names, based on the process with which they were created.

The two basic methods to create carbon black are:

1. Channel process: Many tiny natural gas flames hit a cool metallic surface, the carbon black then forms on this metallic surface before being oxidised at a high temperature. The small spheroid particles formed using this process have the highest surface area, smallest particle size and the highest volatile content of any carbon black particle.

2. Thermal process: The carbon black is formed in a preheated firebrick-lined chamber due to the thermal decomposition of natural gas in the absence of air. This creates coarser carbon black with a lower surface area and larger particle sizes.

(Pierson, 1993: 229)

The oil furnace process is a continuous process where carbon black is produced by the pyrolysis of heavy aromatic petroleum oils at temperatures between 1400 ^{0}C and 1800 ^{0}C. A big advantage of this process is that the manufacturing conditions can be well controlled to get a specific grade of carbon black.

Lampblack is a soft, amorphous and flocculent type of carbon black that is used as a black pigment. It is made by burning coal tar and petroleum oil, before the particles are calcined in the flue gas where it is carried to a large chamber, this expansion then causes the particles to settle. Different feed-to-air ratios has a large effect on the characteristic and properties of the formed lampblack (Pierson, 1993: 230-231).

Acetylene black is made by the thermal decomposition of acetylene. In this strongly exothermic reaction the acetylene gas as put into a retort at 800 ^{0}C in the absence of air where it decomposes. This reaction does not require additional heat.

Acetylene black can be compared to high grade lampblack but with a higher liquid-absorption capacity, higher electrical conductivity and overall

greater purity than that of lampblack. This makes acetylene black useful when electrical conductivity is needed, and is used as a filler in rubbers and plastics, and in the making of dry cells (Pierson, 1993: 231).

Carbon black can also be produced from vegetable products (as opposed to petrochemical feedstock), carbon black produced from these vegetable products tend to have much larger particle sizes.

The differences that the manufacturing process has on the final carbon black properties can be seen when you compare the properties and composition of carbon black in Table 2-5 with the properties of acetylene black as given in Table 2-6.

Table 2-5: Properties and composition of carbon black (Pierson, 1993: 229)

Composition	
Hydrogen	0.5-1.0 %
Nitrogen	0.02-0.09 %
Oxygen	2.5 -7.0 %
Sulfur	0.01 – 0.03 %
CO2	0.1-1.5 %
CO	0.2 – 4.0 %
Carbon	balance
Properties	
Surface area	25 – 150 m^2/g
Particle size	10 – 500 nm
Oil absorption	0.5 – 1.5 cm^3/g

Table 2-6: Composition and properties of acetylene black (Pierson, 1993: 232)

Composition	
Polymerization products	<1 %
Carbon	99 %
Ash	0.03 – 0.04 %
Moisture	0.05 – 0.06 %
Properties	
Density	2.05 g/cm^3
Apparent density	0.02 g/cm^3
Surface area	65 m^2/g
Particle size	3 – 130 nm
Undertone	blue

Carbon black is mainly used in rubber to increase the strength, hardness, stiffness, wear resistance and heat resistance. Carbon black can also be used in typographical inks, paints, enamels, lacquers, etc.

It is clear that the method that is used to make the carbon black has a big impact on the properties of the final carbon black.

Other advantages of carbon black is that it is very cheap, helping keep down the cost of the synthesized composites (costs 10-20 % that of purified natural graphite) and carbon black's production volume is very big (9 times that of natural graphite) (Magasinski *et al*, 2010).

In 2008 approximately 9.8 million metric tonnes of carbon black was produced. More than 95 % of carbon black is produced by the oil furnace process, with the other processes making up the rest (acetylene black process, channel black process, gas black process, thermal black process and the lamp black process).

2.7.2. Carbon black's structure

Carbon black has very little inorganics or extractable organic compounds. The particle morphology of carbon black is described as aciniform (grape-

like) aggregates which are made out of fused spherical particles. These aggregates are then also clustered into larger agglomerates (Long *et al*, 2013).

Carbon blacks are usually found as complex particle aggregates and agglomerates and not as free individual particles (Long *et al*, 2013).

More properties of carbon black, as described by (Long *et al*, 2013) are given in Table 2-7.

Table 2-7: Properties of carbon black (Long *et al*, 2013)

Property	
Morphology	Aciniform (grape-like) aggregates and agglomerates
Nodule size	15-300 nm
Aggregates size	85-500 nm
Agglomerate size	1-100+ micrometer
Total carbon	97-99 %
Elemental carbon	>97 %
Organic Carbon	< 2 %
Hydrogen to carbon ratio	<0.008
Trace inorganic species	<1 %
Solvent-Extractable Organic Matter	0.02-0.14%
Total PAH content	0.1-330 (mg/kg)
Surface Area	12-240 (m2/g)
Density	1.7-1.9 (g/cm3)

Carbon black is mainly made up out of particle aggregates and agglomerates with sizes larger than 100 nm and up to hundreds of microns. The carbon black aggregate is considered the smallest indivisible entity. Long *et al* (2013) defines the carbon black aggregate as: “a discrete, rigid, colloidal mass of extensively coalesced particles, it is the smallest dispersible unit”.

The basic building blocks of carbon black products are called primary particles or nodules, these particles have a turbostratic arrangement and are made up of randomly stacked, concentric sheets of graphite platelets.

These nodules are usually only found within the reactor vessel because of their very quick and irreversible fused aggregate formation. Thermal blacks can however have some nodules in between the aggregates, but these nodules made from thermal blacks are usually larger than those of other carbon blacks (larger than 100 nm) (Long *et al*, 2013).

The nodules form first, followed by aggregation and then finally agglomerates (large clusters) are formed as seen in Figure 2-6. These agglomerates can range in size from 1-100+ micrometres. Agglomerates can be made up of many thousand aggregates clinging together by Van der Waals forces. There are no chemical bonds or welding holding the agglomerates together, but these agglomerates are regarded as the predominant carbon black entity since they are not usually broken by normal manufacturing conditions or use. Manufactures usually further pelletize these agglomerates to reduce dust and to make handling and shipping easier, leading to a final product with diameters of 100-1000 micrometre (Long *et al*, 2013).

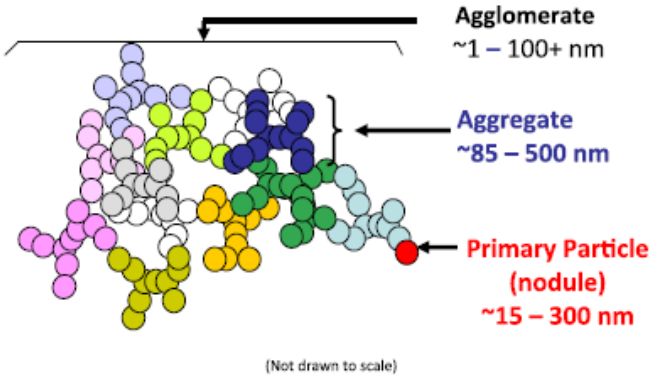

Figure 2-6: The normal structure of carbon black (Long *et al*, 2013).

Table 2-8 summarises some of the main difference between carbon black and other carbon materials.

Table 2-8: Main differences between carbon black and carbon-based nanomaterials (Long *et al*, 2013)

Carbon material	**Distinct property**
Carbon black	Aciniform aggregates
SWCNT and MWCNT	Fibrous materials High aspect ratio Needle like fiber shape Nanoscale dimensions
Fullerenes	Symmetrical closed-cage structure Hexaganol and pentagonal rings Nanoscale dimensions
Graphene-family nanomaterials	Single atom thick 2 d sheet of hexagonal carbon atoms Plate like structure of graphene sheets Nanoscale dimensions

Carbon black can be described as a nanostructured material (its internal or surface structure is in the nanoscale, but the strongly fused aggregates can be much larger) rather than a nanoparticle or nano-object (Long *et al*, 2013).

Sircar & Wells (1982) tested the effect that carbon black has on the thermal conductivity of elastomers. They found that the way in which the carbon black was added to compatible blends did not affect the thermal conductivity values and that the carbon black increased the thermal conductivity of all the tested elastomers. They also found a linear relationship between the volume concentration carbon black and the thermal conductivity, except when the carbon black concentration was very high.

The thermal conductivity of carbon black in the bulk phase is much different from that of the individual carbon black particles and the density of carbon

black is 1900 kg/m^3. The apparent conductivities of acetylene black was found to be 45-60 mW/(m·K) under atmospheric air pressure and 3.5-5 mW/(m·K) under primary vacuum (Maquin *et al*, 2000).

Smaller carbon black particles have larger surface areas. The surface area affects the intensity of the black colour, the conductivity and the UV absorption. A larger surface area leads to better absorption because of the larger surface area that is available.

Carbon black absorbs energy from all wavelengths of light; this is what gives it its black colour. To obtain the maximum absorption of light carbon black particles with a high surface are should be chosen.

The primary particle size is the most important factor that determines UV absorption efficiency, the UV absorption increases, with a decreasing particle size, until 20 nm is reached (Pritchard, 1998: 153-157).

2.7.3. Carbon black from environmentally friendly sources

Carbon black from recycled tyres significantly reduces the cost and energy required to make carbon black and reduces the overall environmental impact. This process can be self-sufficient with regards to its energy requirements since the gases from the pyrolysis of the tyres can be used to add the heat necessary for the process (Smith *et al*, 2016).

The particle size distribution of carbon black from recycled tyres can be seen in Figure 2-7. Almost all of the particles are in the micrometre range (1 µm to 100 µm).

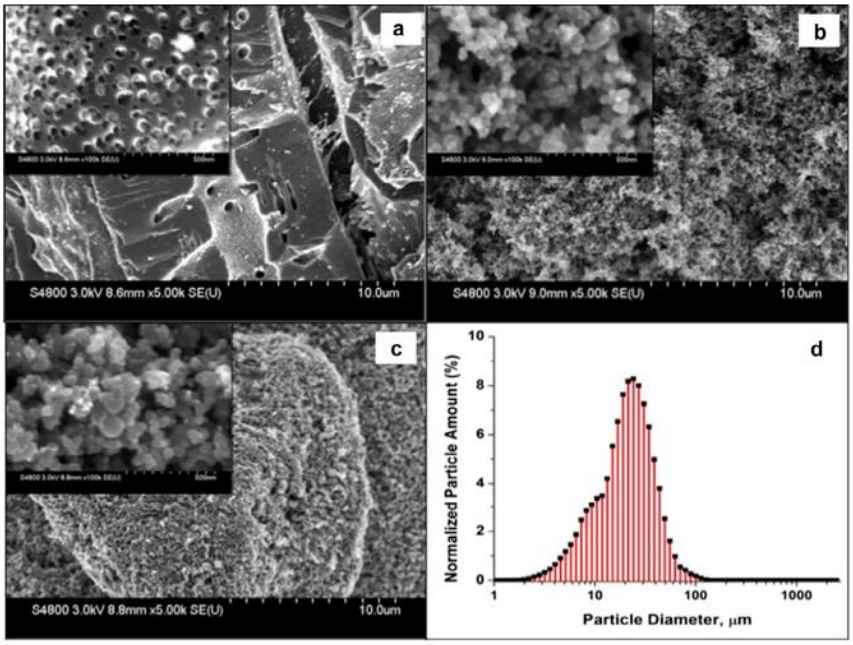

Figure 2-7: SEM micrographs of activated carbon (a), commercial carbon black (b), carbon black from recycled tyres (c), and the particle size distribution of the carbon black from recycled tyres (d) (Smith *et al*, 2016).

According to Hita *et al* (2016) 7×10^6 tons (or more) of waste tyres are created every year. The big increase in tyre consumption in Asia and Oceania will make them the main source of waste tyres for the next two decades, with China producing 5.2×10^6 tons of tyres in 2010 alone.

Tyres are mainly made out of carbon black, steel, natural rubber and synthetic rubber. The carbon black reinforces the rubber and increases the tyres resistance to fracture and abrasion. The main materials in tyres are given in Table 2-9.

Table 2-9: The materials that make out a tyre as a percentage of the total weight of the completed tyre (Hita *et al*, 2016)

Material (wt. %)	PCT		TT	
	USA	EU	USA	EU
Natural rubber	14	22	27	30
Synthetic rubber	27	23	14	15
Carbon black	28	28	28	20
Steel	14-15	13	14-15	25
Others[a]	16-17	14	16-17	10

[a] Fillers, Nylon, accelerators and sulphur, as well as others.

There are 4 billion tyres in landfills and stockpiles with an additional 1.5 billion tyres sold each year. Pyrolysis of tires can be used to create useful products like carbon black (called pyrolytic carbon black). The pyrolysis of tyres creates carbon black, a non-condensable gas mixture and a liquid fuel made up of aromatic and aliphatic compounds. Carbon black makes up 30-40 % of tyres, this carbon black comes from fossil sources and recycling this product would greatly help the profitability of tyre valorisation by pyrolysis. The carbon black obtained from this process was found to have comparable properties to commercial carbon blacks, with regards to their BET surface (Martínez, Murillo & García, 2013).

2.8. Additional additive effects

Additives can have other unexpected effects on the substance in which they are added, some of these effects are discussed below.

2.8.1. Subcooling

Subcooling (or super cooling) is when the PCM only begins to solidify at a temperature lower than its melting temperature.

Subcooling does not influence the melting of the PCM (charging phase) but is an important factor in the cooling process since the crystallization will

start at temperature well below the phase change temperature. This is especially important in TES applications since the latent heat will only be released during crystallization. Nucleation is the main process that starts the crystallization. There are two types of nucleation:

1. Homogenous nucleation where the temperature is low enough for the PCM itself to start the nucleation, or when solid PCM is added to the sub cooled PCM, starting nucleation.
2. Heterogeneous nucleation is where special additives are added to the PCM to start the nucleation.

Some authors have found that some carbon particles can act as nucleating agents, leading to heterogeneous nucleation which increased the crystallization process and therefore reducing the subcooling (reducing solidification time) (Kibria *et al*, 2015).

2.8.2. Viscosity

The particles added to the PCM increases the dynamic viscosity of the composite, limiting the dispersion. Kibria *et al* (2015) found that the nanoparticle concentration and the temperature of the composite influenced the dynamic viscosity of the composite. They found that the increase of the dynamic viscosity was significantly higher than the thermal conductivity enhancement.

Fan *et al* (2014) investigated graphene-based composite PCMs and found that because of the increase in thermal conductivity the melting rate was accelerated by 8 % with a 3 wt.% loading and a boundary temperature of 55 ^{0}C. When Fan *et al* (2014) increased the boundary temperature they found that the melting rate was slowed down, because of the large increase in dynamic viscosity and its effect on the natural convection.

2.8.3. Latent heat of fusion

To understand the effect that carbon additive can have on PCMs, it must first be understood what the latent heat is.

Kibria *et al* (2015) states that the two classes of intermolecular attractions are:

1. Short-range forces (centres of molecules are 3 Ä or less apart), usually a repulsive force.
2. Long-range forces (centres of molecules are more than 3 Ä apart), usually a weak attraction force.

When the PCM goes from a solid to a liquid the heat that is absorbed does not increase the temperature of the material, instead it is used to overcome the weak intermolecular attractions (Kibria *et al*, 2015).

If the concentration of nanoparticles added to the PCM is high enough then they could change the long-range forces. This could lead to an increase in the latent heat if the nanoparticles/wax interaction potential is larger than that between the wax molecules. The smaller SWCNTs increased the latent heat of fusion because of their better dispersion and large surface area which increased the intermolecular attraction with the wax molecules (Kibria *et al*, 2015).

The latent heat of fusion of the PCM would very quickly decrease with an increase in MWCNT loadings, until a certain point is reached. After this point the latent heat would suddenly increase again and create a peak before linearly decreasing. The reason for this behavior is that the dispersion of MWCNT is more uniform at low loadings, causing the MWCNTs to absorb more palmitic acid molecules. This causes more palmitic acid molecules to lose their phase change properties, causing the latent heat to decrease very quickly at low loadings. As the loading

increases the amount of agglomeration also increases which reduces the percentage of palmitic acid molecules that are absorbed by the MWCNTs, culminating in a peak value of latent heat. Further increase in the CNT loading does not further affect the agglomerate, causing the latent heat to linearly decrease (Kibria *et al*, 2015).

Kibria *et al* (2015) also states that an increase and decrease behavior in the latent heat in PCMs with dispersed carbon particles were also observed by other researchers. They further state that there exists an optimum level of nanoparticle concentration where the thermal conductivity increase is a maximum and the reduction in latent heat capacity is a minimum.

2.8.4. Radiative heat transfer in semitransparent media

Yi *et al* (2012) looked at semitransparent media and states that there are solid, mushy and liquid regions in PCMs, each having its own physical properties. Each of the interfaces between the regions is semitransparent and diffuse reflecting. PCMs used in high temperature TES is an example of this type of radiative heat transfer in semitransparent media. The effect of internal thermal radiation in the melting/solidifying of semitransparent PCMs must be taken into account.

They found the following with regards to radiative heat transfer:

- Thermal radiation had a non-linear effect on temperature fields, with complicated mechanisms.
- Radiative heating/cooling can accelerate internal melting or solidification.
- Lowering the optical thickness increases the scattering albedo giving wider mushy zones and slower solidification.

- Different phases in semitransparent PCMs have different physical/thermophysical and radiative properties.

The effect of radiative heat transfer on the solidification of various solid mediums is explained below.

2.8.4.1. Semitransparent, purely absorbing medium

1. Small optical thickness (0.1)
    - Large liquid zone at start and the heat transfer is similar to a liquid only medium.
    - As the PCM solidifies there is a smaller liquid fraction, this causes the temperature and liquid fraction differences to grow larger.

2. Optical thickness increased from 0.1 to 1
    - The difference in temperature fields are smaller.
    - The phase change speed is quicker because of the increase in optical thickness.
    - Certain range, increased optical thickness, bigger thermal emissions, stronger radiative cooling.
3. Optical thickness increased from 1 to 5
    - Small increase in the solidification speed
    - Thermal emission is proportional to the optical thickness
    - Large optical thickness causes heat transfer behavior similar to conduction. The solidification heat transfer is dominated solely by conduction and not radiation together with conduction.
    - As optical thickness increases it reaches a point where the phase change speed does not increase any more (because of the conduction effect).
4. Optical thickness increased beyond 5

- The strong scattering has a very big effect on solidification and increases solidification time.
- The temperature and liquid fraction differences are larger under strong scattering conditions (small optical thickness had a small difference).

2.8.4.2. Opaque surfaces

- Optical thickness of 1, surface emissivity of 0.1: the solidification speed is much slower than non-opaque surface.
- Solidification speed increase with increase in emissivity, but even at 1 it is still lower than semitransparent surfaces.

Yi *et al* (2012)'s main findings are summarized as:

- When the optical thickness is not big there is a significant difference in temperature and liquid-fraction distributions and the differences decrease with an increase in optical thickness
- Increase in optical thickness leads to faster phase change up to a certain point. After this point is reached the heat transfer is mainly controlled by conduction and the speed stops increasing.
- The solidification speed of opaque surfaces increase with an increase in emissivity. Semitransparent surfaces with a moderate optical thickness have a faster solidification speed than opaque surfaces regardless of the emissivity.

These findings show that changing the optical properties of a PCM can have a large effect on the PCM's radiative heat transfer properties during melting/solidification.

2.9. Characterization methods

2.9.1. DSC

Sharma *et al* (2015) reported that almost all of the studies that were reviewed used a DSC to evaluate the thermal properties of the tested PCMs. In DSC analysis the sample and reference are kept at the same temperature, the thermal properties of the sample can then be obtained by measuring the difference between the heat absorbed by the reference and the sample. The problem with the use of DSC is that it uses a very small sample and requires it to be uniform, which is not realistic for PCM composites because they are not homogeneous.

Djefel *et al* (2014) did DSC analysis on stearic acid and various stearic acid composites. Pure stearic acid during the melting process had an extrapolated onset temperature, peak temperature and extrapolated end temperature of 52.85 ^{0}C, 59.14 ^{0}C and 56.30 ^{0}C respectively. During the freezing process the extrapolated onset temperature, peak temperature and extrapolated end temperature were 52.23 ^{0}C, 46.90 ^{0}C and 50.42 ^{0}C respectively. For a 50 wt.% stearic acid and coffee ground composite the extrapolated onset temperature during the melting process was 1.44 ^{0}C lower than the pure stearic acid, this decrease in temperature was also present for composite PCMs with graphite added. The extrapolated end temperatures of the composites showed an increase in temperature compared to that of pure stearic acid. It was also found that the melting temperature range increased for the different composites. The extrapolated onset temperatures of the composite PCMs were closer to that of pure stearic acid during the freezing process. Lastly the extrapolated end temperatures and peaks of the PCMs composites were lower when compared to that of pure stearic acid (Djefel *et al*, 2014).

The melting onset temperature was reduced while the solidification onset temperature was increased when multi-walled carbon nanotubes were added to pure paraffin. The effect that nanoparticles have on the latent heat capacity of the PCM depend on the size, shape, concentration and the intermolecular attraction between the particles and the PCM (Kibria *et al*, 2015).

Zhang & Fang (2006) compared the DSC curves of pure paraffin with an 85.6 wt.% paraffin and expanded graphite composite. They found that the thermal characteristics of the two samples were very similar because there was no chemical reaction during the preparation of the paraffin and expanded graphite composite. They found the latent heat of the PCM by numerical integration of the area under the peaks of the solid-solid and solid-liquid transitions. The total latent heat of the pure paraffin was 188.69 J/g and that of the composite PCM was 161.45 J/g.

An alternative to the DSC method to measure the thermophysical properties of PCMs is the T-history method. The T-history method puts two samples in an air enclosure at a different temperature, the temperatures of the two samples as well as the temperature of the air is then measured. One of the samples is the reference sample with known thermal properties while the other sample is the PCM being measured (Cabeza *et al*, 2015). Cabeza *et al* (2015) gives the advantages of the T-history method over DSC as:

- More precise energy and temperature measurements
- The sample and conditions being tested more closely resemble that of the sample's application (can use a larger mass of sample)
- Subcooling and other properties of the sample can also measured

2.9.2. Test of thermal storage performance

Zhang & Fang (2006) tested the thermal storage performance of a paraffin/expanded graphite composite PCM. They took 7 grams of pure paraffin and 7 grams of the composite, and then put them into identical glass test tubes. A thermocouple was then placed in the centre of the test tube and the two test tubes were put into a waterbath at a constant temperature of 29 ^{0}C. The test tubes were then quickly put into another waterbath at 65 ^{0}C where the PCM will store heat. When the heat storage was complete the two test tubes were then put back into the waterbath at 29 ^{0}C where heat extraction from the PCM took place.

Zhang & Fang (2006) tested a 85.6 wt.% paraffin PCM, with expanded graphite and found that the composite had a 27.4 % reduction in heat storage rate and a 56.4 % reduction in heat release rate. The reason for the larger reduction in the heat release rate is due to the fact that the heat release rate is controlled by thermal conduction (which is increased much more by the expanded graphite's bigger thermal conductivity) while the heat storage rate is controlled by natural convection. The change in charge/discharge rate found by Zhang & Fang (2006) is shown in Figure 2-8.

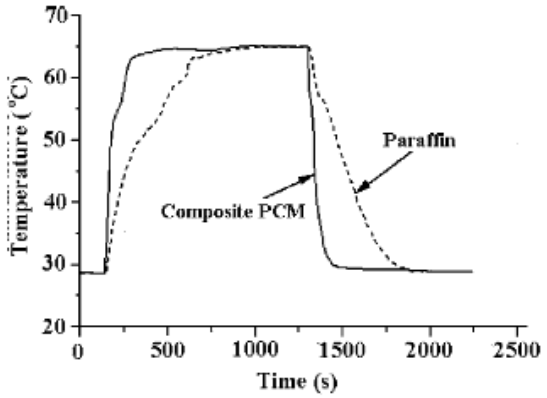

Figure 2-8: Paraffin and composite PCM heat storage and release curve (Zhang & Fang, 2006).

2.10. Nanofluids

Nanofluids have a lot of similarity to the use of PCM composites for direct solar absorption and are more widely investigated. Carbon black and water mixtures are especially important, since the carbon black helps absorb more sunlight and thereby helps increase the temperature of the mixture, similar to the desired effect when using carbon black in PCMs.

Nanofluids are liquids with nanoparticles (particles whose diameter are less than 100 nm) suspended inside them. Nanofluids have very good optical and thermal properties even at low nanoparticle concentrations. The ability of nanofluids to convert the light energy from the sun into thermal energy is extremely important for their use in solar energy applications (Taylor *et al*, 2011).

The important wavelength range for solar energy is 0.25 μm to 2.5 μm. Taylor *et al* (2011) found that nanofluids could absorb more than 95 % of the incoming sunlight (when the nanofluid thickness is more than 10 cm), even with very low nanoparticle volume fractions (less than 10 parts per million). These nanoparticles also do not significantly increase the viscosity or density of the liquid.

According to Taylor *et al* (2011) the perfect volumetric collector should:

- Absorb solar radiation efficiently and convert it to heat inside the working fluid
- Have minimal heat losses due to radiation and convection
- Not cause fouling or clogging

An anti-reflective glazing could be used as a cover on these collectors to reduce the heat losses due to radiation and convection while still allowing sunlight to go through.

Nano-sized particles do not add a significant amount of extra abrasion or clogging when added to the liquid. The low volume fraction of nanoparticles needed also mean that the extra capital investment is low. When the nanoparticle volume fraction is high the incoming light will mostly be absorbed in a thin surface layer, this is not optimal since the thermal energy in this surface layer is easily lost to the environment. When the nanoparticle volume fraction is low the nanofluid will not absorb all of the solar radiation hitting it, the optical properties of the fluid must therefore be very precisely controlled to ensure that the nanofluid operates effectively (Taylor *et al*, 2011).

2.10.1. Preparation of nanofluid

Taylor *et al* (2011) recommends using 1 % sodium dodecyl sulphate as a surfactant and a probe-type sonicator (for 15 to 30 minutes) to disperse the nanoparticles into the base fluid. Using a surfactant to stabilise the nanofluid does not work at high temperatures and therefore needs continuously re-sonicating or the use of more exotic preparation techniques to ensure long term stability for solar applications.

2.10.2. Carbon black's use in nanofluids

Carbon black has potential in the application of solar utilization because it has extremely good absorption over the entire wavelength of sunlight. Carbon black added to water causes the temperature to rise faster when exposed to sunlight, which indicates that it has good solar energy absorption properties. It also increased the thermal conductivity of the water with a near linear correlation between the thermal conductivity and volume fraction carbon black added (Han *et al*, 2011).

Figure 2-9 (a) shows a TEM of a typical carbon black nanofluid, with particles around 20 nm in diameter with some agglomeration. Figure 2-9 (b) shows the size distribution of these particles, the agglomeration of the particles give the higher particle size.

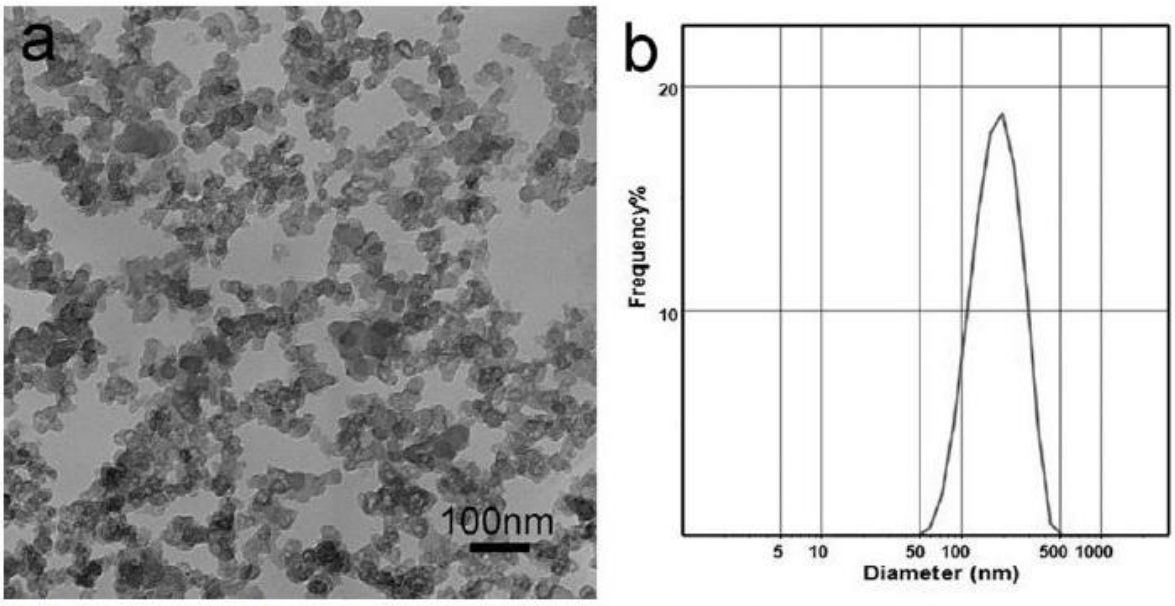

Figure 2-9: Characterization of the typical sample (a) TEM image, (b) size distribution (Han *et al*, 2011)

As seen in Figure 2-10 the temperature of the nanofluids increase faster than that of pure water and the more particles there are the faster it increases, up to a certain volume.

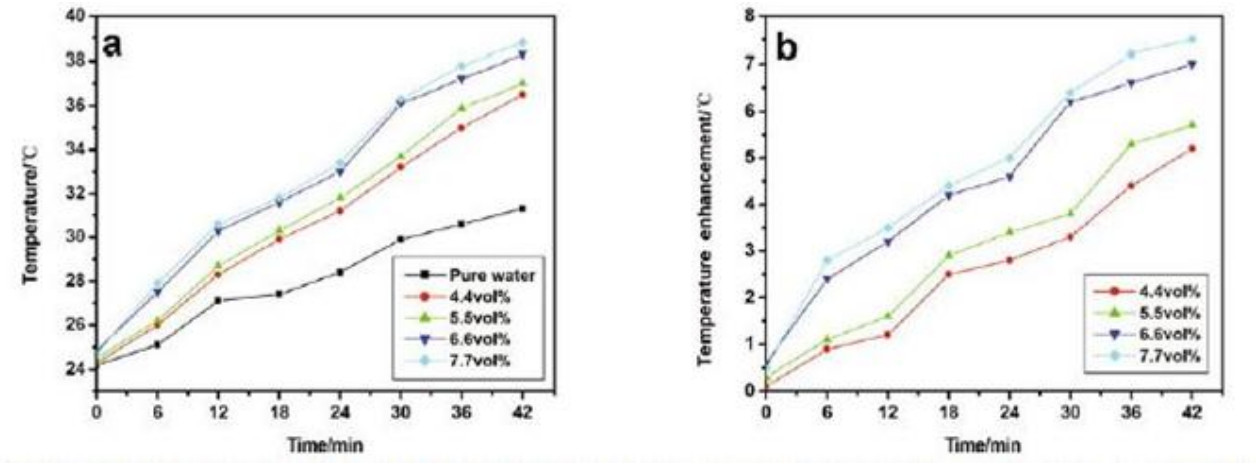

Figure 2-10: Photothermal properties of carbon black nanofluids. (a) Temperature as a function of time. (b) temperature enhancement as a function of time (Han *et al*, 2011).

Figure 2-11 shows the UV-Vis-NIR absorption spectra of carbon black powder. It can be seen that the carbon black has good absorption over the entire range. Figure 2-12 shows the UV-Vis-NIR transmittance spectra of carbon nanofluids and water. The perfect absorption of carbon black nanofluids in the wavelength from 1400 nm to 2500 nm can be seen. The carbon black nanofluids also have a lower transmittance in the wavelength range from 200 nm to 1400 nm which shows that it has better solar absorption than water.

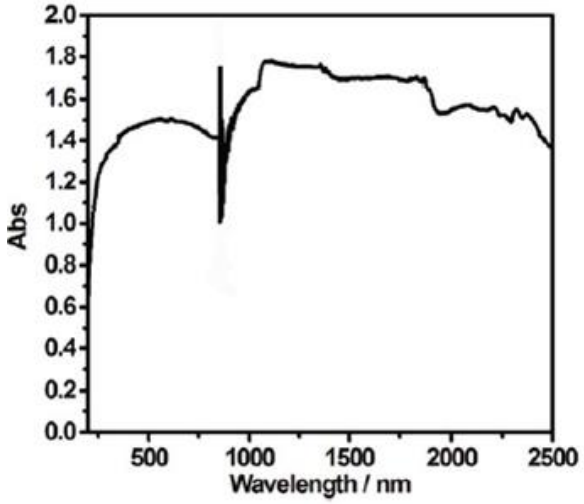

Figure 2-11: UV-Vis-NIR absorption spectra of carbon black powder (Han *et al*, 2011)

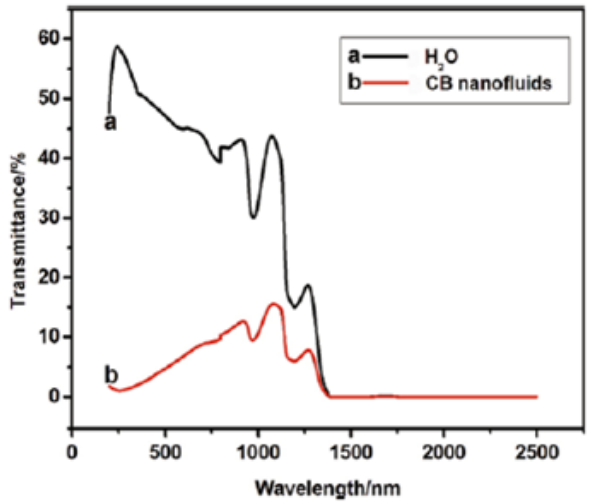

Figure 2-12: UV-Vis-NIR transmittance spectra (Han *et al*, 2011)

The near linear correlation between the volume fraction carbon black and the thermal conductivity can be seen in Figure 2-13. It is clear that the thermal conductivity of the nanofluids increases with an increase in the carbon black volume fraction.

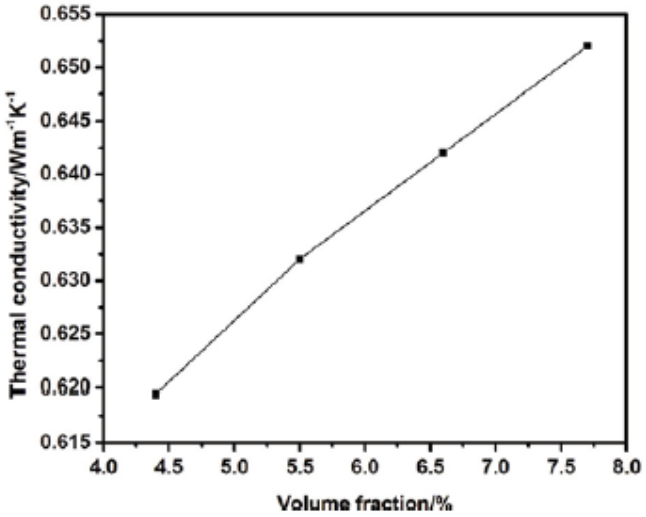

Figure 2-13: Thermal conductivity of nanofluids as a function of carbon black volume fraction at 35 ºC (Han *et al*, 2011).

2.10.3. Challenges

Some of the problems with nanofluids in solar thermal devices as discussed by Mahian *et al* (2013):

High cost: Some nanofluids are difficult to produce which increases its cost.

Instability and agglomerating: Solar systems which make use of natural circulation do not work well with nanofluids. At high temperature gradients the agglomeration of nanoparticles becomes a bigger problem.

Pumping power and pressure drop: Certain nanofluids have higher viscosity compared to the base fluid which increases the pressure drop and therefore increases the required pumping power.

Erosion and corrosion of components: Certain nanoparticles could cause corrosion and erosion of the thermal devices if they are used over a long time span. The nanoparticles also have different erosion and corrosion effects depending on the surface that they are in contact with (Mahian *et al*, 2013).

2.11. Novel experiments and potential applications of PCMs

There are many potential applications for PCMs with improved solar absorption; some of them are briefly discussed below.

2.11.1. Solar water heating

Nearly all domestic solar water heaters in the US are forced-circulation systems, the collectors have black chrome selective surfaces or flat-black absorbers. They can also have heat exchangers using propylene or ethylene glycol in the collector loops (Duffie & Beckman, 2013: 488)

Adding a PCM, especially a PCM that can act as the direct solar absorber and heat transfer fluid could greatly increase the efficiency of these heaters and continue to heat the water, even after the sun went down.

2.11.2. Integral collector storage systems

Integral collector storage systems act as solar collectors and energy storage systems. They consist of a tank, energy-absorbing surfaces which are inside an insulated box and a transparent cover. This configuration is shown in Figure 2-14. At the start of the day water is added to the tubes (black plastic cylinders) and this water is then heated throughout the day (Duffie & Beckman, 2013: 494).

A PCM can be used to replace the black plastic cylinders as the direct solar absorber, increasing the efficiency and keeping the water warm for longer.

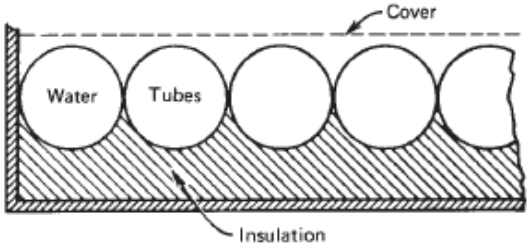

Figure 2-14: A solar heater that combines collection and storage (Duffie & Beckman, 2013: 494).

2.11.3. Pool heating

It requires a significant amount of energy to heat a swimming pool, even though the temperature required for pools are low (Duffie & Beckman, 2013: 502).

Using a PCM to heat the pool can be very useful since the PCM can continue to heat the pool during night time.

2.11.4. Building heating

The two main heat transfer fluids used in building heating are water and air. Building heating consists of the collector, the storage unit and the building being heated. An extra energy source is usually required and the optimum combination of solar energy and conventional energy becomes very important. These systems have collectors that heat up a fluid, the storage unit to store the solar energy and a distribution system to control the dispensing of the solar energy to where it is needed (Duffie & Beckman, 2013: 505).

Using the PCM can combine these systems, while also improving the collection of solar energy.

2.11.5. Movable insulation

Direct-gain and storage walls can have significant energy losses if measures are not taking to minimize them. A storage wall using water tanks were shown to have notable energy losses during nighttime. The large un-insulated areas in passive heating systems (solar absorbing elements) can also have a large amount of energy losses. To counteract these losses movable insulation is used (drapes, screens, shades, shutters or more substantial insulation) (Duffie & Beckman, 2013: 546-547).

Organic PCMs have very low thermal conductivity and can be used as an insulator. Using this PCM as the direct solar absorber in colder times and blocking the absorbing side in the hotter times (then the PCM acts as an insulator), could be used to keep the building hot in the winter and cold in the summer. This approach would need some heat transfer enhancement to ensure that the heat from the low thermal conductivity PCM can be effectively used when needed.

2.11.6. Collector-storage walls and roofs

A high capacitance solar collector is directly connected to the area that needs to be heated. Solar radiation hits the outside surface, this energy is then transferred to the inside of the room by convection and radiation. Openings in the wall can allow air (natural or forced circulation) to transfer the heat into the room (Duffie & Beckman, 2013: 557).

2.11.7. Flat-plate Collectors

A box containing a copper plate with copper pipes soldered onto them with a glass (or multiple glass) covers. The copper pipes and plates are usually painted black. This flat plate collector can heat water up to temperatures of 80 ^{0}C (Chen, 2011: 233).

Adding the PCM composite to directly absorb the sunlight (instead of having only air between the copper plates and the glass cover) could improve the efficiency of the solar collector and allow the water to be heated even when there is no longer sunlight.

2.12. Modelling

2.12.1. Model with no phase change

A basic model of a solar simulator was made. It was modeled as a light source hitting a glass pane, then going through a small air gap then another glass pane, then a larger air gap before finally hitting the PCM. The PCM was first modeled as a solid with constant physical properties (melting was not taken into account). It could therefore heat up past its melting point without a change in properties or absorbing extra energy to use when undergoing phase change. The annotated rig can be seen in Figure 2-15 and the resistance network is shown in Figure 2-16.

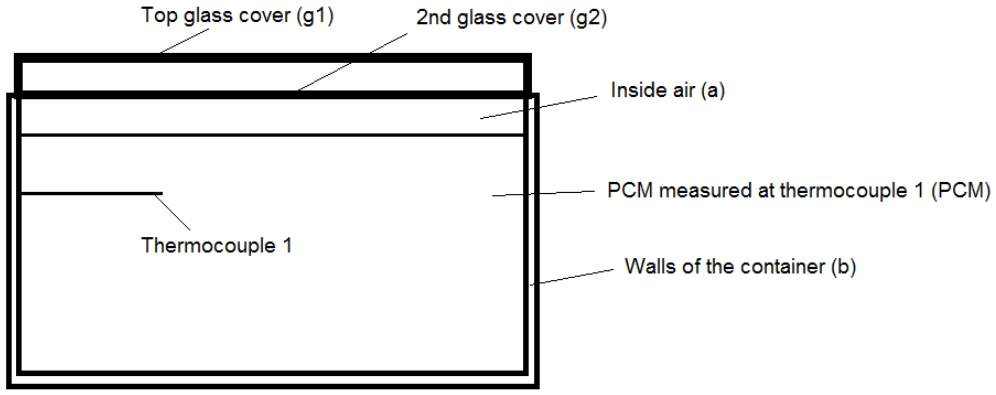

Figure 2-15: Annotated rig, showing the subscripts used in the model

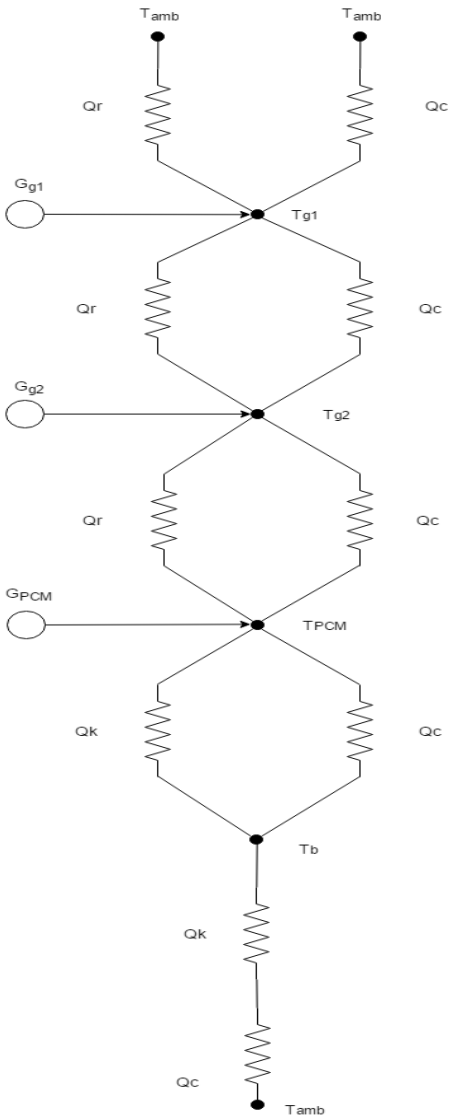

Figure 2-16: The simplified thermal network of the modelled system.

The simplified model is a modified version of Harmim *et al* (2012)'s mathematical model of a box-type solar cooker.

Assumptions:

- The outer box/insulation is treated as a single material with a uniform temperature
- The radiation is constantly and uniformly hitting from directly above the solar oven
- The temperature of each part of the solar oven is at a uniform temperature (entire node is at the same temperature)

- The thermo-physical properties of all of the materials stays the same (no melting)
- The ambient temperature remains constant at 25 °C

2.12.1.1. Energy balances

The main heat transfer mechanisms for every resistance were modeled.

For the first glass pane, there is radiation hitting the glass, radiation and convection heat transfer between the two glass panes, and radiation and convection between the glass pane and the surroundings (ambient):

$$\left(MC_p\right)_{g1}\frac{dT_{g1}}{dt} = S_g G_{g1} + S_g\left(hr_{g2-g1} + hc_{g2-g1}\right)\left(T_{g2} - T_{g1}\right)$$

$$-S_g hr_{g1-amb}\left(T_{g1} - T_{amb}\right) - S_g hc_{g1-amb}\left(T_{g1} - T_{amb}\right) \qquad (1.)$$

For the second glass pane there is radiation hitting the glass (after passing through the first glass pane), radiation and convection heat transfer between the two glass panes, and radiation transfer between the PCM and the glass:

$$\left(MC_p\right)_{g2}\frac{dT_{g2}}{dt} = S_g G_{g2} + S_{PCM} hr_{PCM-g2}\left(T_{PCM} - T_{g2}\right)$$

$$-S_g\left(hr_{g2-g1} + hc_{g2-g1}\right)\left(T_{g2} - T_{g1}\right) \qquad (2.)$$

For the PCM there is radiation hitting the PCM (after passing through both glass panes), radiation heat transfer between the PCM and the bottom glass pane, convection between the PCM and the inside air and some heat conduction through the PCM:

$$\left(MC_p\right)_{PCM}\frac{dT_{PCM}}{dt} = S_{PCM} G_{PCM} - S_{PCM} hr_{PCM-g2}\left(T_{PCM} - T_{g2}\right)$$

$$-S_{PCM}hc_{PCM-a}(T_{PCM}-T_a)-S_{PCM}hk_{PCM}(T_{PCM}-T_{amb}) \qquad (3.)$$

For the air between the glass and PCM there is convective heat transfer between the PCM and the inside air as well as convective heat transfers between the inside air and the outer box walls:

$$(MC_p)_a\frac{dT_a}{dt}=S_{PCM}hc_{PCM-a}(T_{PCM}-T_a)-S_bhc_{a-b}(T_a-T_b) \qquad (4.)$$

For the box wall there is convective heat transfer between the inside air and the box wall and conduction heat transfer through the box walls (with insulation):

$$(MC_p)_b\frac{dT_b}{dt}=S_bhc_{a-b}(T_{PCM}-T_{g2})-S_bh_{b-amb}(T_b-T_{amb}) \qquad (5.)$$

2.12.1.2. Radiation heat transfer coefficients

The radiation heat transfer coefficient between the top glass cover and the surrounding room is given as:

$$hr_{g1-amb}=\varepsilon_{g1}\sigma(T_{g1}^2-T_{amb}^2)(T_{g1}+T_{amb}) \qquad (6.)$$

The radiation heat transfer between the two glass covers is:

$$hr_{g2-g1}=\frac{\sigma(T_{g1}^2+T_{g2}^2)(T_{g1}+T_{g2})}{\frac{1}{\varepsilon_{g1}}+\frac{1}{\varepsilon_{g2}}-1} \qquad (7.)$$

The radiation heat transfer between the top of the PCM and the bottom glass cover is:

$$hr_{PCM-g2}=\frac{\sigma(T_{PCM}^2+T_{g2}^2)(T_{PCM}+T_{g2})}{\frac{1}{\varepsilon_{PCM}}+\frac{1}{\varepsilon_{g2}}-1} \qquad (8.)$$

2.12.1.3. Convection heat transfer coefficients

The convection heat transfer coefficient between the top glass cover and the surrounding air is given in Equation 9, the solar simulator is indoors but a fan was used to keep the lamp cool. The convection heat transfer was therefore calculated using this correlation for wind speed (Duffie & Beckman, 2013: 165):

$$hc_{g1-amb} = 5.7 + 3.8U \quad (9.)$$

Where U is the wind speed (the experiment was carried out indoors but with a fan on to keep the lamp from overheating).

Nusselt number was used to estimate the convection heat transfer coefficient between the two glass covers with the following correlation from Rohsenow, Hartnett & Cho (1998):

$$Nu = [Nu_{ct}, Nu_l, Nu_t]_{max} \quad (10.)$$

Where

$$Nu_{ct} = (1 + (\frac{0.104Ra^{0.293}}{1+(\frac{6310}{Ra})^{1.36}})^3)^{\frac{1}{3}} \quad (11.)$$

and

$$Nu_l = 0.242(Ra\frac{e}{S_0})^{0.273} \quad (12.)$$

And lastly

$$Nu_t = 0.0605Ra^{\frac{1}{3}} \quad (13.)$$

The Nusselt number used to estimate the heat transfer coefficient between the PCM and the inside air was calculated using the correlation from Churchill & Chu (1975):

$$Nu = (0.825 + \frac{0.387Ra^{\frac{1}{6}}}{(1+(\frac{0.492}{Pr})^{\frac{9}{16}})^{\frac{8}{27}}})^2 \quad (14.)$$

2.12.1.4. Absorbed solar radiation

The solar radiation hitting the top glass cover, bottom glass cover and lastly the PCM are given in Equations 15-17:

$$G_{g1} = I(t)(\alpha_{g1} + \tau_{g1}\alpha_{g1}\rho_{g1}) \quad (15.)$$

$$G_{g2} = I(t)\tau_{g1}(\alpha_{g2} + \alpha_{g2}\rho_{g2}\rho_{g1} + \tau_{g2}\alpha_{g2}\rho_{PCM}) \quad (16.)$$

$$G_{PCM} = I(t)\tau_{g1}\tau_{g2}(\alpha_{PCM} + \alpha_{PCM}\rho_{g2}\rho_{PCM}) \quad (17.)$$

The system of equations was solved using the lsode function for solving differential equations in Octave.

2.12.2. Stefan problem (moving phase boundary)

Yi *et al* (2012) states some problems with modeling Stefan problems, especially when considering radiative effects in semitransparent PCMs:

- The phase interface moves, while the control volumes are set. This causes errors when the interface does not land exactly on the control volume interface. This error can be reduced by choosing smaller control volumes.
- The radiative properties of the PCM changes with both time and space, and is significant.

Yi *et al* (2012) gives the three methods that can be used to solve Stefan problems (for heat conduction) as:

1. Enthalpy
2. Moving mesh
3. Fixed grid front tracking

Yi *et al* (2012) looked at phase change problems in semitransparent media (like PCMs used in TES systems) and found that they not only use conduction but the combination of transient heat transfer using conduction, convection and radiation. They found that because of their complexity these phase change problems in semitransparent media cannot be efficiently solved by most numerical methods (finite volume method, finite element method, discrete transfer method). Most models only consider the change in thermophysical properties but assumed that the radiative properties are constant. They found that this assumption will lead to large errors if it is used in semitransparent PCMs.

The melting process as defined by Agyenim *et al* (2010) is:

1. Only conduction heat transfer as the PCM heats up (sensible heat)
2. Heat conduction between the boundary wall to the PCM and the solid-liquid interface
3. As the amount of melted PCM increases there is a transition from conduction to natural convection.
4. Purely convective regime, PCM is almost entirely liquid and due to the buoyancy effect the liquid core temperature distribution does not depend on time, but rather on height and depth.

The model:

The phase change or Stefan problem was solved using the method suggested by Date (1992), using the control volume as shown in Figure

2-17. Their proposed method produced nonwavy temperature and heat flux histories, regardless of the initial and boundary conditions, interface velocity, Stefan number, Biot number or the time step. Their method also allows for line-by-line integration of the finite-difference equations, easy tracking of the interface boundary, possible extension to multidimensional problems and requires a fewer amount of nodes.

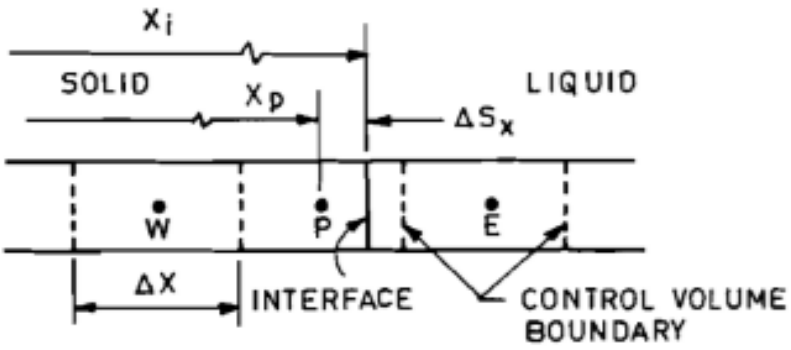

Figure 2-17: A typical phase change node P and the control volume as used by (Date, 1992)

Assumptions:

- Liquid phase is assumed to be stagnant (no convection)
- One dimensional
- No bulk convection
- Uniform properties
- No radiation heat transfer

In this model the enthalpy, rather than the temperature is used as the main dependent variable. The energy equation for the solid and liquid phase is then written as:

$$\frac{\partial}{\partial \tau}(\rho H) = div(K\ grad\ T) \qquad (18.)$$

With the stated assumptions the equation can then be written as:

$$\rho \frac{\partial}{\partial \tau}(H) = K \frac{\partial^2 T}{\partial x^2} \quad (19.)$$

The following dimensionless variables are defined:

Dimensionless enthalpy:

$$\phi = \frac{H - H_s}{\lambda} \quad (20.)$$

Dimensionless temperature:

$$\theta = \frac{C_p(T - T_m)}{\lambda} \quad (21.)$$

Dimensionless distance:

$$X = \frac{x}{L} \quad (22.)$$

Dimensionless time:

$$\tau = \frac{\alpha t}{L^2} \quad (23.)$$

The equation then becomes:

$$\frac{\partial \phi}{\partial \tau} = \frac{\partial^2 \theta}{\partial X^2} \quad (24.)$$

With

$\theta = \phi$ for $\phi \leq 0$ (solid)

$\theta = 0$ for $0 \leq \phi \leq 1$ (phase change)

$\theta = \phi - 1$ for $\phi \geq 1$ (liquid)

Which is generalized as:

$$\theta = \phi + \phi' \quad (25.)$$

With $\phi' = 0.5(|1-\phi| - |\phi| - 1)$

And with

$\phi' = 0$ in the solid phase

$\phi' = -\phi$ during phase change

$\phi' = -1$ in the liquid phase

But $\theta = \phi + \phi' = 0$ at the phase-change node, which means that the temperature of the entire node is held at T_m during phase change, this can lead to wavy temperature profiles. This creates wavy profiles when a coarse mesh is selected. To solve this Date (1992) refined θ, by separately calculating the nodal temperature for the phase-change node.

Theta is then further defined as

$$\theta = \phi + \phi'' \qquad (26.)$$

where $\phi'' = \phi' + \theta_{pc}$

The implicit finite difference equation is then:

$$\phi_j^n(1+2S) = S\left(\phi_{j+1}^n + \phi_{j-1}^n\right) + S\left(\phi_{j+1}^{\prime\prime n} - 2\phi_j^{\prime\prime n} + \phi_{j-1}^{\prime\prime n}\right) + \phi_j^0 \quad (27.)$$

The ϕ'' values lag behind by one iteration.

This equation is unconditionally stable according to the Scarborough criterion. Solving this equation using the tridiagonal matrix algorithm produces much faster convergence when compared to solving the equation point by point. The use of the tridiagonal matrix algorithm is also necessary in order to predict smooth heat flux and temperature histories (Date, 1992).

The equation was solved using the Thomas algorithm used for solving tridiagonal matrices. See Appendix A for additional information on the Thomas algorithm.

2.13. Conclusions

At present concentrated solar power (CSP) is the most economical viable way to produce large amounts of electricity from solar energy. The use of PCMs are preferred since they can store solar energy as latent heat and can be used to generate electricity even when there are periods of no solar radiation.

Carbon black shows excellent optical properties, absorbing solar radiation over a very wide wavelength and has been successfully used to enhance solar absorption in nanofluids. This proves that carbon black could potentially be used to make PCM composites for direct solar applications.

PCMs and carbon particle composites can be used in a CSP plant: their excellent thermal and optical properties could make the use of PCM composites viable as the direct solar absorber, the working fluid and the energy storage device, decreasing cost and increasing efficiency.

3. Experimental

3.1. Apparatus

The two main experiments were conducted to test the use of the PCM composite as a direct solar absorber. A small scale experiment was carried out first, followed by a larger (but still laboratory scale), more comprehensive experiment. The light source, PCM and carbon black used were the same in both these experiments.

3.1.1. Solar simulator/light source

The experiments were carried out using a very compact quartz metal halide lamp with single-pinch GX-22 lamp cap. The lamp is a Philips Master MHN-SE 2000W/956 GX22 400V HO lamp.

The lamp had a colour temperature of 5600 K while the effective surface temperature of the sun is approximately 6000 K (Duffie & Beckman, 2013: 210).

The relative energy distribution of different types of radiation for a clear sky is given in Figure 3-1. The photometric data of the lamp from the specification sheet is given in Figure 3-2, while the actual measured data using an Apogee PS-100 Spectroradiometer is given in Figure 3-3. The spectroradiometer's wavelength sensitivity range is 350 nm to 1000 nm. It can be seen that the lamp gives a good approximation of solar radiation, with most of the energy between 400 nm and 800 nm wavelengths.

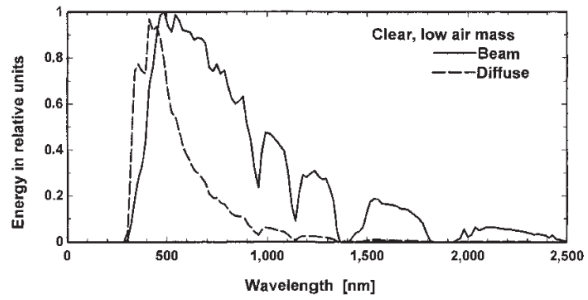

Figure 3-1: Energy distribution of solar radiation for a clear sky (Duffie & Beckman, 2013: 62).

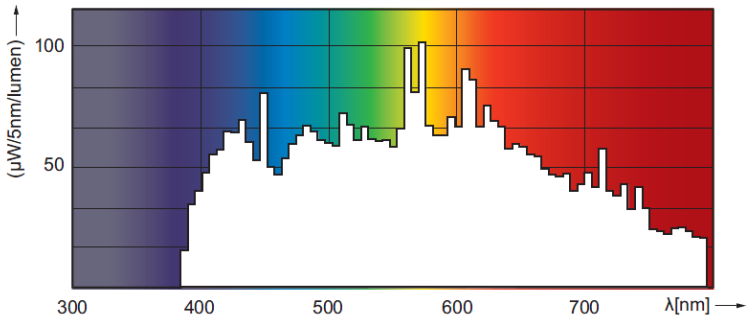

Figure 3-2: Photometric data of the lamp, obtained from the lamp's data sheet, showing the energy of the lamp at different wavelengths (Royal, 2013).

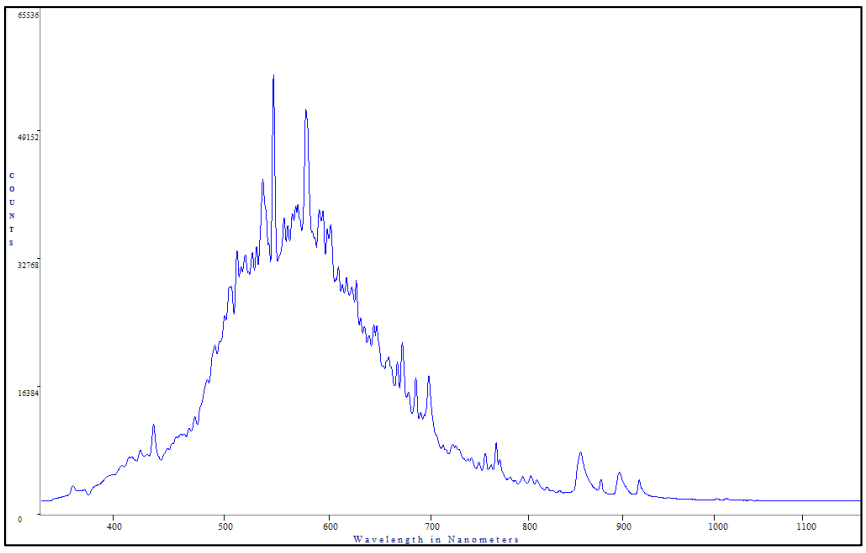

Figure 3-3: The measured visible to near infrared range spectroradiometer data of the lamp.

The total shortwave radiation of the lamp was measured using an Apogee MP-200 Pyranometer. The radiation was measured between 895 W/m^2 and 905 W/m^2 which is similar to the real solar data obtained from SAURAN, as discussed earlier.

3.1.2. PCM

The PCM was obtained from IOI Oleochemicals and is a fatty acid. The products name is Palmac 55-16 which contains a minimum of 94 % palmitic and stearic acid. The composition of the fatty acid (obtained from the manufacturer, using GLC) was given as:

- C12 = 1.0 % Maximum
- C14 = 2.0 % Maximum
- C16 = 52.0-56.0 %
- C18 = 42.0-47.0 %
- C18:1 = 0.5 % Maximum
- Others = 1.0 % Maximum

This product was made from only vegetables and was derived from palm oil or palm kernel oil.

The density of the PCM was measured as 0.9767 g/cm^3 with a standard deviation of 0.0015 g/cm^3. The latent heat of the PCM was measured as 186 J/g and the PCM has a melting point of around 55 °C.

3.1.3. Carbon black

The carbon black that was used for all of the experiments was 60 micron corax N660.

Carbon black with a particle size of 60 µm was used, because this particle size is in the range of the carbon blacks Smith *et al* (2016) found from recycled car tyres, as discussed earlier.

3.1.4. Small scale experiments

The small scale experiments were designed to give an idea of the factors involved and especially the range of carbon black concentrations that needed further testing.

A small Tupperware container was filled with the PCM (or the PCM composite); a glass cover with a hole through it for a thermocouple was then placed on top of the container. The entire setup was then sealed using a silicone sealant. The top glass cover with the thermocouple hole in the middle is shown in Figure 3-4. The entire setup is shown in Figure 3-5.

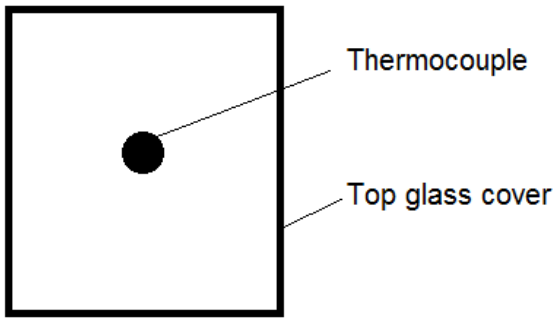

Figure 3-4: Glass cover that was added on top of the PCM container, showing the position of the thermocouple (top view).

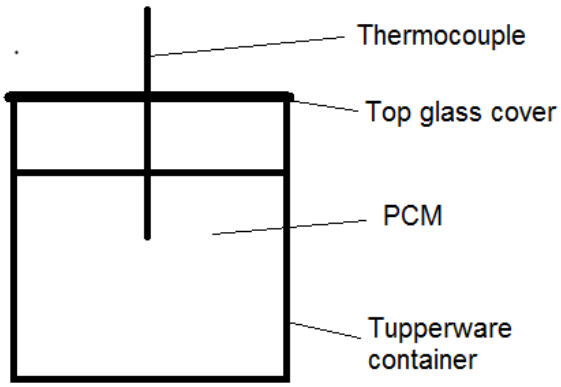

Figure 3-5: Small container filled with the PCM, showing the thermocouple and the sealed glass cover at the top (side view).

3.1.5. Large scale experiments

The design of the solar oven is given in Figure 3-6. This solar oven was then put under the solar simulator in a small room with a fan; the temperature of the room would slightly heat up over the course of the experiment.

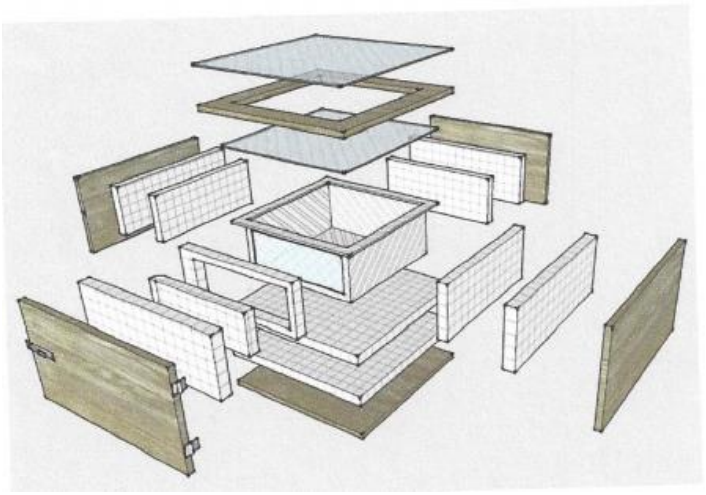

Figure 3-6: Expanded view of the solar box.

The original design had some drawbacks: more thermocouples were needed inside the PCM and it took too long to completely heat or cool all of the PCM inside the oven. Consequently modifications were made to the original design, firstly four thermocouples were added as seen in Figure 3-7 and Figure 3-8, and secondly a heating/cooling coil was added at the bottom of the solar simulator as seen in Figure 3-9.

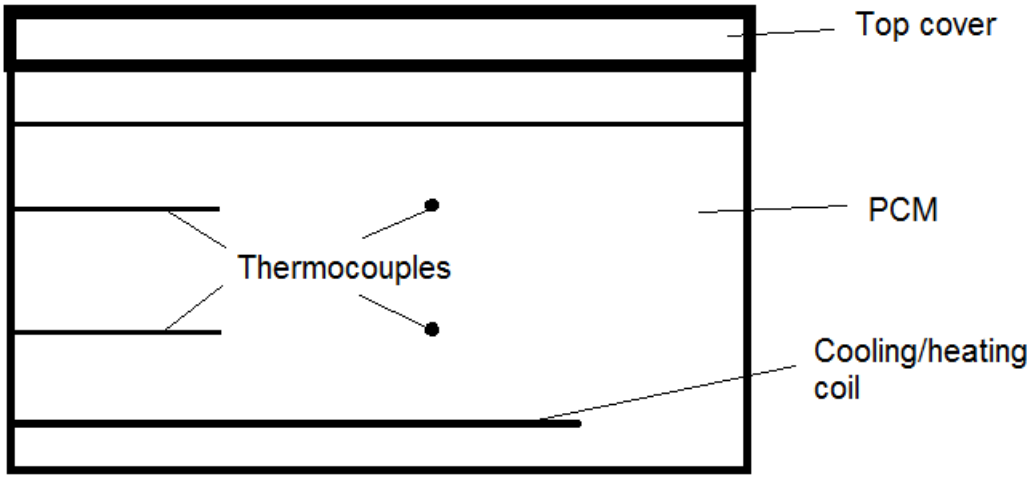

Figure 3-7: Side view of the solar box, showing the four thermocouples and the heating/cooling coil. The top thermocouples was 2 cm below the top of the PCM, while the bottom thermocouples were 9 cm below the top of the PCM.

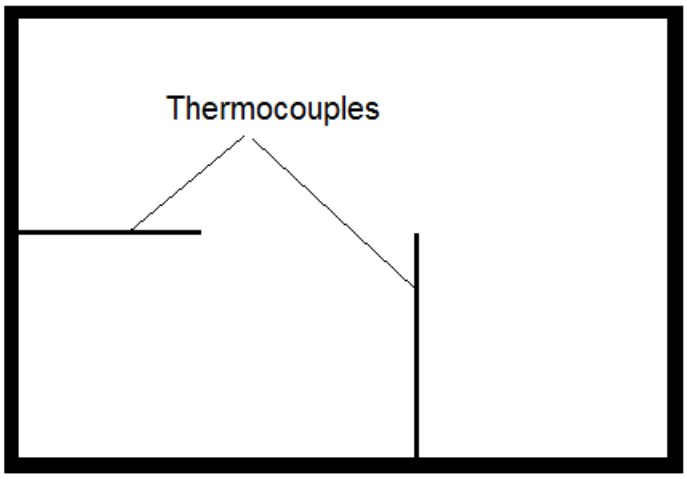

Figure 3-8: Top view of the solar box showing only the thermocouples.

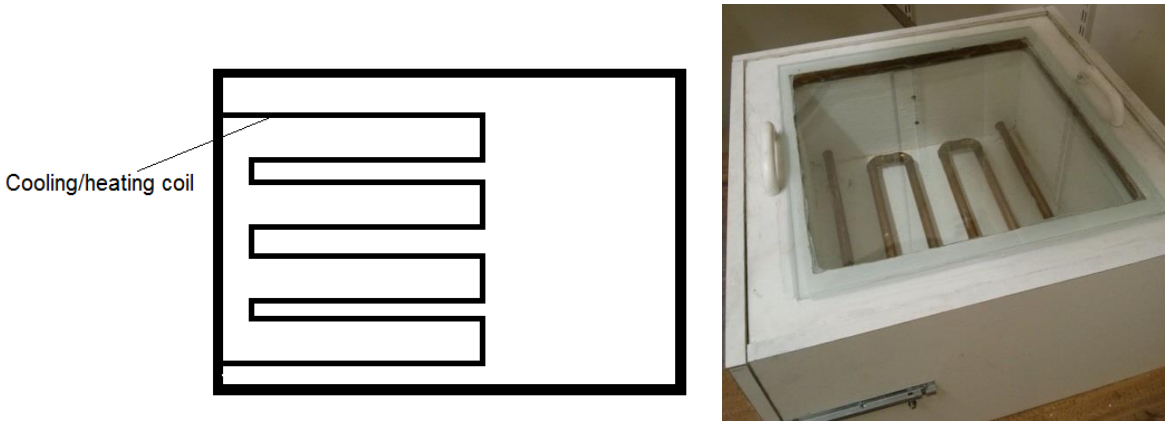

Figure 3-9: Top view of the solar box showing only the cooling/heating coil (left), with a photo of the solar box showing the cooling coil (right).

The coil was attached to a waterbath and used to heat/cool the PCM.

3.2. Planning

Independent variable:

The concentration of the carbon black: a small scale experiment was first conducted to narrow down the range of carbon blacks loadings that needed to be tested, very low concentration carbon black showed the most potential, with good dispersion and temperature increases. The dispersion of the carbon black and the effect that the carbon black has on the temperature increase of the PCM were studied.

Dependent (measured) variables: The temperature of the PCM and the photos showing the dispersion.

Background variables: Ambient temperature

Experimental design:

The pure PCM was first tested for multiple cycles to ensure that the changes observed are not due to the PCM itself changing over multiple cycles. Organic PCMs were chosen because of their stability over many cycles, (Sarı *et al*, 2004) concluded that the thermal properties of lauric

acid, stearic acid, myristic acid, palmitic acid and palmitic acid/stearic acid eutectic mixtures were stable over 360 repeated melt/freeze cycles. The changes observed are therefore only because of the change in the carbon black loading and not because of a change in the properties of the PCM over multiple cycles.

Many runs to show repeatability, the longest run was more accurate since the temperature of each run at the start was different and it therefore had more data to compare (longer time).

The melting front is somewhat unpredictable for multiple runs and has a big influence on the temperature values that are measured. To test for this, temperature measurements were taken at different heights and at different areas at the same height. The experiments were also run for a long enough time that the melting front moved well past the thermocouples. Some of the temperature measurements were also taken at a height that was close to the top of the PCM to ensure that the melting front was well past this point at the end of the experiment so that the effects of this variable melting front were lessened.

Running the experiment for more than 5 hours each time also meant that any variability in the light source would be evened out.

A glass side panel was added to the experiment so that the dispersion and the melting front of the PCM could be viewed (as well as the top glass cover showing the top of the PCM). The most important parameters were therefore the temperature at various positions (measured by the thermocouples) as well as the dispersion (seen through the glass window/photos).

Photos of the sample from the top view and the side view, through the glass were taken. To further analyse the appearance of the PCM, samples were taken of each run and put into test tubes to compare to each other.

The same PCM and carbon black was used in all of the experiments to cancel out any errors

3.3. Method

3.3.1. Small scale experiments

The PCM was melted on a hot plate at 60 ^{0}C, the carbon black was then added and magnetically stirred at 600 rpm for 20 minutes. This PCM composite was then added to the container and the thermocouple was inserted in the middle of the liquid PCM composite. After the PCM composite solidified, the rig was sealed with a silicone sealant. The light source was switched on for 5 minutes to start up, then the container was put directly beneath the light source and the PCM's temperature was continuously measured.

3.3.2. Large scale experiments

12 kg of PCM was added to the rig and melted under the lamp, to add carbon black a liquid sample was taken from the rig. The carbon black was then added to the sample and stirred on a magnetic stirrer at 600 rpm for 20 minutes. This mixture was then added back to the liquid PCM in the solar box and stirred. The solar box was then left to cool/solidify. The solar box was then put under the light source and the temperatures at four different places were continuously measured.

The heating/cooling coil (attached to a waterbath) was used to ensure that all of the PCM had melted before adding more carbon black and as a cooling coil to make sure that the PCM had solidified and cooled down before the next run was started.

3.4. Auxiliary experiments

3.4.1. Thermal energy storage capacity (rate of charge/discharge)

A setup similar to that of Zhang & Fang (2006) was used.

A series of glass test tubes were filled with 7 g of pure PCM or a PCM composite. The various PCM composites were prepared in the same way as those used in the other experiments (20 minutes on a magnetic stirrer). These test tubes were then subsequently put into waterbaths at 29 ^{0}C and 65 ^{0}C respectively, while they performed energy storage or energy discharge and their temperatures were recorded.

3.4.2. Transmittance/absorbance characteristics

Novel Solar Simulator experiment:

The solar simulator was used as the light source and the amount of shortwave radiation passing through a certain amount of liquid PCM or PCM composite was measured using an Apogee MP-200 Pyranometer. A setup was created where the light had to pass through a 100 mL glass beaker (that was insulated to reduce/eliminate the amount of radiation that would enter from the surroundings) to hit the pyranometer sensor located beneath it. The beaker was then filled up to varying depth with melted PCM and the radiation coming through to the bottom was measured.

Novel UV-vis experiment:

To get a more detailed picture of the transmittance/absorbance of the PCM composite a novel UV-vis setup was used. A stable LED light bulb was used as the light source and the samples were put into standard 1 cm path length cuvettes. The various PCM composites were prepared in the same way as those used in the other experiments (20 minutes on a magnetic stirrer).

The light source and cuvettes were then put into a box with insulation to block out stray radiation. The cuvettes were surrounded by extra insulation so that the light goes from the light source passes through only the cuvette and hits the sensor behind the cuvette. An Apogee PS-100 Spectroradiometer was used to measure the photometric and the radiometric data. The setup is shown in Figure 3-10 and Figure 3-11.

Figure 3-10: Side view of the setup used in the novel UV-vis experiment, with the light source on the left and part of the spectroradiometer, sticking out of the insulated box, on the right.

Figure 3-11: Top view of the setup used in the novel UV-vis experiment, with some of the insulation, and the LED bulb visible on the left.

Light spectra

To get a Beer-Lambert law relationship, two specific wavelengths were chosen. There are two peaks in the relative strength of the light, at around 450 nm and 550 nm as seen in Figure 3-12. The light is strongest at the peaks, these two wavelengths were therefore chosen to analyse the samples transmission and absorption.

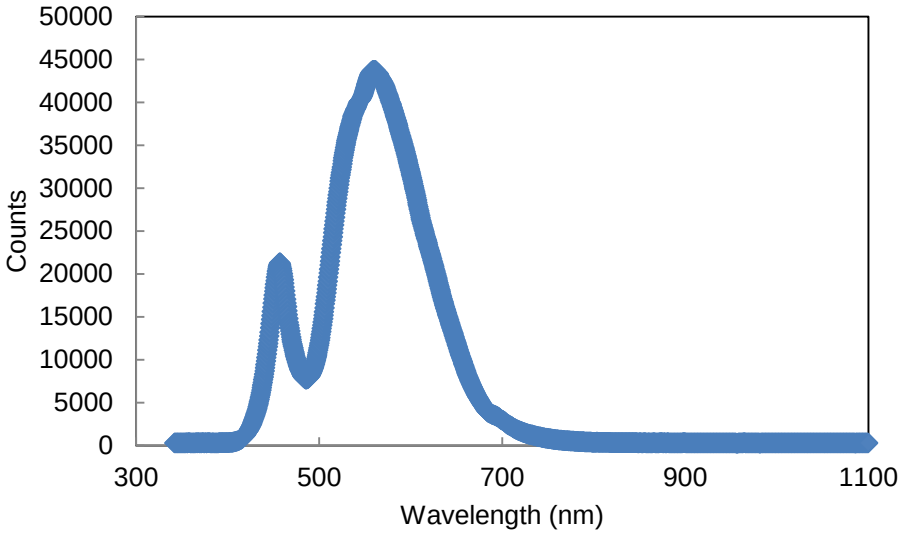

Figure 3-12: Measured spectra of the light, showing the relative strength for certain wavelengths.

3.4.3. Differential scanning calorimetry (DSC)

Various PCM and PCM composites (0 % carbon black to 8 % carbon black) were analysed in a DSC using the dynamic method and sealed aluminium pans.

The various PCM composites were prepared in the same way as those used in the other experiments (20 minutes on a magnetic stirrer). The following procedure was followed using Nitrogen gas (50.0 mL/min):

- Hold for 1.0 min at 30.00 °C

- Heat from 30.00 °C to 100.00 °C at 5.00 °C/min
- Hold for 1.0 min at 100.00 °C
- Cool from 100.00 °C to 30.00 °C at 5.00 °C/min
- Hold for 1.0 min at 30.00 °C
- Heat from 30.00 °C to 100.00 °C at 5.00 °C/min

To test the stability of the PCM and PCM composites (0 % carbon black to 1 % carbon black) multiple melting and freezing cycles were run. The procedure for these tests, using Nitrogen gas (50.0 mL/min), is given below:

- Heat from 30.00 °C to 80.00 °C at 10.00 °C/min
- Cool from 80.00 °C to 30.00 °C at 10.00 °C/min
- Heat from 30.00 °C to 80.00 °C at 5.00 °C/min
- Cool from 80.00 °C to 30.00 °C at 5.00 °C/min
- Heat from 30.00 °C to 80.00 °C at 10.00 °C/min
- Cool from 80.00 °C to 30.00 °C at 10.00 °C/min
- Repeat the last two steps for a total of 100 cycles (200 steps)
- Heat from 30.00 °C to 80.00 °C at 10.00 °C/min
- Cool from 80.00 °C to 30.00 °C at 10.00 °C/min
- Heat from 30.00 °C to 80.00 °C at 5.00 °C/min
- Cool from 80.00 °C to 30.00 °C at 5.00 °C/min

As seen in the procedure, to start off with the sample was quickly heated and cooled down again to erase the thermal history, after that the sample was then heated and cooled slower to get more accurate data. 100 of the faster cycles were then run before finally being melted and cooled at the slower pace again. The data from the two slower runs were then compared to see the stability of the PCM or PCM composite.

3.4.4. Settling experiments

Composite carbon black and PCM samples (0 % to 4 % carbon black) were prepared using the same procedure and the same materials as the small and large scale experiments (mixed on a magnetic stirrer at medium intensity for 20 minutes).

These liquid samples were then put into standard 1 cm path length cuvettes and their transmittance/absorbance data was recorded while they solidified. After they solidified they were put into an oven and kept at 65 °C for 14 days (in liquid form for the entire duration), taking new photos of them every day.

3.4.5. Density

The absolute density of the PCM and the carbon black was measured using a pycnometer, with Helium as the analysis gas, 5 purges and an equilibrium rate of 0.050 psig/min.

3.4.6. SEM

The surface of the carbon black was investigated to see the topography and to get an idea of the sizes of the carbon black agglomerates and aggregates.

Scanning electron microscope (SEM) micrographs were obtained using an ultra-high-resolution field-emission microscope (Zeiss Ultra Plus 55 FEGSEM) equipped with an in-lens detection system and operated at an acceleration voltage of 1 kV. A working distance of between 2 mm and 3 mm was used. The powder was lightly deposited on carbon tape and examined without any additional sample preparation.

4. Results and Discussion

4.1. Small scale experiments

In this section the ability of the PCM/PCM composite to absorb the radiation from the solar simulator was investigated. The stability of the PCM composite was also studied and potential problems were explored, before starting with the more comprehensive experiments.

4.1.1. Repeatability of small scale experiments

Figure 4-1 shows the temperature profile of the PCM with no carbon black, it increases to around 55 ^{0}C (sensible heat part) then stays constant as the PCM melts, absorbing the energy as latent heat. This melting temperature of 55 ^{0}C is in good agreement with that found using DSC. At the end of the experiment no all of the PCM has melted and the PCM is still using some of the heat/radiation for phase change.

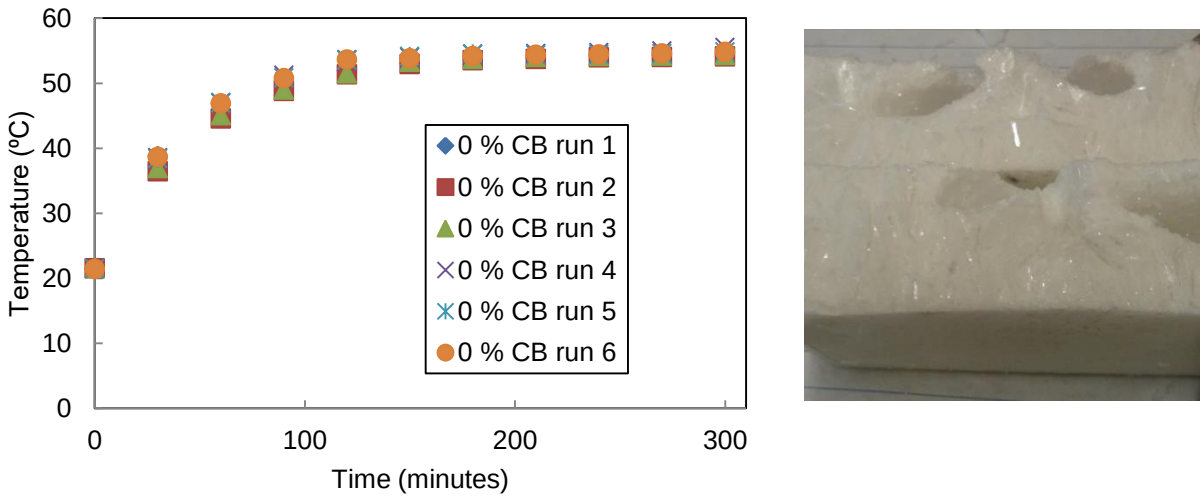

Figure 4-1: Multiple pure PCM runs are very similar showing very good repeatability for multiple phase change cycles (left). A photo of the pure PCM broken in half (right).

This stability over multiple cycles is one of the advantages of this organic based PCM. The air gaps in the solid PCM, as seen in Figure 4-1 is due to the difference in the solid and liquid density of the PCM.

Figure 4-2 shows that when the PCM and carbon black is well mixed at the start that there is almost no deviation in the results of multiple experiments and the runs are repeatable, with good carbon black dispersion.

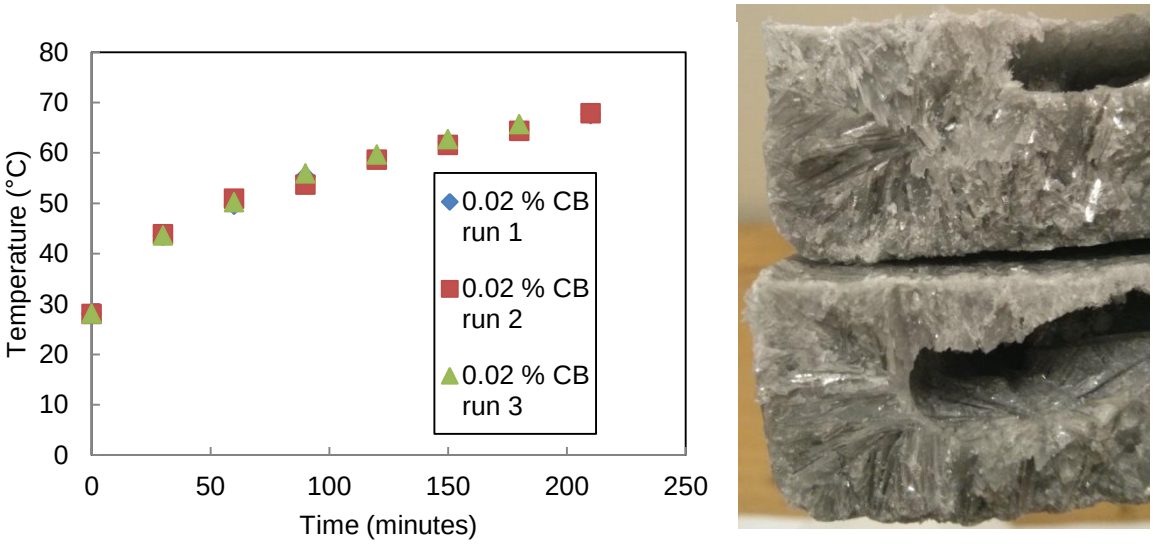

Figure 4-2: Temperature profile for three runs with 0.02 % carbon black (left). Photo of 0.02 % carbon black PCM after the third run (right).

Similarly Figure 4-3 to Figure 4-6 show that multiple runs (at low carbon black loadings) are repeatable, that the carbon black has not settled out and that it does not require additional stirring to ensure good dispersion

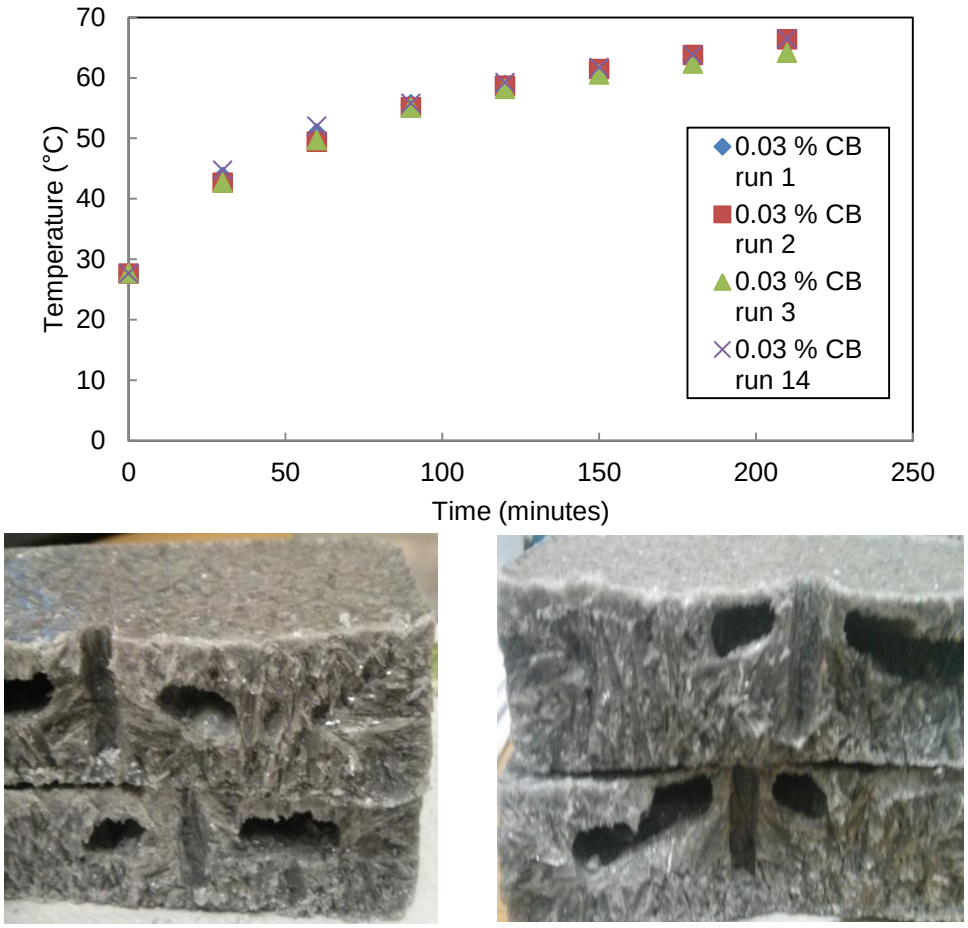

Figure 4-3: Temperature profile for 0.03 % carbon black loadings (top) showing almost no deviation. Photo of the 0.03 % carbon black after the first run (bottom left) and after 4 runs (bottom right).

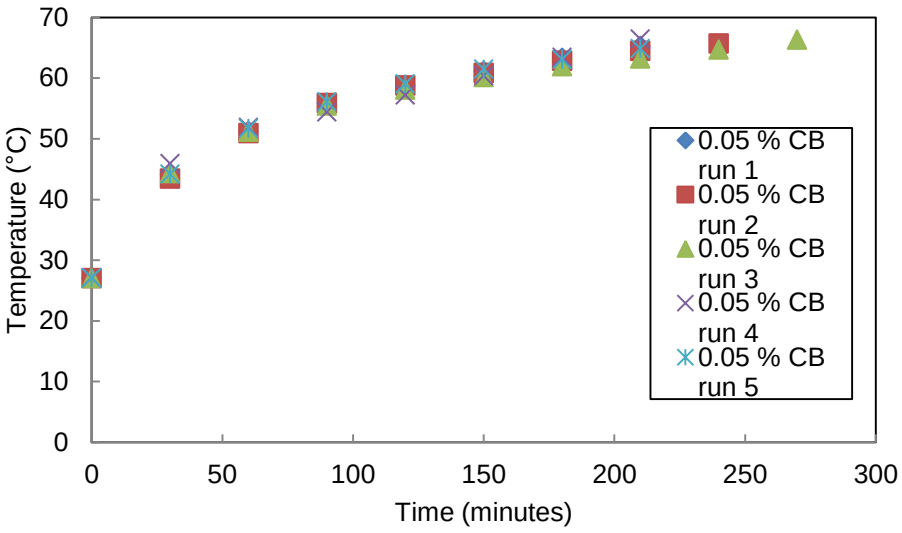

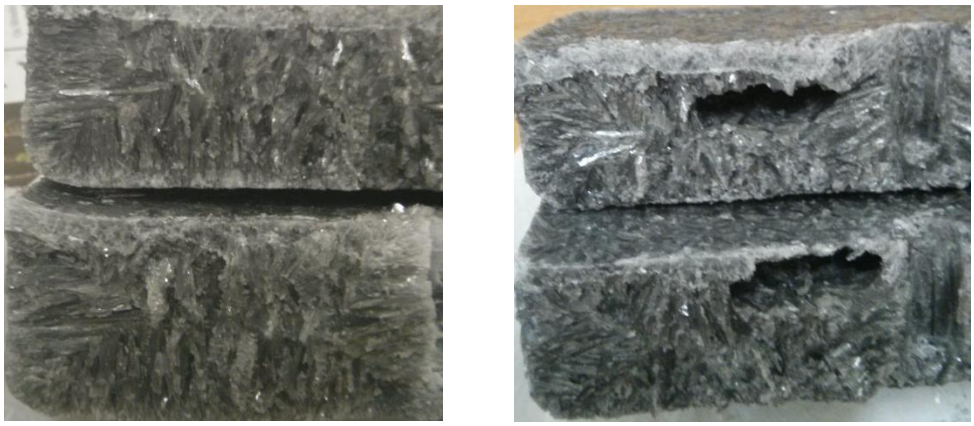

Figure 4-4: Temperature profile for 0.05 % carbon black loadings (top) showing almost no deviation. Photo of the 0.05 % carbon black after the first run (bottom left) and after 5 runs (bottom right).

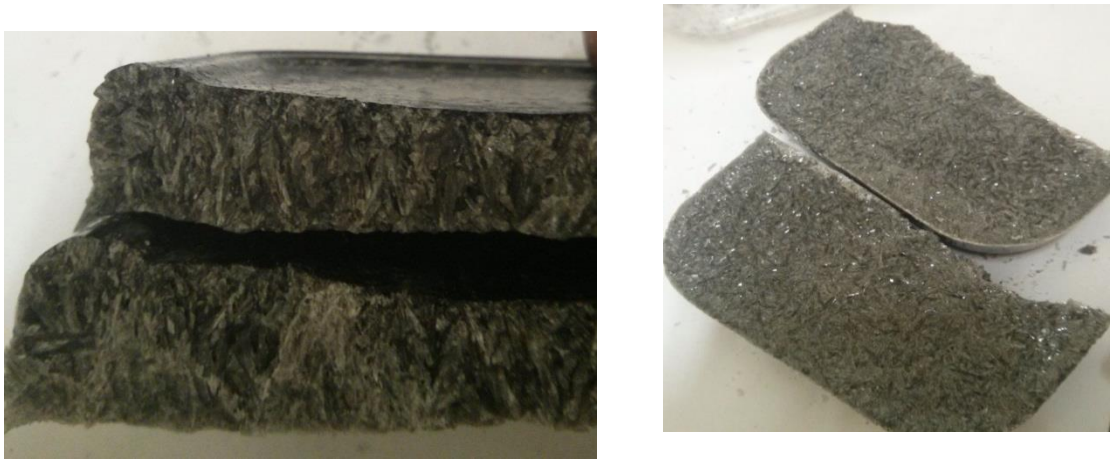

Figure 4-5: 0.1 % carbon black loading side view (left) and top view (right).

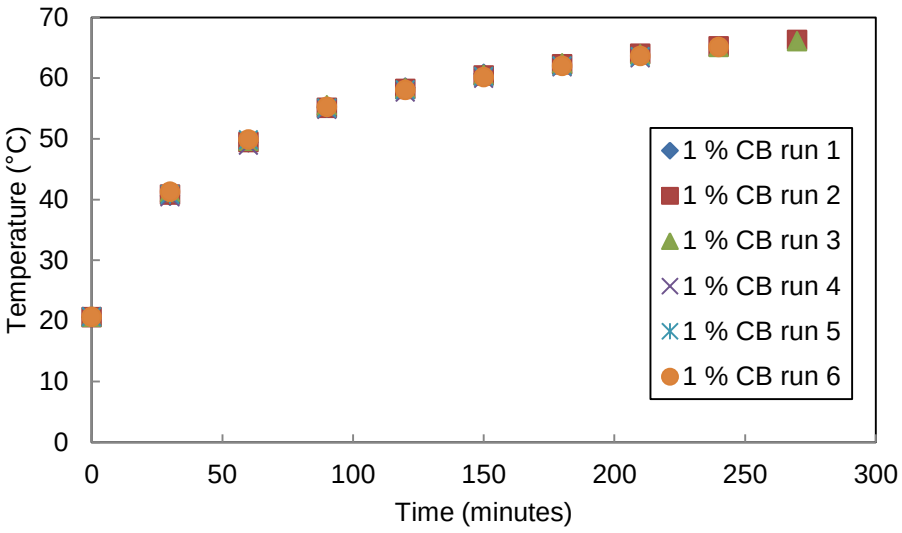

Figure 4-6: Temperature profile of multiple experiments with 1 % carbon black, showing almost identical melting times. The maximum standard deviation for the 1 % carbon black runs over 5 hours was 0.46 ^{0}C.

Additional temperature profiles of the PCM with 1 % added carbon black can be seen in Figure 4-7. The experiment was run for a certain amount of time, before the light source was switched off and the PCM was then allowed to cool down. This was to get an idea of the time that would be needed to cool down the PCM at different temperatures, which would help with the design of the more comprehensive large scale experiments.

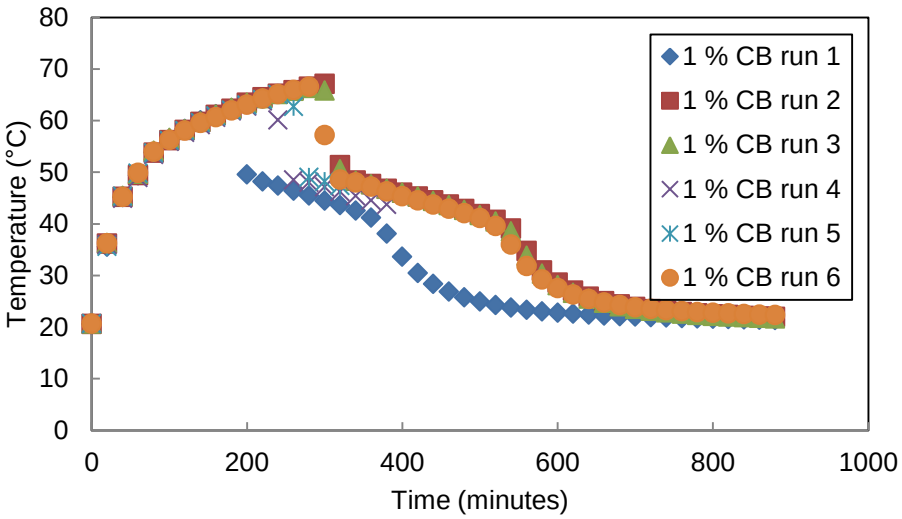

Figure 4-7: The heating and cooling of various 1 % carbon black runs (top). The 1 % carbon black is shown in liquid form (bottom left) and solid form (bottom right).

The temperature rises slowly and then has a quick drop as the light is switched off. There are three different regions:

1. The radiation heat transfer increases the temperature of the PCM and starts to melt the solid PCM.
2. The light source is then switched off and the liquid PCM temperature quickly drops and then cools down to around 45 ^{0}C.
3. In the last phase the liquid PCM has completely solidified and this solid PCM cools down to room temperature. The cooling time is very

long even though a relatively small amount of PCM was used. This can be explained by the very small thermal conductivity of the PCM and is a major drawback in the use of PCMs.

4.1.2. Carbon black dispersion at high concentrations

There is a large amount of settling out at high carbon black concentrations. Figure 4-8 shows an 8 % carbon black composite that was stirred when the carbon black was added and then left to solidify without further agitation, compared to an 8 % composite that was left on a magnetic stirrer to solidify. The 8 % composite that was left on the magnetic stirrer showed much better dispersion, but because of the large amount of carbon black its texture was more flaky/powdery compared to the waxy texture of the normal PCM.

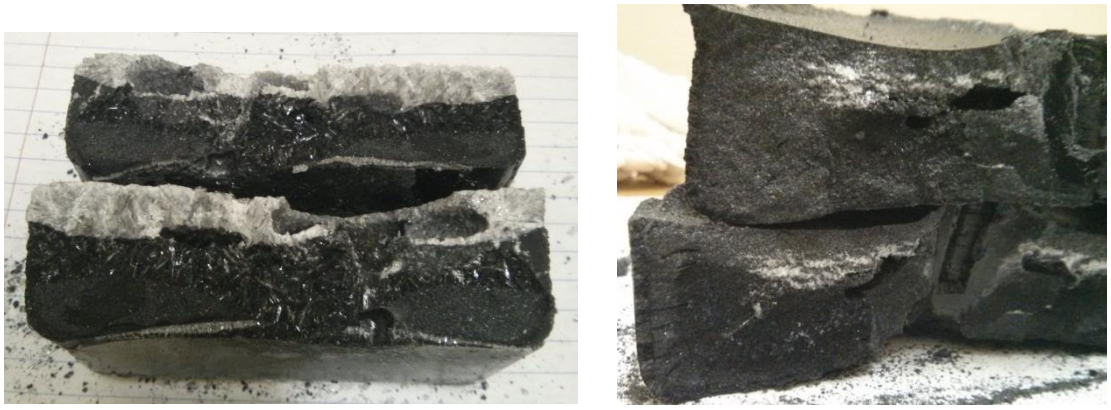

Figure 4-8: PCM with 8 % carbon black when only stirred at the start (left) and when continually stirred on a magnetic stirrer while solidifying (right).

4.1.3. Radiation absorption improvement

The temperature of the PCM increases faster when carbon black is added. The temperature difference between each run and the pure PCM run can be seen in Figure 4-9. 0.04 % Carbon black loading showed the largest

temperature difference, with the PCM composite 16 ^{0}C hotter than the pure PCM after 150 minutes. 0.01 % Carbon black had the highest temperature difference after 200 minutes with a value of 16 ^{0}C (note that the 0.04 % carbon black experiment did not go up to 200 minutes).

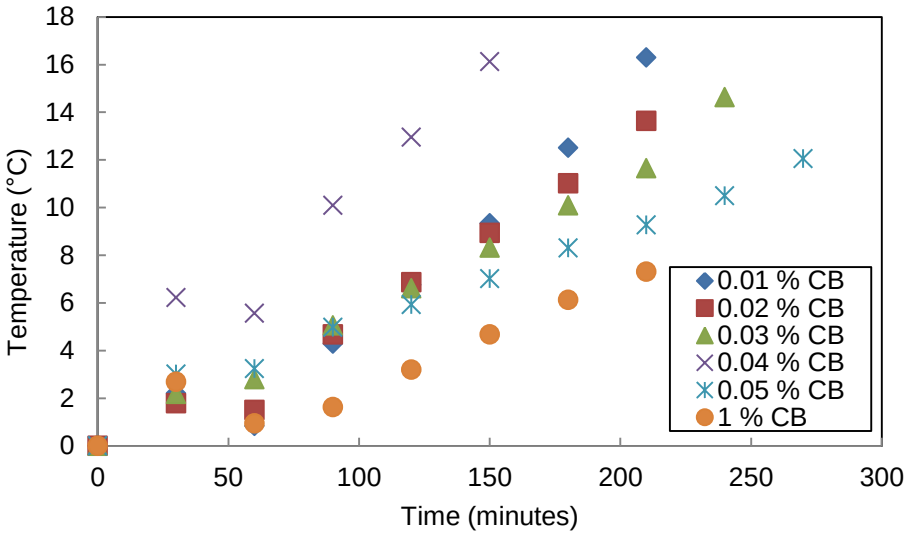

Figure 4-9: The temperature difference between each run and the pure PCM is shown.

The observed trend is that the lower the percentage carbon black (but still above 0 %) the higher its temperature is at a given time. The 0.04 % carbon black and the 8 % carbon black experiment however do not follow this trend, showing faster temperature increases. This shows that there are multiple factors affecting the optimal carbon black loading in the PCM.

Figure 4-10 shows the time it took each experiment to reach 60 ^{0}C, the time to reach 60 ^{0}C slowly increased with an increase in carbon black, except for the 0.04 % run which only took 85 minutes to reach 60 ^{0}C.

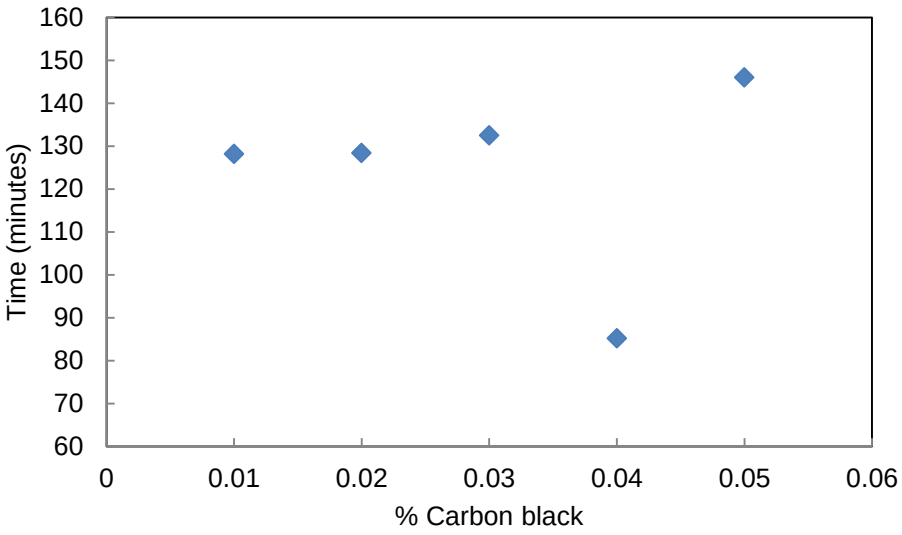

Figure 4-10: The time it took various carbon black loadings to reach 60 ^{0}C. The PCM with no carbon black was tested for 300 minutes but had not reached 60 ^{0}C by that time.

The small scale experiment provided the following information to take into account when doing the more comprehensive experiment:

- A very small amount of carbon black is needed to enhance the absorption of radiation.
- Simply increasing the carbon black loading does not uniformly increase the effectiveness of the PCM composite. The excellent radiation absorption properties of carbon black is being counteracted by another factor which decreases the PCM composite's efficiency as the carbon black concentration is increased.
- The low carbon black loadings (which gave the best radiation absorption properties) are easily dispersed in the PCM and do not require frequent stirring to ensure that it does not settle out after multiple runs.
- The cooling times of the PCM and the PCM composite are very long and the carbon black does not appear to offer meaningful enhancements to the thermal conductivity of the PCM composite.

- There are multiple factors affecting the optimal carbon black loading and the values of the temperatures at various depths inside the PCM are needed.

4.2. Large scale experiments

The position of the thermocouples in the large scale experiment is given in Figure 4-11.

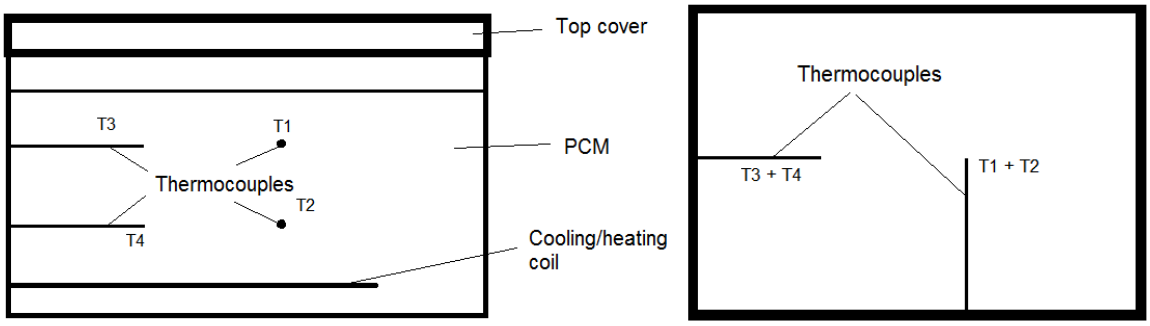

Figure 4-11: The side view (left) of the large scale rig and the top view (right) showing the positions of the thermocouples where the temperature data was recorded (T1 to T4). The thermocouples T1 and T3 were around two cm below the top of the PCM and T2 and T4 were located nine cm below the top of the PCM.

4.2.1 Radiation absorption improvement

The most important aspect of the PCM composite is its ability to absorb the incoming solar radiation, storing this energy as latent and sensible heat. In this section different carbon black loadings are compared in order to find the optimal carbon black concentration.

Figure 4-12 shows the change in colour of all of the carbon black concentrations tested. Starting at around 0.5 % carbon black (bottom row) there is hardly any visible change in colour with an increase in carbon black loading.

Figure 4-12: Solid samples of all of the large scale experimental runs (0 % carbon black to 6 % carbon black).

Figure 4-13 shows that a concentration of 0.06 % carbon black had the fastest increase in temperature of all the tested carbon black concentrations. Other low concentrations carbon black also showed good improvement (0.03 % to 0.08 % carbon black). The full run with all of the tested carbon black concentrations can be seen in Appendix E.

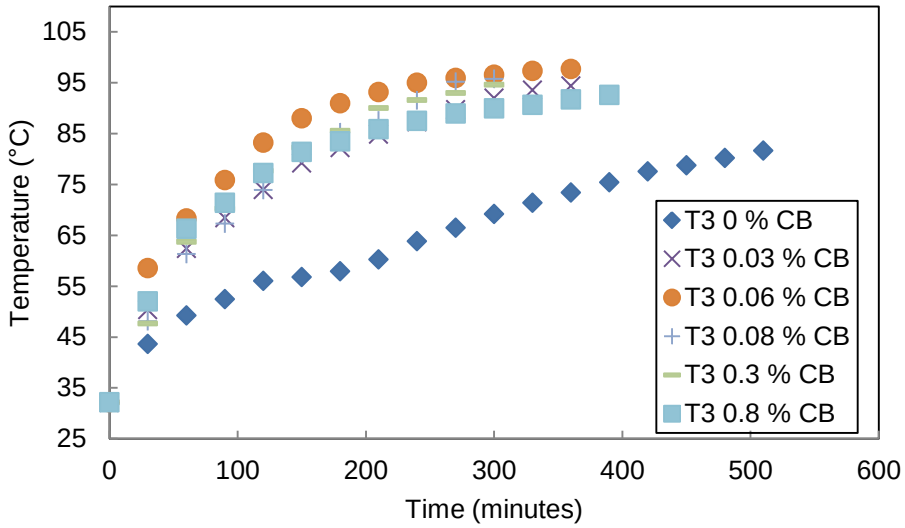

Figure 4-13: Temperature change over time of the PCM and PCM composites as measured by thermocouple 3.

The temperature did not uniformly increase with an increase in carbon black loading, but there is a trend showing that the temperature increased faster for the lower carbon black concentrations (but still more than 0 % carbon black).

Temperature 1 is measured at a level similar to Temperature 3, with a similar curve and can be seen in Appendix E.

Temperature 4 is the temperature measurement deeper inside the PCM. At this depth the lower concentrations carbon black performed even better than at the shallower depth, with four of the five best performers between 0.01 % and 0.08 % carbon black, as seen in Figure 4-14. The full run with all of the tested carbon black concentrations can be seen in Appendix E. Temperature 4 also has much more variability than the other runs, as seen and discussed in Figure 12-25 in Appendix E.

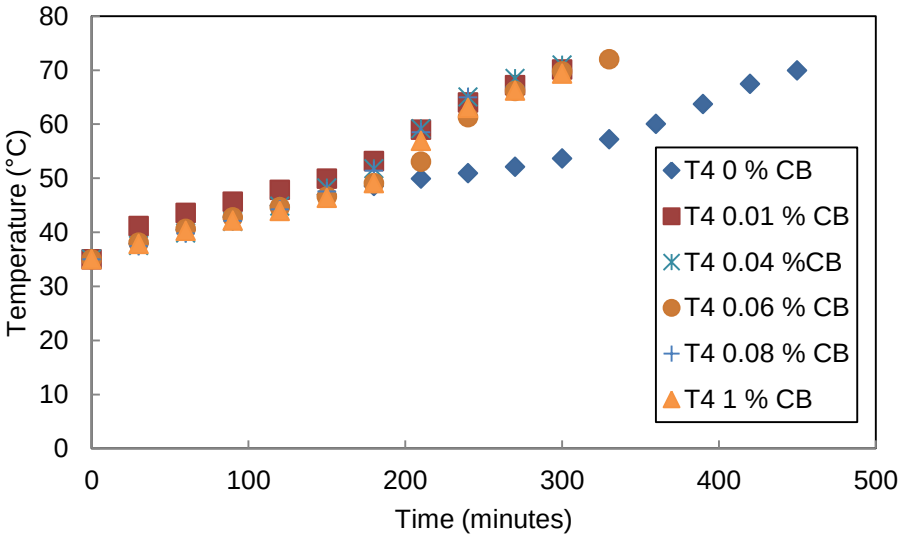

Figure 4-14: Temperature change over time of the PCM and PCM composites as measured by thermocouple 4.

The time it took the PCM to reach 65 ^{0}C is shown in Figure 4-15. The time to reach 65 ^{0}C evens out after 1 % carbon black, with only small variations. This means that once a certain saturation value is reached there is no more improvement with an increase in carbon black loading. These experiments show that similar to the small scale experiments there is a certain optimal concentration showing a much shorter heating time, for Temperature 1 and 3 this concentration is 0.06 %.

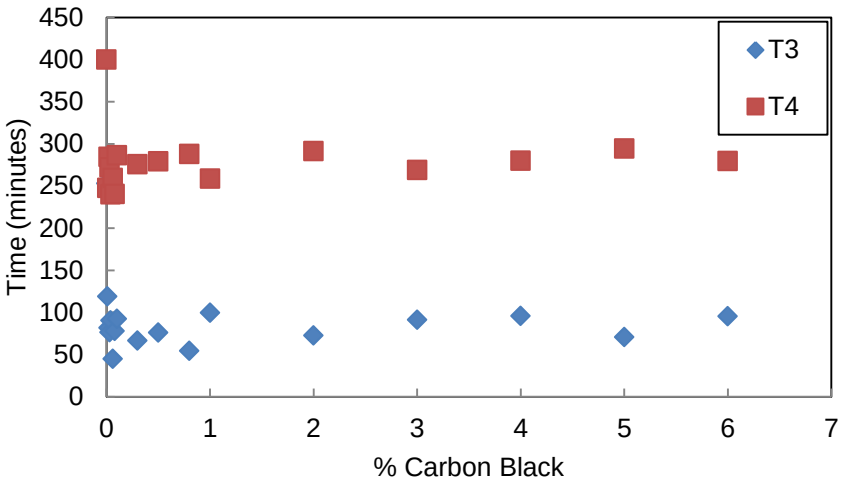

Figure 4-15: Time it took different thermocouple readings (and therefore different depths) to reach 65 ^{0}C at specific carbon black loadings. It took the pure PCM at T4 400 minutes to reach 65 ^{0}C while the pure PCM at T3 took 253 minutes.

The time it took Temperature 3 to reach 75 ^{0}C is shown in Figure 4-16. Figure 4-16 shows the same trend as the previous graphs, with a sharp decrease in heating time required and then eventually evening out to a constant value.

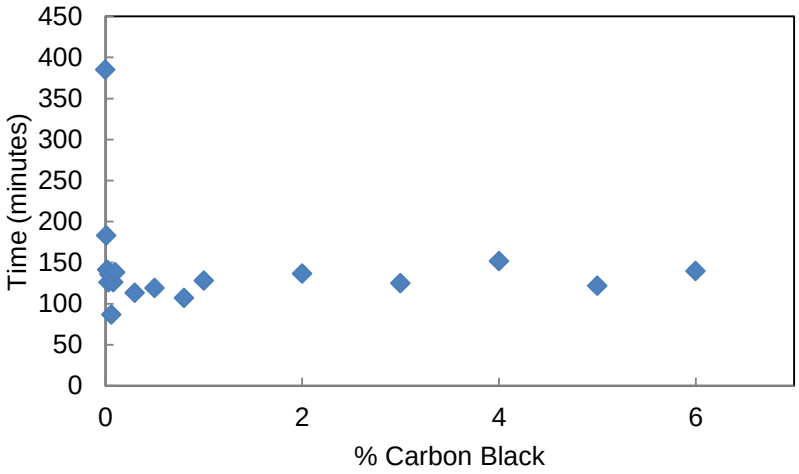

Figure 4-16: Time it took for Temperature 3 to reach 75 ^{0}C at specific carbon black loadings.

Figure 4-17 shows a closer look at the lower concentration carbon black runs of Figure 4-16. The time required to reach 75 ^{0}C goes down, reaches a minimum at 0.06 % carbon black and then goes back up.

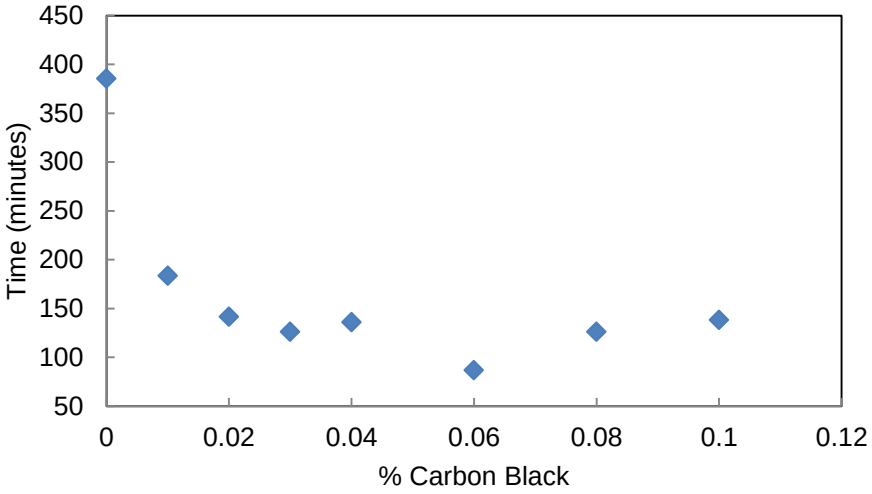

Figure 4-17: Time it took for Temperature 3 to reach 75 ^{0}C at specific carbon black loadings.

It took the pure PCM at thermocouple 3, 385 minutes to reach 75 ^{0}C, but it took the 0.06 % carbon black composite only 86 minutes (350 % faster). All of the tested PCM composites from 0.01 % to 6 % reached 75 ^{0}C in less than half the time it took the pure PCM.

The time it took Temperature 3 to reach 90 ^{0}C are similar to those of Figure 4-17 and can be seen in Appendix E.

Temperature 2 is the thermocouple reading furthest down inside the PCM and the time it took to reach 47 ^{0}C is shown in Figure 4-18. To reach this thermocouple heat must be transferred through radiation to the top of the PCM, convection through the liquid layer and conduction of heat through the solid PCM. There are also various other factors to consider, including the heat conduction to the PCM further down, the conduction to the outer walls and the internal radiation. All of these effects also change with the moving phase change boundary. The very low thermal conductivity of the

PCM also means that it takes a long time to see any of the changes, because of the slow temperature increase. All of the different factors affecting the temperature mean that it is much harder to find out exactly what causes the temperature differences seen in Figure 4-18.

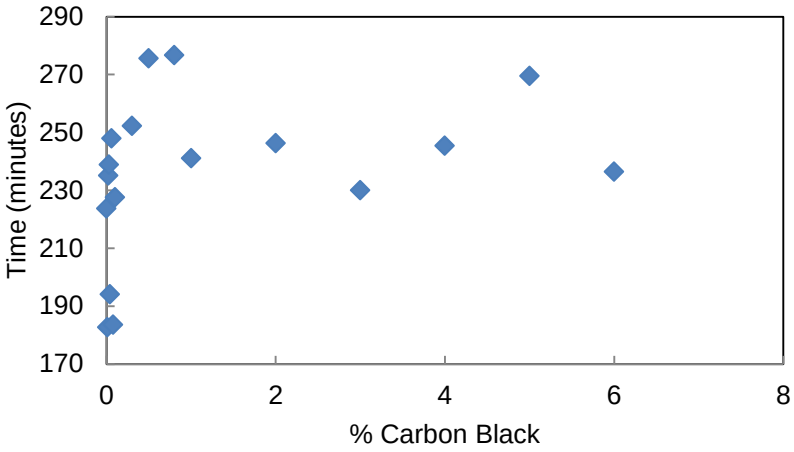

Figure 4-18: Time it took for Temperature 2 to reach 47 ^{0}C at specific carbon black loadings.

It took the pure PCM at thermocouple 2, 220 minutes to reach 47 ^{0}C, but it took the 0.01 % and 0.08 % carbon black composites only around 183 minutes (20 % faster).

Table 4-1 ranks each experiment after 4 hours, from the highest temperature to the lowest temperature. Temperature 3 is the temperature measurement taken at the top part of the PCM while Temperature 4 is taken deeper inside the PCM and therefore has a different optimal carbon black concentration.

Table 4-1: Temperature of the PCM after 4 hours for Temperature 3 and Temperature 4, ranked from the highest temperature (1) to the lowest temperature (17)

	% Carbon Black																
	0	0.01	0.02	0.03	0.04	0.06	0.08	0.1	0.3	0.5	0.8	1	2	3	4	5	6
T3	17	16	12	9	10	1	3	7	2	4	8	11	13	5	15	6	14
T4	17	3	9	7	1	5	2	15	13	12	11	4	14	6	10	16	8

Table 4-1 shows that the fastest increase in temperature for thermocouple number 3 is between 0.06 % carbon black and 0.5 % carbon black, while the fastest increase in temperature recorded by thermocouple number 4 is between 0.01 % carbon black and 0.08 % carbon black. This shows that the deeper the thermocouple is inside the PCM composite the lower the optimal carbon black concentration.

This downward shift in optimal carbon black concentration is due to the radiation being absorbed by the top part of the PCM and the reduction in the natural convective heat transfer of the PCM with an increase in carbon black loading. The natural convective heat transfer in the PCM plays a bigger role the further away you go from the radiation source.

The optimal carbon black concentration needs enough carbon black to absorb a large portion of the incoming radiation while also allowing some to pass through to heat up the un-melted PCM beneath the liquid level. At a height deeper inside the PCM the optimal carbon black concentration is lower. The deeper you go, the more radiation you need to pass through to hit the un-melted PCM beneath the moving liquid layer as opposed to having the radiation absorbed in the top liquid part.

The low percentages carbon black runs start off slower due to the solid PCM absorbing less radiation with lower percentages carbon black. As the PCM starts to melt, the properties change and there is a tradeoff between having a higher concentration carbon black to absorb the radiation, having the radiation go through to hit the un-melted PCM beneath the moving liquid layer and the influence of the carbon black on the natural convection and conduction. This shows that there is an optimal carbon black concentration dependent on the depth, size, orientation and heat transfer boundary conditions of the PCM.

Radiation is more efficient to add energy to the PCM compared to the heat transfer through convection, hence the trade-off.

(Taylor *et al*, 2011) found a similar result with the use of nanofluids to absorb solar radiation. If the concentration of the nanoparticles are too high most of the radiation will be absorbed by a thin layer on the surface which is easily lost to the environment and when the concentration of nanoparticles are too low the nanofluid does not absorb all of the incoming solar radiation. They further suggest that the optical properties of the nanofluid be precisely controlled so that the nanofluid operates optimally.

(Yi *et al*, 2012) also found a similar trade-off when the optical thickness of the PCM was changed: Phase change speed increases with the increasing of optical thickness with respect to absorption coefficient. When the optical thickness is increased to a certain point, the solidification heat transfer is dominated mainly by conduction, and consequently the phase change speed does not increase any more.

4.2.2. Repeatability of large scale experiments

Figure 4-19 shows the melted PCM (stearic/palmitic acid eutectic mixture with no carbon black) that was used in the large scale experiments; it had an almost clear, see-through colour.

Figure 4-19: Pure PCM in beaker (top left), in the large scale experiment top view (top right) and in the large scale experiment side view (bottom).

The data for the large scale experiment, showing the PCM with no carbon black can be seen in Figure 4-20. The runs showed comparable results with good repeatability.

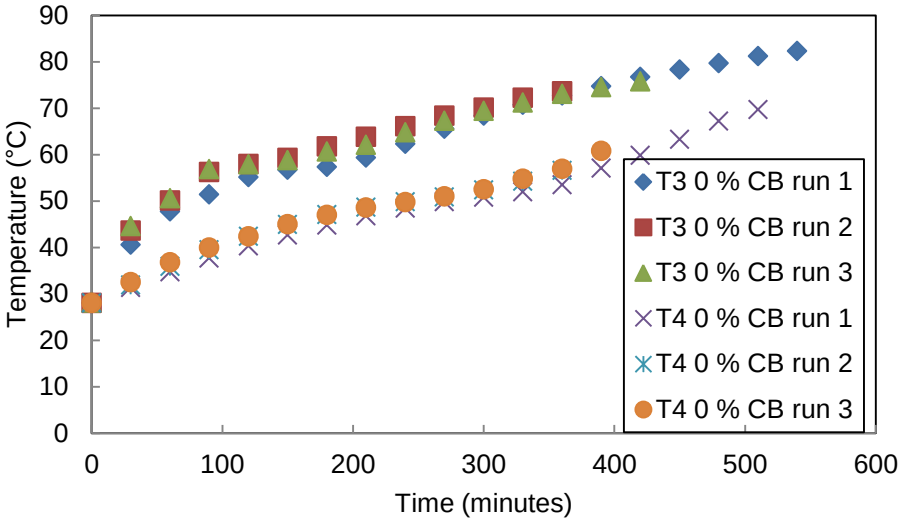

Figure 4-20: The temperature of the pure PCM experiment as recorded by Thermocouple 3 (T3) and Thermocouple 4 (T4) is shown.

There are large similarities when comparing Figure 4-20 with Figure 4-21 from Baran & Sari (2003), who also used a setup with an eutectic mixture

of palmitic acid and stearic acid. Baran & Sari (2003) used a PCM encased in a HTF pipe, the heat added by Baran & Sari (2003) was due to conduction with the HTF pipe, until a liquid layer formed in the PCM which then lead to the heat mainly being added by convection. Compared to our experiments where the heat was added due to the radiation from the lamp, followed by convection/conduction. The similarities of the two graphs show that the natural convective heat transfer inside the organic PCM is very important, independent of what type of heat transfer is present at the boundary.

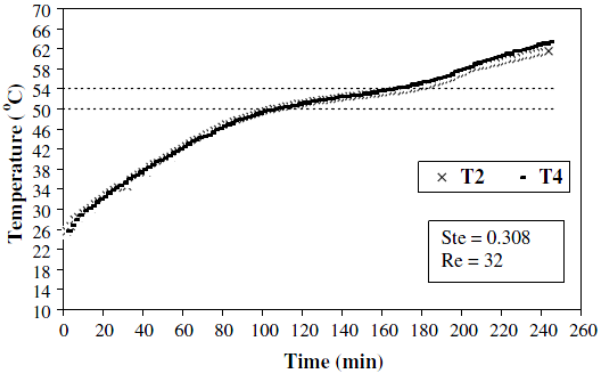

Figure 4-21: Temperature change over time of the stearic/palmitic acid PCM (Baran & Sari, 2003).

The melted PCM will move to the top of the rig while any solid PCM will go to the bottom, because the melted PCM has a lower density and viscosity. This is called the buoyance effect and enhances the natural convection heat transfer. This phenomena in palmitic acid/stearic acid eutectic compounds was discussed by Baran & Sari (2003) and found in various other PCMs (and other experimental configurations) by other researchers.

The graphs above do not clearly show the effect of the latent heat of fusion (flat graph at the melting temperature) because of the natural convection which is enhanced by the buoyance effects. There is a heat transfer to the

bottom of the PCM and a mass transfer of the melted PCM to the top. This was not observed in the small scale experiment because of its small size.

The transient temperature profile of the 0 % carbon black PCM and the other composite PCMs followed similar trends. At the start the radiation from the light source goes through the two glass covers and hits the top of the PCM. The heat transfer to the solid PCM at the start is almost exclusively through radiative heat transfer. The large amount of radiation being absorbed by the top PCM layer (especially for the experiments with carbon black added) causes the absorbing operation of the sensible heat to be quickly realised. This causes a thin liquid layer to form at the top of the PCM. There is therefore a liquid layer at the top followed by a softened solid PCM layer and lastly the solid PCM.

As the PCM absorbed the latent heat of melting the solid-liquid interface moved downward. There was therefore radiation heat transfer some distance into the PCM, convection heat transfer between the solid PCM and the liquid layer and conduction heat transfer inside the solid PCM. At some depth (further discussed in the Characterisation section) all of the radiation was absorbed in the liquid layer, the melting front was therefore governed by the natural convection in the melted PCM. The temperature gradient and distance between the top of the liquid PCM (heated by the radiation from the lamp) and the solid-liquid PCM interface governed the natural convection. This distance increased as more PCM melted, reducing the effect of heat conduction while increasing the effect of natural convection.

The buoyance effects also increased with an increase in the liquid layer. This increase in buoyancy which increased the convective heat transfer causes the melting front to be controlled by convection. Conversely when the liquid PCM is cooled the solidification front is controlled by conduction.

Kibria *et al* (2015) found that carbon additives increase the conduction heat transfer but weakened the natural convection in the liquid state. The carbon black additive in our experiments therefore decreases the natural convection even though it does not provide the increased conduction heat transfer but instead provides increased radiation absorption.

Fan *et al* (2014) similarly found that there was a competition between the increased heat conduction and reduction of natural convection. In their experiments they found that increasing the boundary temperatures led to more rigorous natural convection which in turn slows the melting because the natural convection contribution is reduced by the fast growing dynamic viscosity. In our experiments the higher carbon black concentrations mean that there is a higher boundary temperature which could lead to this same situation.

It becomes clear that you want to use a low as possible additive loading so that the dynamic viscosity does not increase significantly and the latent heat storage capacity is not reduced.

The carbon additives can also have an effect on the thermal performance of the system based on the geometry of the storage and the thermal gradients. Further investigation might therefore be required to test the carbon black in different geometry storage containers and more temperature readings need to be taken to more precisely see the effect of the different thermal gradients.

Figure 4-22 shows the appearance of the liquid phase 0.01 % carbon black composite. It is clear that even at this very low concentration the liquid is very different from that of the pure PCM shown earlier.

Figure 4-22: 0.01 % carbon black in beaker (left) and top view of large scale experiment (right). Note that the top two thermocouples are still visible beneath the liquid layer, shown in the right figure.

Figure 4-23 shows the side view of the 0.01 % carbon black composite. The colour of the solid PCM is much lighter than that of the liquid layer.

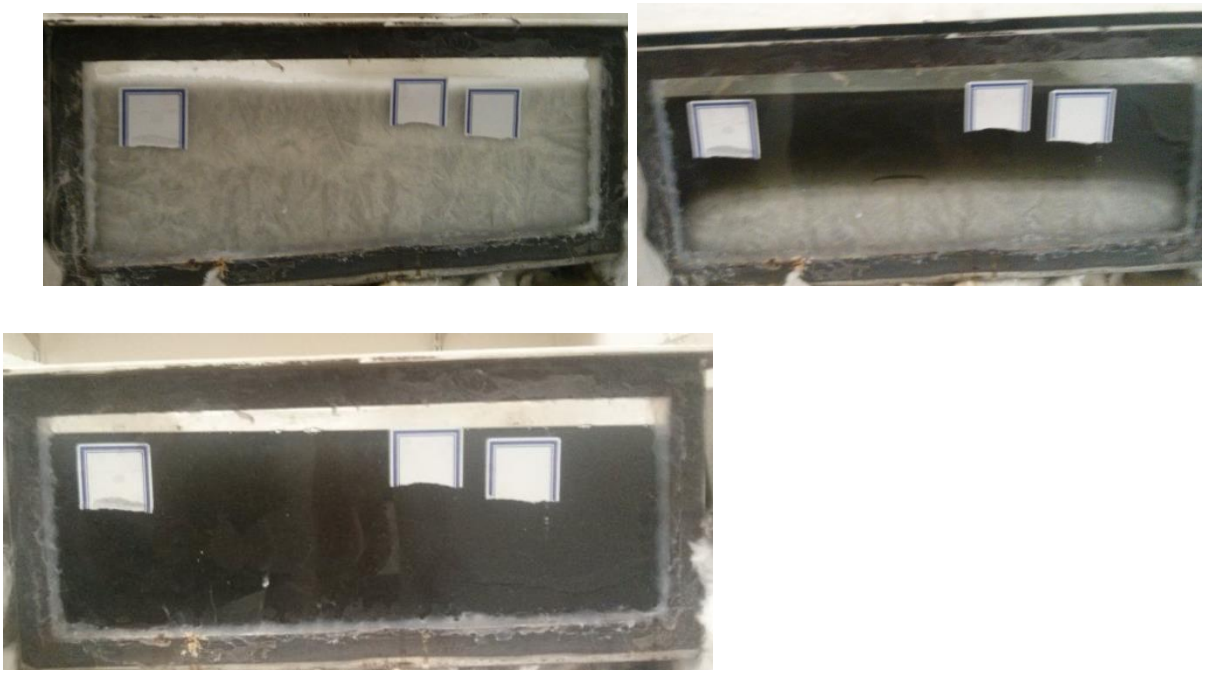

Figure 4-23: side view of 0.01 % carbon black showing the difference in its solid form (top left), mixture of solid/liquid form (top right) and liquid form (bottom).

Note the liquid bubble forming between the solid/liquid layer (top right picture in Figure 4-23), if there are many or large air bubbles present it could reduce the heat transfer between the solid and liquid layer.

The temperature profiles of the top and bottom thermocouples of the 0.01 % carbon black loading experiments can be seen in Figure 4-24.

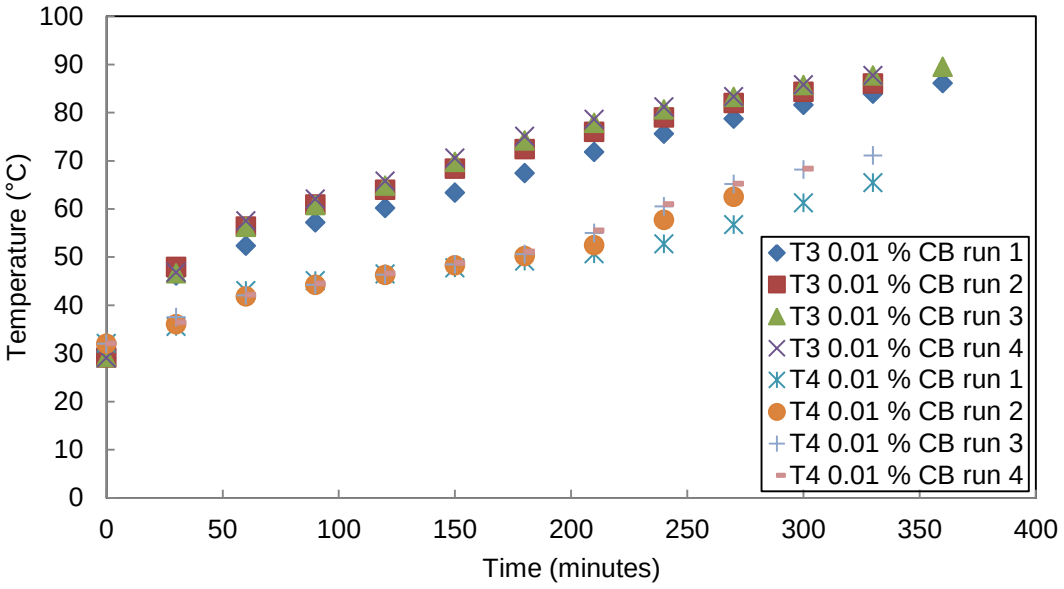

Figure 4-24: Temperature change over time of the 0.01 % carbon black composite as recorded by Thermocouple 3 (T3) and Thermocouple 4 (T4).

Figure 4-22 shows the appearance of the liquid and solid phases of the 0.02 % carbon black composite. The thermocouples are no longer visible through the liquid layer and the colour of the solid phase is also much darker than that of the 0.01 % carbon black composite.

Figure 4-25: 0.02 % carbon black top view in liquid phase (top left), top view in solid phase (top right) and side view of the solid phase (bottom).

A dip in T3 0.02 % CB run 4 can be seen in Figure 4-26, this sharp decrease was caused by the light source being off for a short time. This dip is only visible on the top thermocouple and is not seen in the lower thermocouple reading. This reinforces the idea that the top thermocouple gets most of its energy from the radiation of the lamp while convection/conduction is responsible for the heat in the lower thermocouple reading.

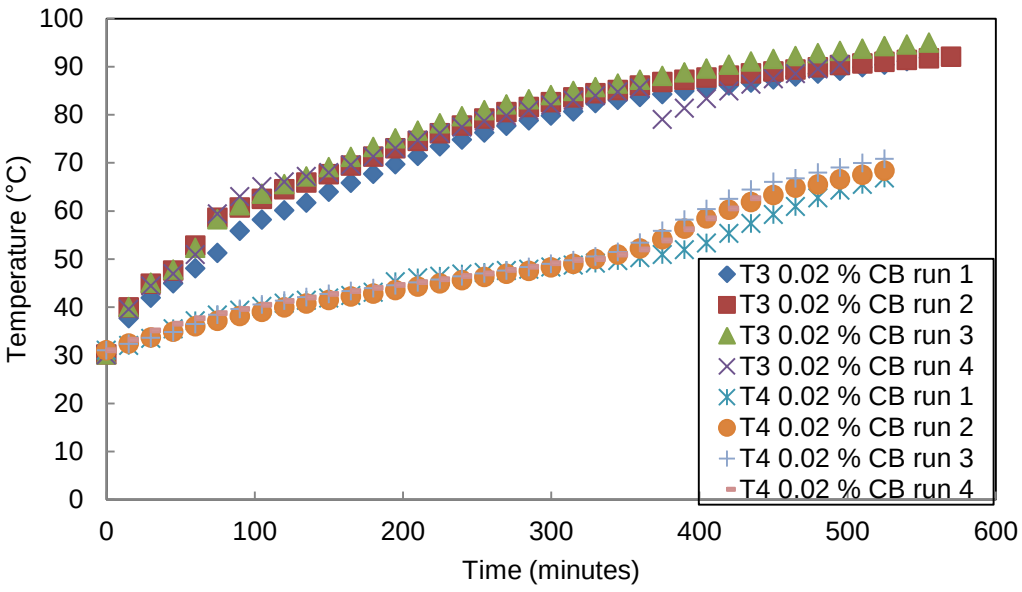

Figure 4-26: Temperature change over time of the 0.02 % carbon black composite, as recorded by Thermocouple 3 (T3) and Thermocouple 4 (T4).

The PCM and 2 % carbon black composite showed that even at higher concentrations, multiple runs show small deviations and good repeatability, as seen in Figure 4-27.

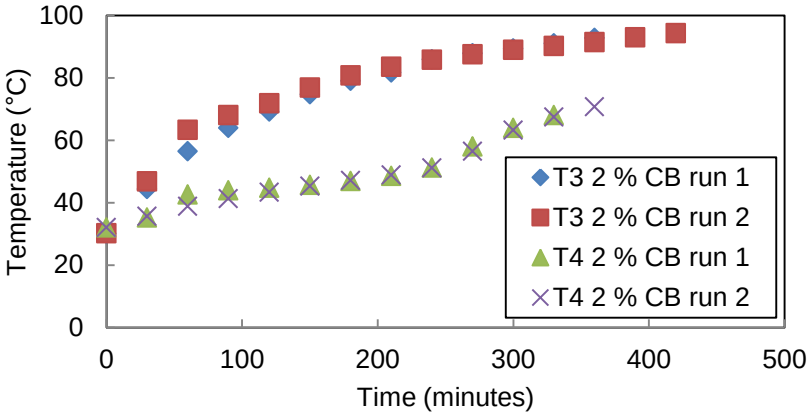

Figure 4-27: Temperature change over time of the 2 % carbon black composite, measured at Thermocouple 3 and 4 (Top),a photo showing the difference between the solid and liquid phase of the 2 % carbon black composite (bottom left) and a photo showing the top view of the solid phase of the 2 % carbon black composite (bottom right).

Multiple runs also showed small deviations and good repeatability, even at a high loading of 6 % carbon black as seen in Figure 4-28. It should be noted that the fact that the values for subsequent runs are so similar does

not mean that the dispersion is still good. It was shown that the carbon black stops providing any additional benefit after a certain point is reached. This means that even though some of the carbon black settles out there is still enough carbon black dispersed in the PCM to provide this maximum efficiency. Figure 4-29 shows how the carbon black settled out at the bottom, as seen in the side view.

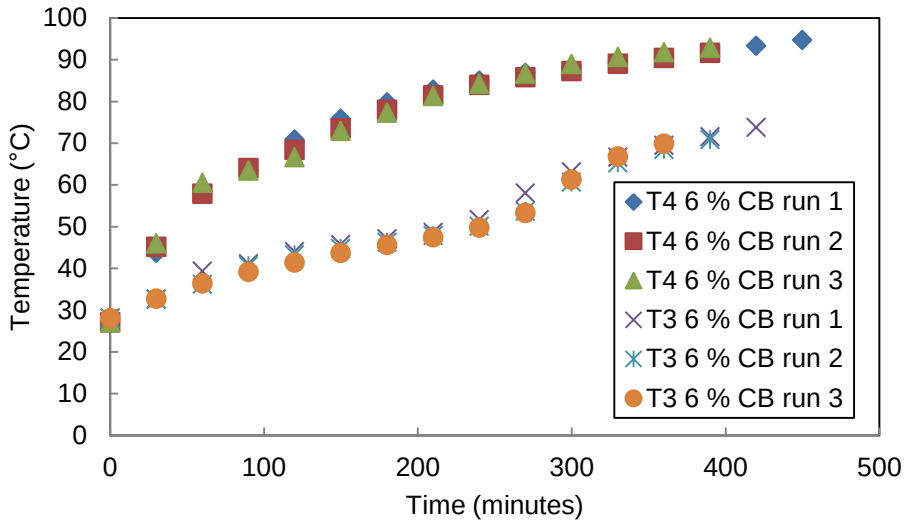

Figure 4-28: Temperature change over time of the 6 % carbon black composite, measured at Thermocouple 3 and 4.

Figure 4-29: Top view of the liquid phase of the 6 % carbon black composite (top left), the top view of the solid 6 % carbon black composite showing a similar colour to that of the previous runs (top right) and the side view of the 6 % carbon black composite showing the darker colour at the bottom where the carbon black is not well dispersed (bottom).

4.3. Characterisation

4.3.1. Differential scanning calorimetry (DSC)

4.3.1.1. Effect of different carbon black loadings

The complete set of DSC data is summarized in Table 4-2 and the DSC curves can be seen in Appendix C. Table 4-2 shows that the latent heats calculated during the heating and cooling are in good agreement.

Table 4-2: DSC data of the PCM composites

	Cooling			2nd Heating		
% Carbon Black	**Onset Temp. (^{0}C)**	**Peak Temp. (^{0}C)**	**ΔH Cooling (J/g)**	**Onset Temp. (^{0}C)**	**Peak Temp. (^{0}C)**	**ΔH Heating (J/g)**
0	53.25	50.51	186.1694	54.71	58.63	186.479
0.01	53.35	50.46	183.9671	57.11	59.33	185.9025
0.02	53.18	50.14	184.3902	54.76	59.08	184.6636
0.04	53.19	49.43	181.5968	54.98	59.78	182.3661
0.08	53.23	49.79	189.4276	54.91	59.72	189.5123
0.1	53.15	49.98	194.4562	54.97	59.28	195.3742
0.5	53.23	49.66	183.9941	54.82	59.51	184.2714
1	53.25	50.3	208.0555	54.84	58.89	209.7028
4	53.3	50.48	199.7085	54.77	58.81	201.232
8	53.22	50.16	175.4823	54.93	59.2	177.8699

Carbon black had no meaningful impact on the onset temperature or peak temperature of the PCM as seen in Table 4-2.

There was however some changes in the latent heat. The sharp drop, followed by an increase and lastly the linear decrease in latent heat was also found by (Kibria *et al*, 2015) and discussed earlier: The dispersion at low carbon black concentrations are very good, reducing the PCM's latent heat. When the carbon black concentration is increased the agglomeration also increases which leads to less PCM molecules being absorbed by the carbon black, causing the latent heat to increase (the carbon black/wax interaction potential was larger than those of the wax molecules). Lastly the increase in carbon black does not increase the agglomeration anymore,

which leads to the linear decrease in latent heat due to the higher concentration carbon black (and therefore less pure PCM with high latent heat).

The limitations of DSC needs to be noted, DSC uses a very small sample size, it is therefore very hard to use on PCMs with additives since the dispersion needs to be excellent and the small sample needs to be a good representation of the total material being tested. This limitation can be solved by the use of the T-history method as discussed earlier and outlined by Cabeza *et al* (2015).

4.3.1.2. Effect of multiple heating/cooling cycles

Figure 4-30 shows the effect of 100 freezing/melting cycles on the stability of the PCM/PCM-composite. The data from the 100 heating/cooling cycles for each PCM composite were superimposed on each other and show very good stability.

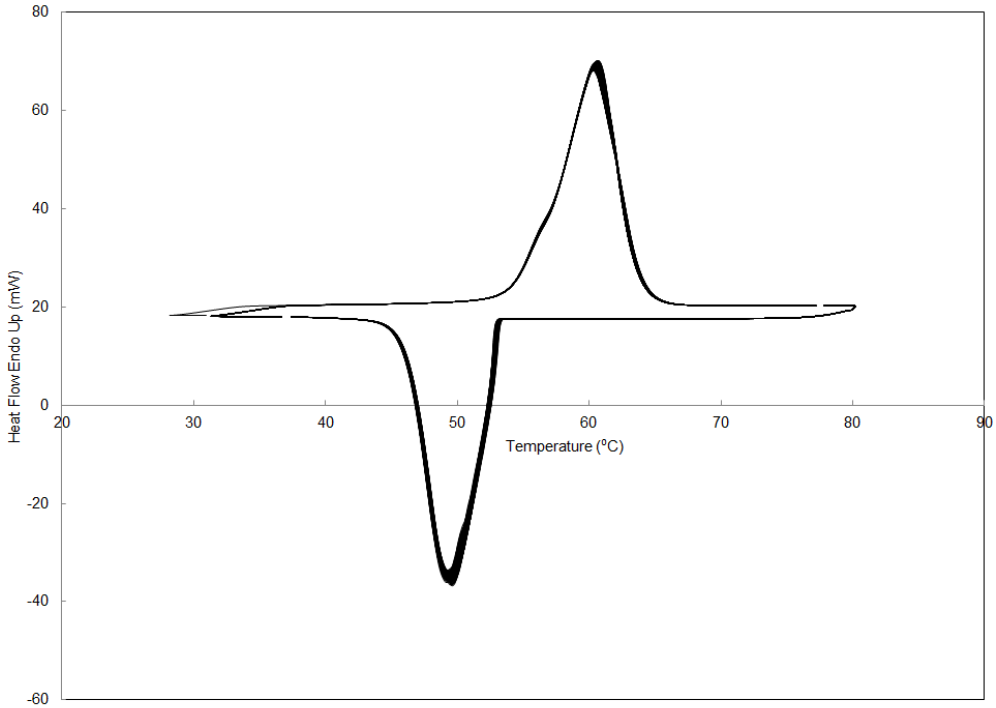

Figure 4-30: 100 consecutive heating and cooling cycles of the PCM and 0.08 % carbon black.

The multiple cycle DSC graphs of other concentrations of carbon black can be seen in Appendix C.

The properties of the PCM/PCM-composite before and after the 100 freezing/melting cycles are shown in Figure 4-31 and Figure 4-32. The properties are very similar before and after the freezing/melting cycles, showing that the PCM has very good stability.

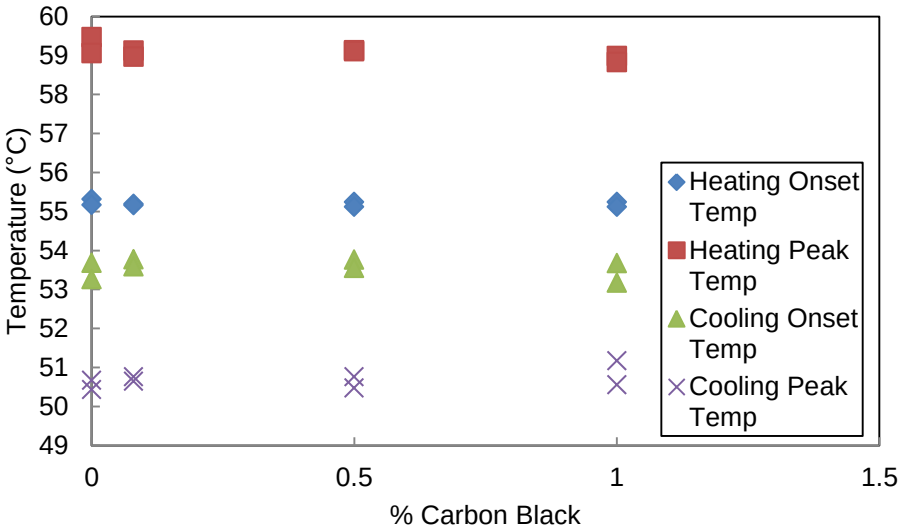

Figure 4-31: Temperature properties before and after 100 heating/cooling cycles.

Figure 4-31 shows that the heating onset temperature, the heating peak temperature, cooling onset temperature and the cooling peak temperature of the PCM/PCM-composite did not significantly change after the 100 melting/freezing cycles.

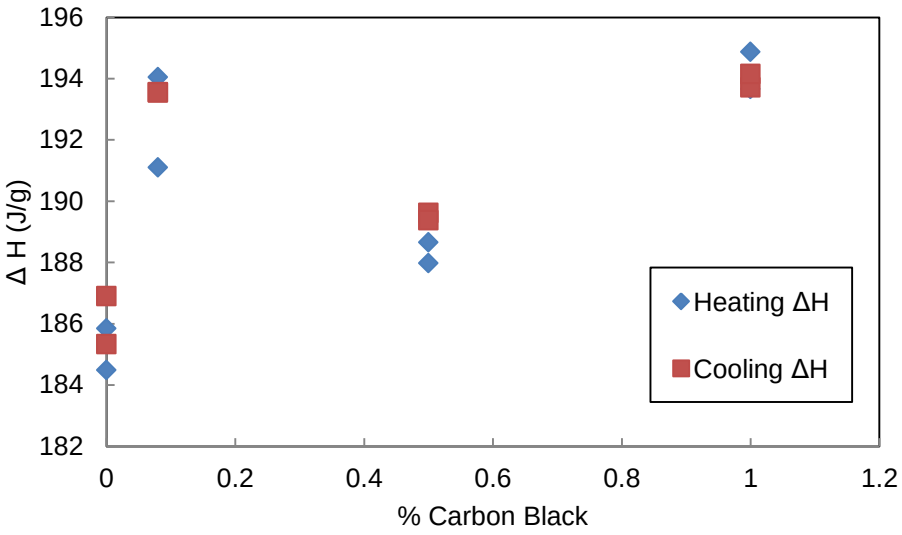

Figure 4-32: Latent heat properties before and after 100 heating/cooling cycles.

The latent heat of the PCM/PCM-composite as seen in Figure 4-32 also showed good stability, with hardly any change in the latent heat of the PCM before and after the 100 melting/freezing cycles.

This means that the organic PCM appears to be stable over multiple cycles and therefore well suited for TES applications. This also shows that the properties of the PCM used in the small scale and large scale experiments did not change over the course of the heating/cooling cycles.

4.3.2. Transmittance/absorbance characteristics

4.3.2.1. Novel solar simulator experiment

Figure 4-33 shows that the amount of radiation passing through a certain length of liquid PCM. The amount of radiation passing through the liquid sample decreased substantially for an increase in carbon black loadings. For all of the concentrations tested the maximum length that the radiation can still go through was less than 40 mm. Almost no radiation passes through the PCM composite with carbon black percentages of more than

0.05 %, even at a liquid layer depth of only 6.5 mm. The complete run can be seen in Appendix B.

When Figure 4-33 is plotted on a semi-logarithmic scale a linear decrease in the amount of radiation passing through the liquid layer can be seen. This relationship could help calculate the optimal carbon black loading for the specific TES application (different size PCM); by knowing exactly how much radiation will be absorbed by a certain concentration carbon black at a certain depth. For example, from the graph you would expect a 0.01 % carbon black composite at a depth of 20 mm to let around a 100 W/m^2 of the original 900 W/m^2 through.

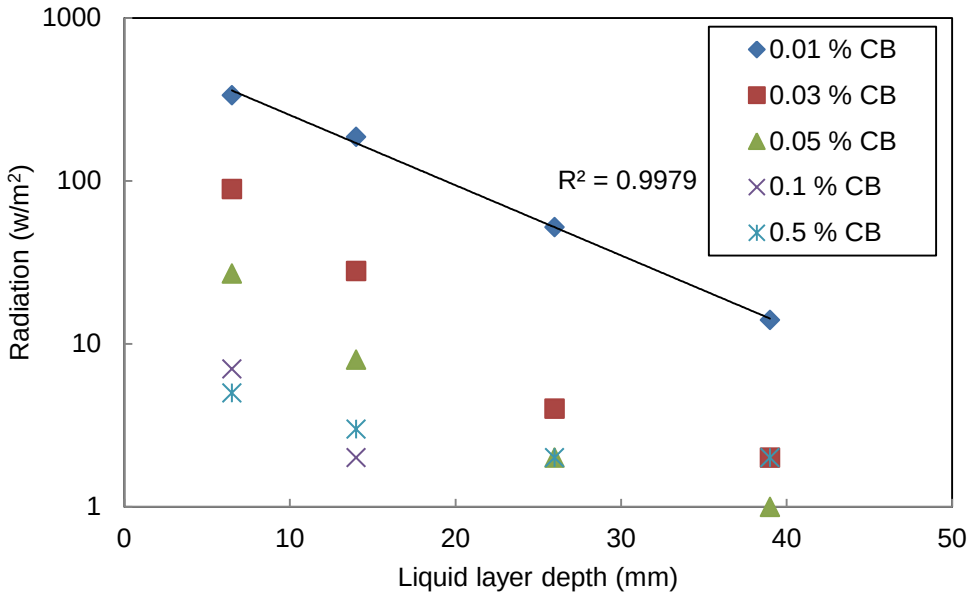

Figure 4-33: Radiation passing through a certain depth of PCM composites on a semi-logarithmic scale.

When the amount of carbon black at different heights is plotted in Figure 4-34 it can be seen that this relationship only holds for low percentages of carbon black (less than 1 % carbon black).

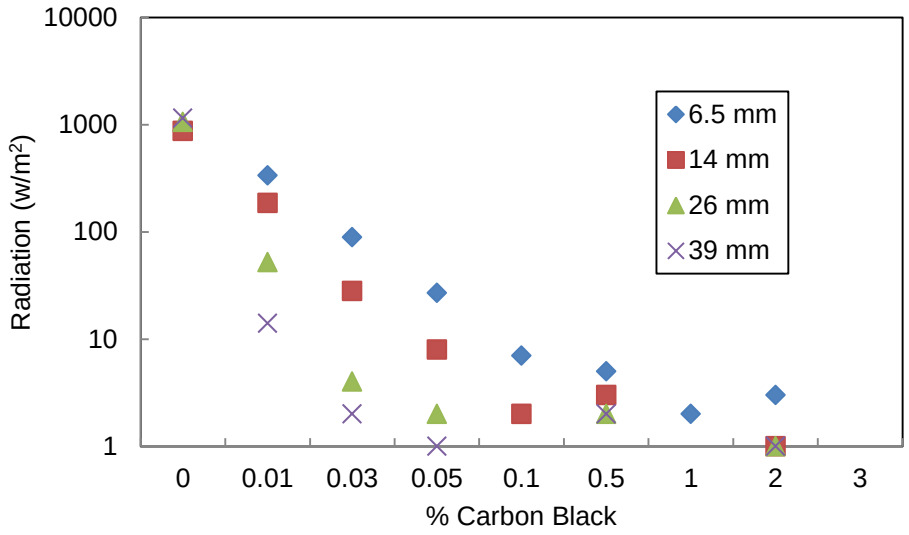

Figure 4-34: Radiation passing through certain depths of PCM composites on a semi-log scale.

The relationship does not hold when the radiation passing through the PCM is very small (either high carbon black concentrations or a large liquid layer to pass through) this is because there is still some stray radiation hitting the sensor because the sensor is not perfectly insulated. Other factors which also influence this relationship are:

- Not parallel monochromatic light
- Test was done in a beaker not cuvette (shape of the beaker could influence refraction)
- Strongly absorbing media, 0.1 % carbon black loading absorbs almost all of the incoming radiation
- The PCM has its own separate absorption properties

Figure 4-35 could give an indication for the amount of carbon black that would be needed (similar to Figure 4-33, depending on what data you want), when you wish to absorb a certain amount of radiation at different depths. For example, from the graph you would expect a 0.02 % carbon

black liquid composite with a depth of 6.5 mm to let around 200 W/m^2 through of the original 900 W/m^2 radiation.

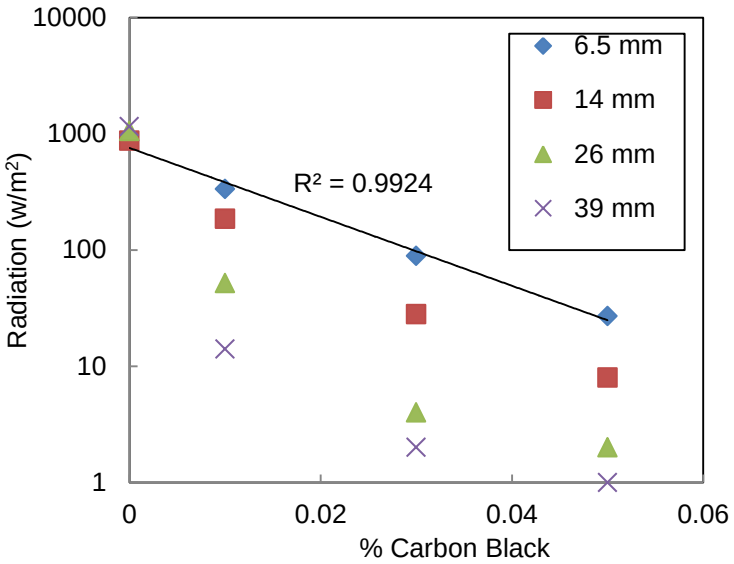

Figure 4-35: Radiation passing through certain depths of PCM composites on a semi-log scale.

The radiation penetration depth calculation is very similar to the Beer-Lambert law, but with a real world test, using the carbon black in the real PCM and a light source similar to the sun. This data gives a good indication of the transmittance/absorbance of the large scale and small scale experiments using the solar simulator. This can then be used in the modelling and to explain the effects that were observed in those experiments. It is useful to know how far the radiation passes into the sample so that the regions that are radiation/convection/conduction controlled are known.

To get a more general idea of the absorbance/transmittance of the PCM composite a further novel UV-vis experiment was conducted, using a controlled light source and standard cuvettes.

4.3.2.2. Novel UV-vis experiment

In this first experiment, the cuvettes with PCM were heated to 65 ^{0}C and then left to cool down and solidify while the radiation passing through them was recorded. The samples became more opaque as they solidified and less radiation was able to pass through as seen in Figure 4-36.

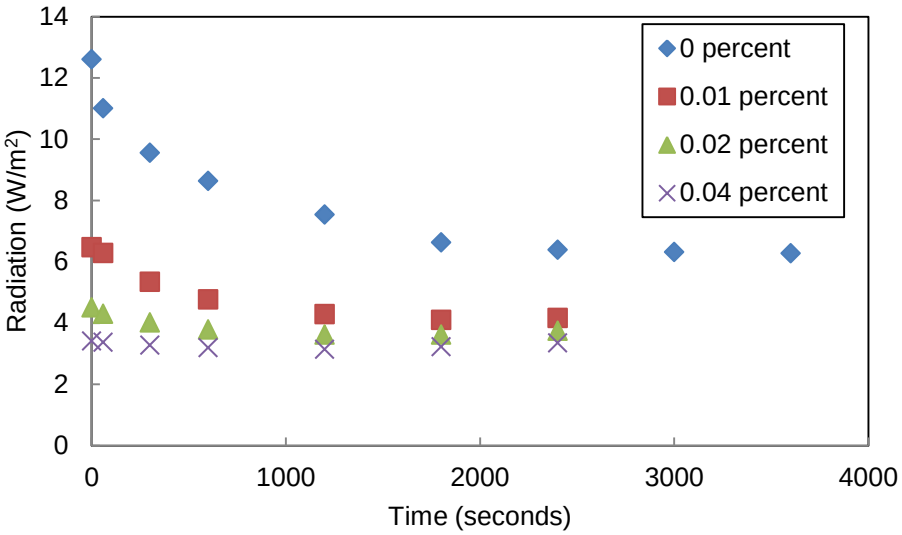

Figure 4-36: Radiation passing through samples (starting as a liquid at 65 ^{0}C) as they were cooling down and eventually became completely solid.

Carbon black loadings at concentrations higher than 0.04 % showed no difference in the amount of radiation passing through them as they solidified. This indicates that at concentrations higher than 0.04 %, using this light source and a 1 cm path length cuvette, the samples were already completely opaque. The small amount of radiation passing through when the samples were completely opaque is due to stray radiation. The full run with all of the tested carbon black loadings can be seen in Appendix B.

The samples were tested with a light source using 450 nm and 550 nm wavelengths. The results were very similar and the 450 nm experiments can be seen in Appendix F.

The Beer-Lambert law is only applicable to very dilute solutions. The strength of the light passing through the sample dropped very quickly before levelling out, as seen in Figure 4-37. This strong absorption of the carbon black as well as “high” carbon black concentrations means that the Beer-Lambert law might not hold.

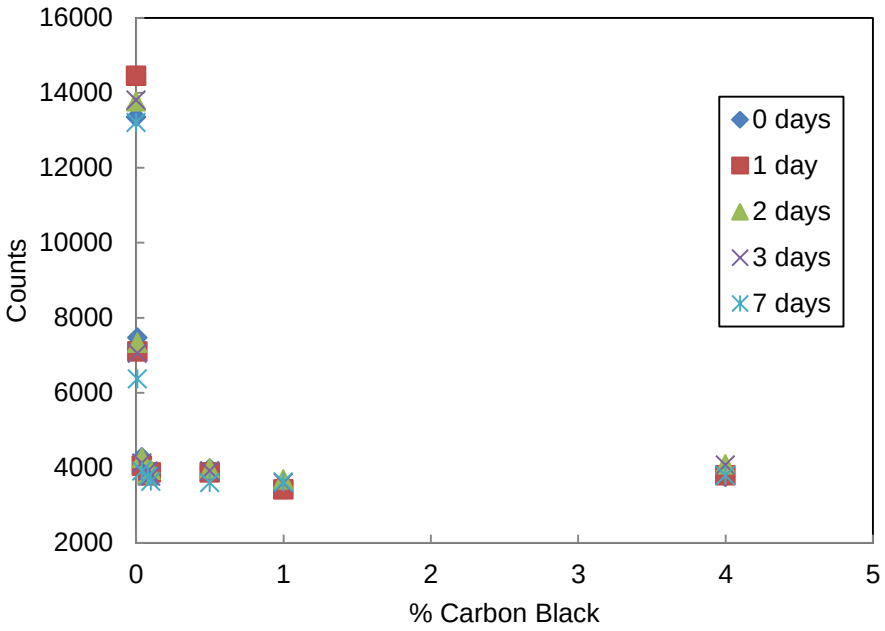

Figure 4-37: Relative strength of the 550 nm wavelength light passing through a liquid PCM sample with a certain carbon black loading.

The absorptivity of the samples at the higher carbon black concentrations was slightly lower every day as seen in Figure 4-38. This is because some of the carbon black started to settle out, leading to more radiation passing through the sample and a lower absorptivity. This settling out can also visually be seen in the photos of the following section. The dispersion at the lower concentrations was much more stable, showing very small or hardly any reduction in absorptivity.

Similar to that of the transmittance, the absorptivity increased sharply at very low carbon black concentrations before levelling out.

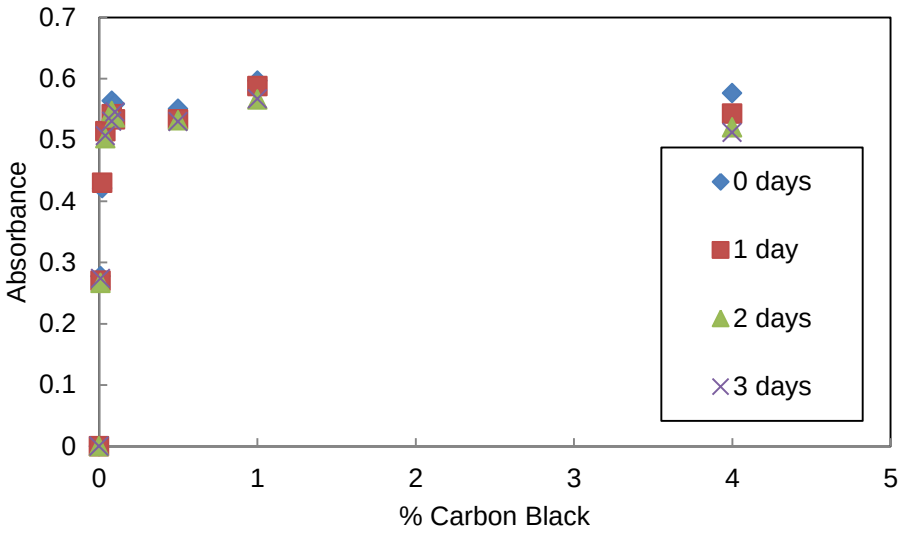

Figure 4-38: Absorptivity of the PCM composites at a wavelength of 550 nm.

Figure 4-39's trendline is not perfectly linear since the concentration at 0.02 % carbon black is already high and started to saturate. The high concentration could lead to electrostatic interactions between the molecules or changes in the refractive index at these high concentrations.

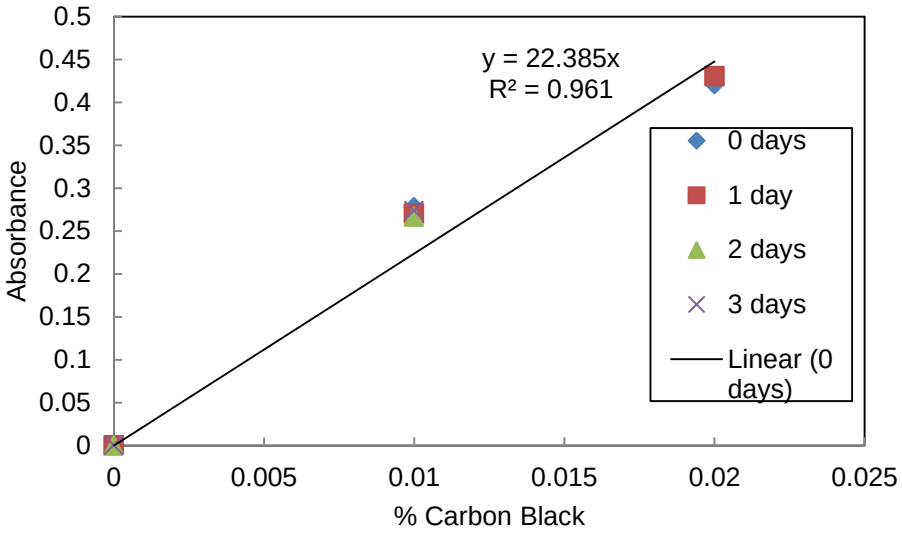

Figure 4-39: Absorptivity of the PCM composites at a wavelength of 550 nm, for the lower carbon black concentrations with a linear trendline.

The path length was 1 cm, the absorptivity coefficient at 450 nm was found to be 28.551 $M^{-1}cm^{-1}$, and 27.778 $M^{-1}cm^{-1}$ at 550 nm. The absorptivity coefficient is usually tied to a certain wavelength, but because carbon black absorbs almost all of the light at a wide range of wavelength the values are very similar for this experiment.

4.3.3. Settling experiments

The solid PCM and PCM composites inside the 1 cm path length cuvettes are shown in Figure 4-40. The carbon black appears to be well dispersed at the start, while there is some settling out at the higher carbon black concentrations after the first melting cycle.

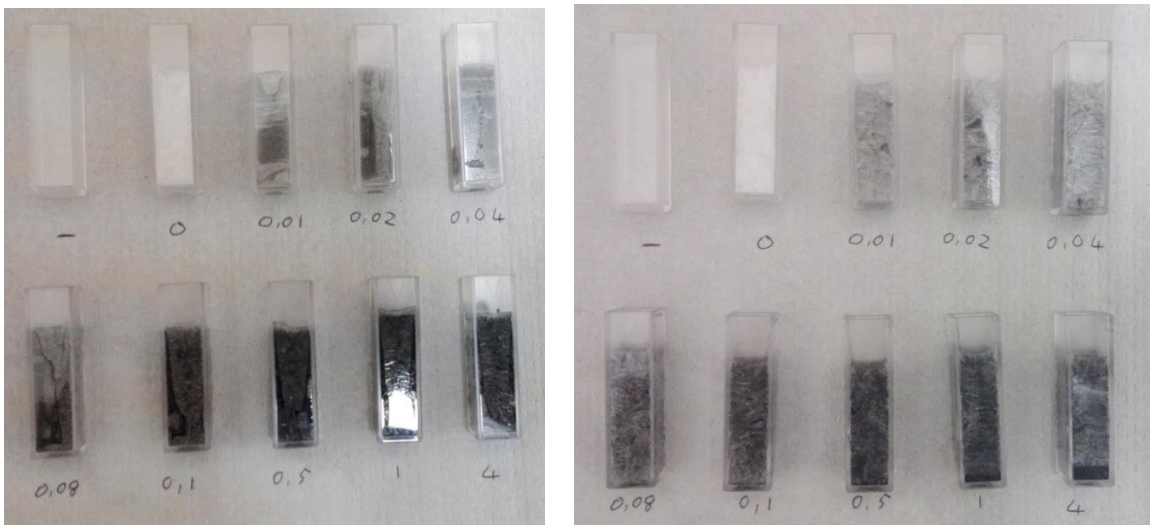

Figure 4-40: Solid PCM composites at the start of the experiments (left), note that some look to already be settling out but this is only due to the way the PCM solidified against the cuvettes and is not due to them settling out. The solid PCM composites after the first melting/solidifying cycle (right) showing some settling out at 1 % and 4 % (second row, far right).

The liquid PCM/PCM-composite samples are shown in Figure 4-41. The colour of the PCM composite becomes visibly darker until around 0.04 %, after this loading the colour appears similar independent of the carbon

black concentration. At the start the liquid samples did not show any visible settling out of carbon black.

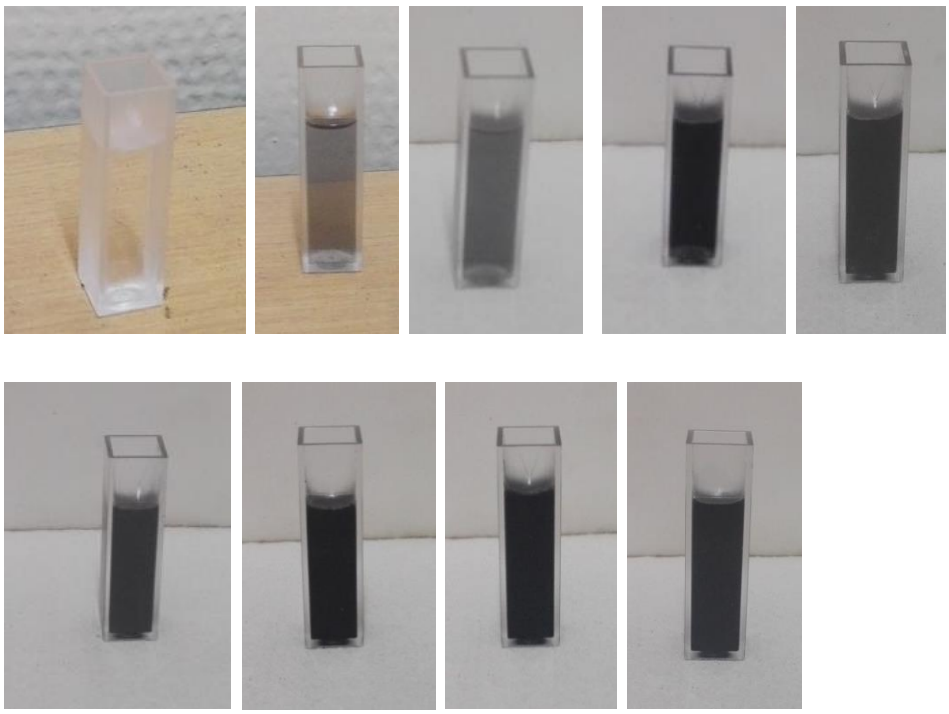

Figure 4-41: Liquid PCM composites melted at 65 ^{0}C, the top row from left to right is: 0 %, 0.01 %, 0.02 %, 0.04 % and 0.08 % carbon black. The bottom row from left to right is 0.1 %, 0.5 %, 1 % and 4 % carbon.

The samples were kept in an oven at 65 ^{0}C for 14 days; photos of these liquid samples were taken every day and are shown in Figure 4-42. The colour of the samples appear to stay mostly constant for the first 9 days, thereafter the colour of the samples (especially those of higher concentrations carbon black) appear less black and more grey as time passes.

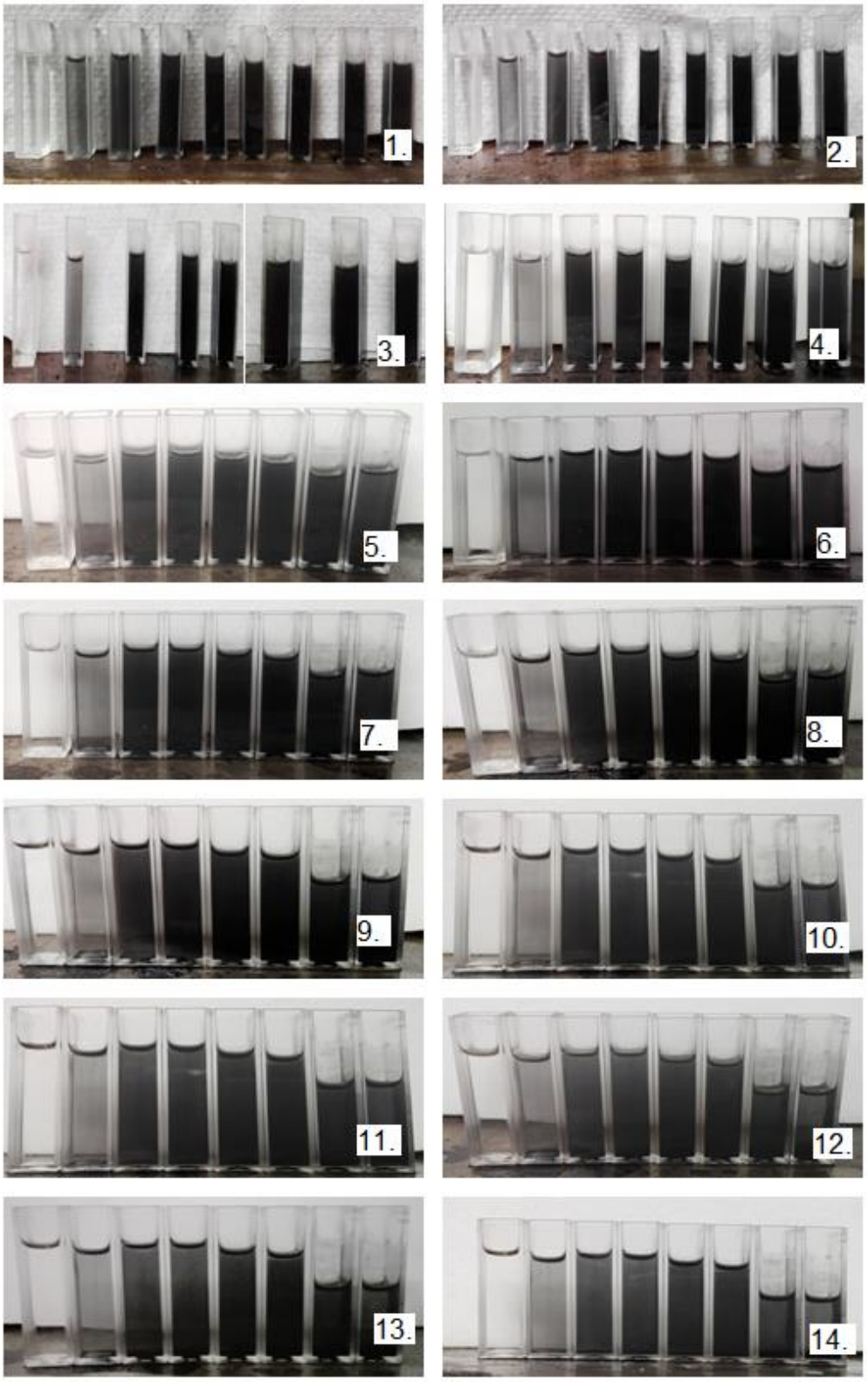

Figure 4-42: Photos of the PCM/PCM-composites, for 1-14 days. The concentration carbon black in the cuvettes, from left to right is: 0 %, 0.01 %, 0.02 %, 0.04 %, 0.08 %, 0.1 %, 0.5 %, 1 %, 4 %. Note that from day 3 the 0.02 % carbon black cuvette is no longer there.

These experiments show that while the dispersion is good after only 20 minutes on a magnetic stirrer, after a couple of days the carbon black can start to settle out (if it is left in a liquid form), especially the high carbon black concentrations and might require additional measures to re-disperse the carbon black particles.

4.3.4. Thermal energy storage charge/discharge rate

The charge and discharge rate of the carbon black was measured, by putting 7 g of the pure PCM and the PCM composites in separate glass test tubes which are then put into subsequent waterbaths at 29 ^{0}C and 65 ^{0}C respectively.

Figure 4-43 and Figure 4-44 show the thermal energy storage charge and discharge rate of the 7 g PCM/PCM composites.

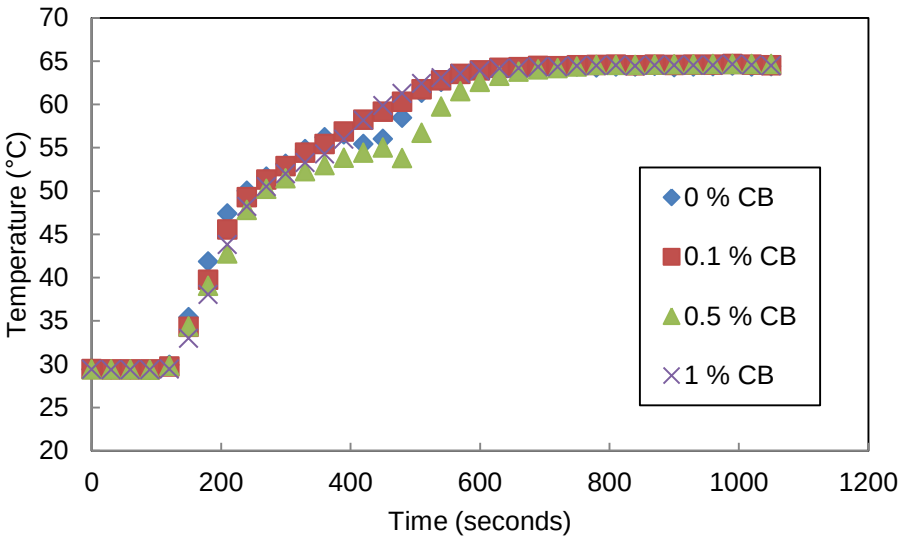

Figure 4-43: The energy storage charge of the pure PCM and low concentration carbon black composites.

There is almost no difference in the charging time when carbon black is added, this is due to the small amount of carbon black added and the charging phase being dominated by convection.

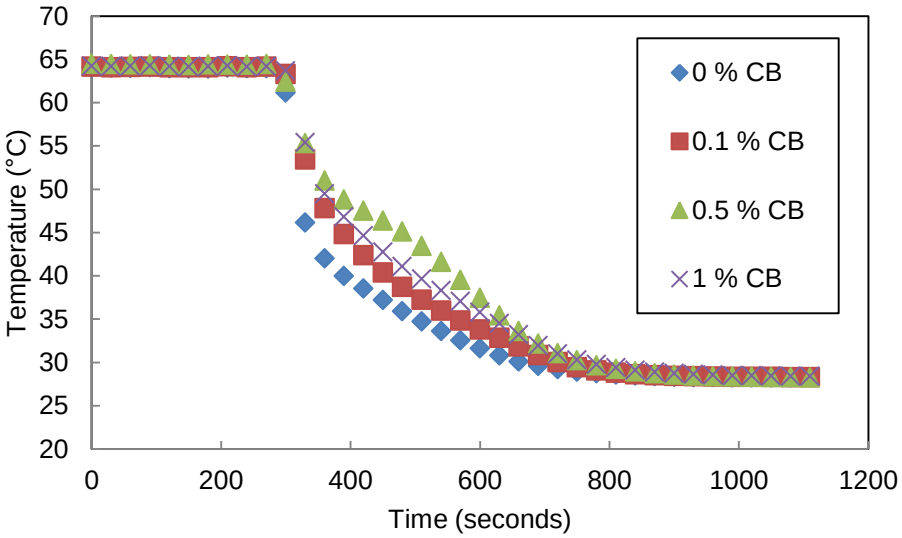

Figure 4-44: The energy storage discharge of the pure PCM and low concentration carbon black composites.

The difference in the temperature between the pure liquid phase and pure solid phase can be explained by a different moving phase boundary during heating/cooling. The overall time to completely heat/cool for all of the PCMs appears to be unaffected by the addition of carbon black.

More tests are shown in Appendix G, showing that larger carbon black loadings also do not show any significant changes in the charge and discharge rate.

Therefore it can be seen that the rate of charge/discharge of the TES system does not significantly change when carbon black is added to the PCM.

4.3.5. Density

The absolute density of the PCM was measured using a pycnometer, with Helium as the analysis gas, 5 purges at a temperature of 23.89 ^{0}C and an equilibrium rate of 0.050 psig/min.

The density of the PCM was 0.9767 g/cm^3 with a standard deviation of 0.0015 g/cm^3.

Similarly the absolute density of carbon black was measured using a pycnometer, with Helium as the analysis gas, 5 purges at a temperature of 23.97 ^{0}C and an equilibrium rate of 0.050 psig/min.

The density of the carbon black was 1.8901 g/cm^3 with a standard deviation of 0.0049 g/cm^3.

4.3.6. Scanning electron microscopy (SEM)

The SEM micrographs of the carbon black are shown in Figure 4-45 to Figure 4-51, in order of increasing magnification.

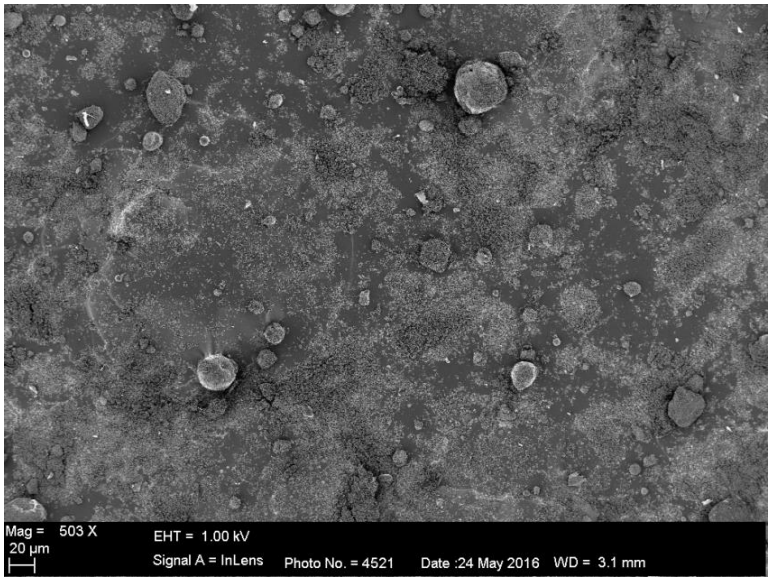

Figure 4-45: The overall structure of the carbon black is shown, the globular structure in the top right is the same as the one shown in the following figures.

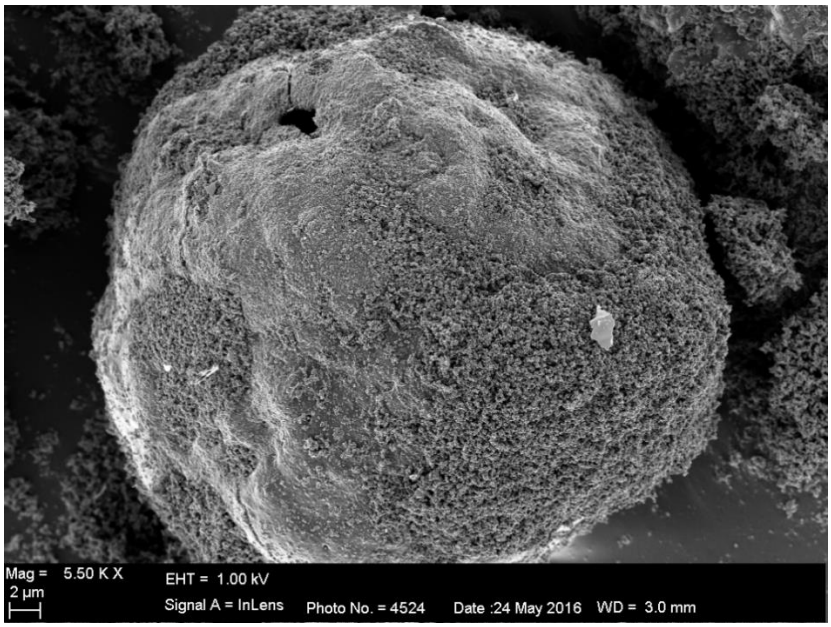

Figure 4-46: Globular structure in the carbon black, showing the characteristic look of carbon black particles on its surface.

Figure 4-47: Globular carbon black structure with carbon black agglomerates visible in its pores.

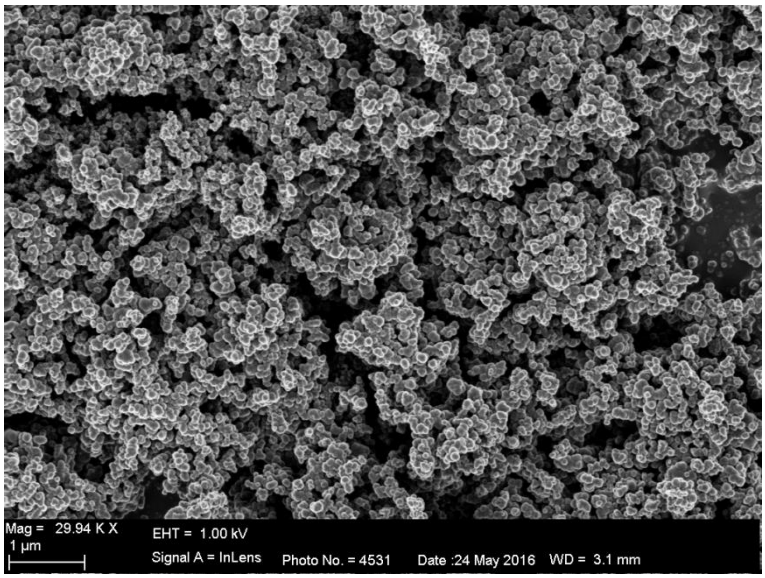

Figure 4-48: Characteristic micrograph of the carbon black, showing the mostly spherical primary particles that make up the grape-like structure.

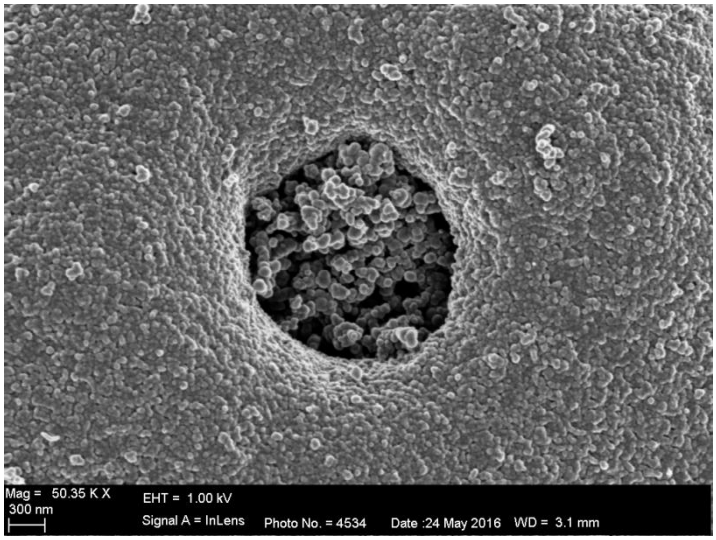

Figure 4-49: Pore on the globular structure showing what looks to be a centre filled with carbon black agglomerates.

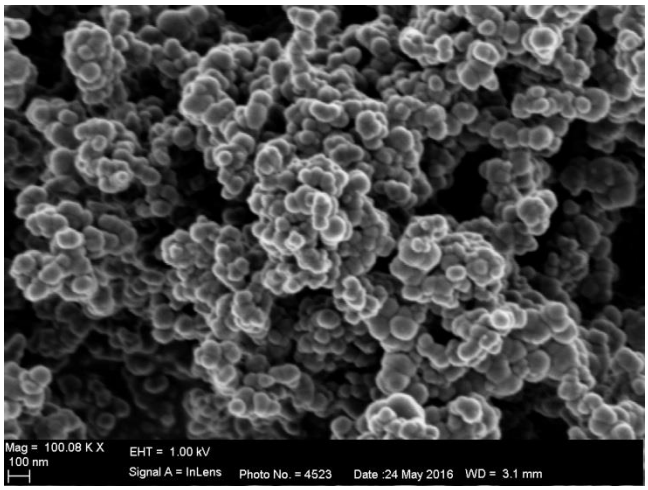

Figure 4-50: Grape like carbon black agglomerate structure, made out of carbon black aggregates which in turn are made out of the spherical primary carbon black particles.

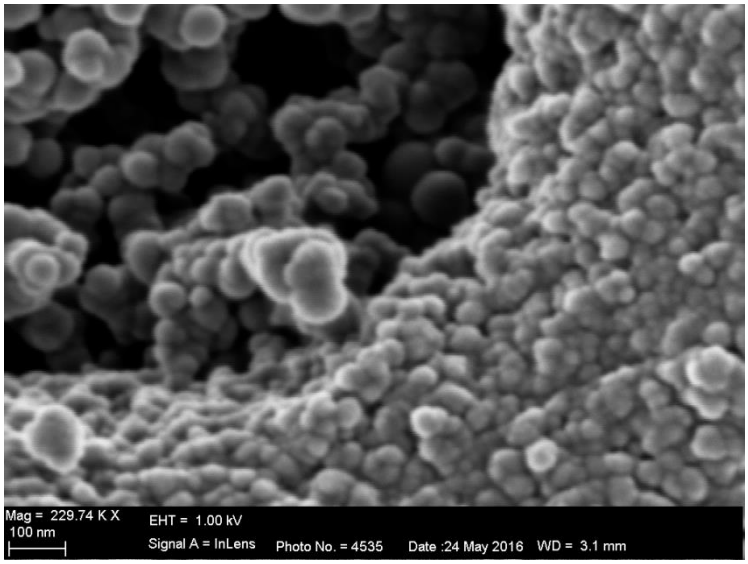

Figure 4-51: Up close look at the inside of the pore on the globular structure, showing the carbon black aggregates inside.

The globular structures seen in these SEM micrographs are around 60 micron in size which is in agreement with the particles size given by the carbon black manufacturer. The structure of the carbon black also suggests that the carbon black has been processed by the manufacturer into these agglomerates to reduce dust and ease handling, as discussed earlier.

Additional SEM micrographs can be seen in Appendix H.

4.4. Modelling

Assumptions:

- Physical properties (density, thermal conductivity, specific heat) are the same for the solid and liquid phase
- Physical properties do not change with temperature
- Liquid phase is stagnant (no convection)
- One dimensional

Two simple models were made. First the solar box was modelled with no phase change (Figure 4-52 and using the data in Table 4-3) and secondly the phase change problem was modelled separately (Figure 4-53).

The model predicts starting temperatures close to that of the 0.04 % carbon black runs since the absorptivity of the PCM is very high with most of the incoming radiation being absorbed, unlike the pure PCM which does not absorb such a large portion of the incoming radiation. The model predicts a higher temperature before evening out because it does not take into account the heat that is absorbed as latent heat when the PCM melts.

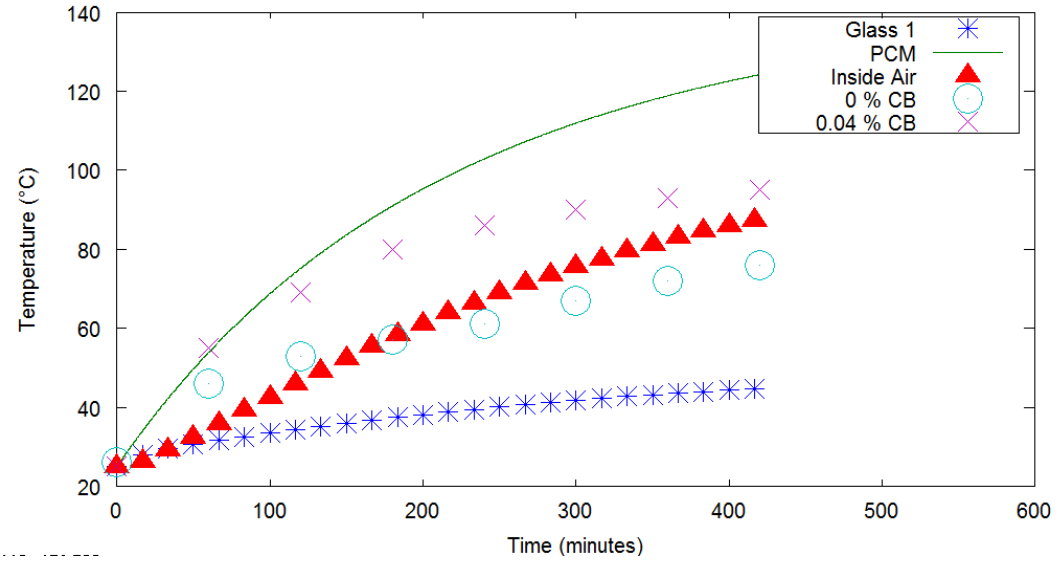

Figure 4-52: Modeled values for the top glass cover temperature, PCM temperature, inside air temperature, and the experimental data for the 0 % carbon black PCM and 0.04 % carbon black composite.

Table 4-3: Values of certain properties used in the model

Property	Value
Emissivity of glass	0.2
Emissivity of PCM	0.95
Emissivity of box walls	0.2
Cp of glass	840 J/(Kg·K)
Cp of box	1700 J/(Kg·K)
Cp of air	1000 J/(Kg·K)
Cp of PCM (average of liquid and solid PCM)	2610 J/(Kg·K)
Insulation thermal conductivity	0.033 W/(m·K)
Air thermal conductivity	0.029 W/(m·K)
PCM thermal conductivity (stearic acid)	0.25 W/(m·K)
Solar radiation	900 W/m^2
Density of PCM (from pycnometer)	976.7 kg/m^3
Latent heat of PCM (from DSC)	186000 J/kg
Ambient temperature	25 ^0C
Wind speed	1 m/s
Transmittance of glass	0.75
Reflectivity of glass	0.05
Reflectivity of PCM	0.01
Mass of PCM (2 cm layer)	2.4 kg

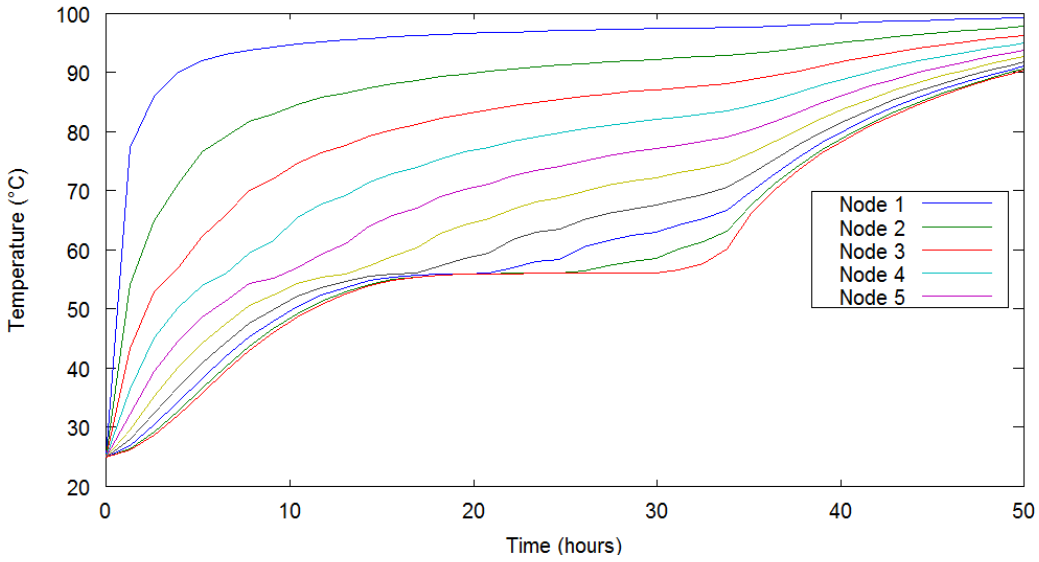

Figure 4-53: Temperature of the pure PCM with phase change included.

The time to completely melt the PCM, according to the model, is very long (more than 30 hours), because of the low thermal conductivity and the fact that the model does not take into account the natural convection. This proves that the natural convection does play a big part in the heat transfer and cannot be ignored (the radiative effects of the semi-transparent media are also not taken into account).

(Kibria *et al*, 2015) reviewed the thermal conductivity improvements of PCMs and found that graphite nano-composites can show 12 times higher thermal conductivity compared to pure stearic acid. Using a 12 times higher thermal conductivity the melting time will be significantly reduced, as shown in Figure 4-54.

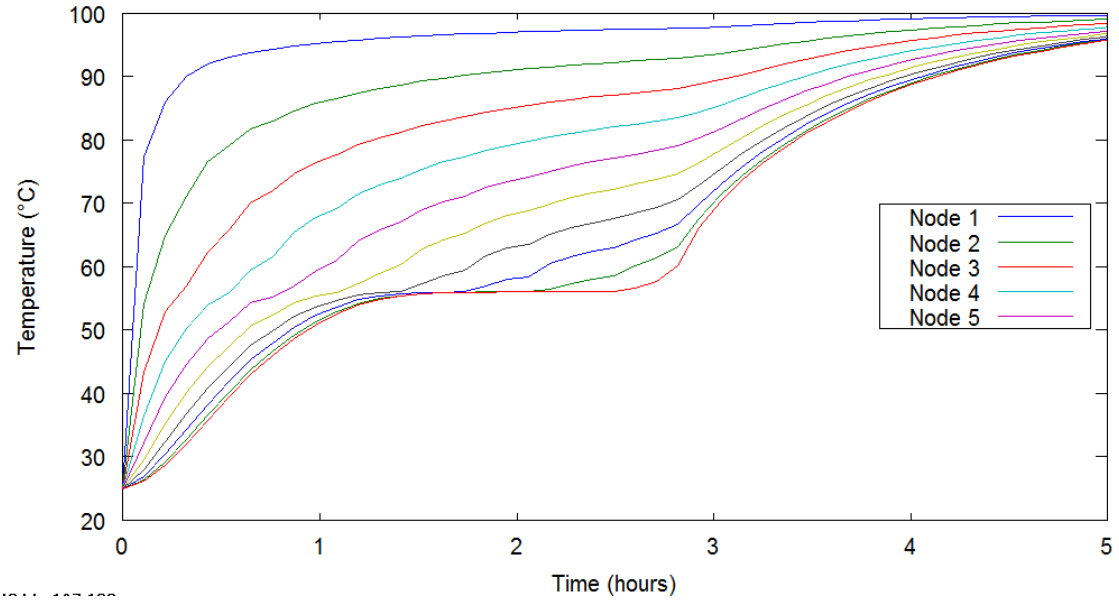

Figure 4-54: Temperature of the PCM with phase change included and a 12 times higher thermal conductivity than that of the pure PCM modelled earlier.

5. Conclusions

Carbon black is very effective at increasing the solar absorption of PCMs, requiring very low carbon black loadings for optimal absorption. The 0.06 % carbon black composites showed the fastest temperature increase and reached 75 ^{0}C much faster (350 %) than the pure PCM. All of the tested PCM composites (0.01 % to 6 % carbon black) reached 75 ^{0}C in less than half the time it took the pure PCM.

The carbon black and PCM samples were stable for up to 9 days, with no added surfactants or treatments (after the initial preparation). This stability without using a surfactant to stabilise the PCM composite is very important since the use of a surfactant does not work at high temperatures.

Carbon black does not have a meaningful effect on the thermal conductivity of the PCM, as seen in the energy charge/discharge experiments and the long cooling times of the PCMs. The carbon black also did not have a negative impact on the melting/solidifying onset temperature or the latent heat of the PCM. This proves that at these low concentrations carbon black can help reduce the shortcomings of the PCM without adversely affecting its energy storage properties.

The optimal carbon black concentration changes with the size of the PCM, a shallower PCM (2 cm deep) showed the fastest temperature increase at concentrations between 0.06 % and 0.5 % carbon black, while the deeper PCM (9 cm deep) showed the fastest temperature increase at concentrations between 0.01 % and 0.08 % carbon black. This can be explained by the very high concentrations carbon black absorbing more radiation but there is a trade-off in effectiveness:

1. The thermal conductivity of the PCM is very low, if all of the radiation is absorbed at the top of the PCM it takes a long time to transfer the

heat from the top of the PCM to the rest of the PCM through convection/conduction. On the other hand if some of the radiation is allowed to pass through the top of the PCM the heat transfer is faster (now mainly through radiation).

2. If the concentration of the carbon black is too high most of the radiation will be absorbed by a thin layer on the surface which is easily lost to the environment and when the concentration of carbon black is too low the PCM does not absorb all of the incoming solar radiation.
3. The carbon black can increase the dynamic viscosity of the PCM and reduce the natural convection of the PCM.

Carbon black does absorb the radiation in all of the tested wavelengths and using the solar simulator it was shown that at concentrations higher than 0.05 % carbon black the liquid is almost completely opaque at a liquid depth of 6.5 mm. Similarly at a liquid depth of 40 mm all of the radiation is absorbed at all of the tested carbon black loadings (0.01 % to 5 %).

Adding heat transfer enhancements (e.g. graphite) like those reviewed in the Literature Review section this novel PCM composite could be used as a combined direct solar absorber, heat transfer fluid and energy storage system. The carbon black provides better solar absorption, while the heat transfer enhancements makes the PCM a good heat transfer fluid and the PCM itself providing the efficient energy storage.

The simplified model found that there are other factors to take into account like the natural convection and the radiative effects of a semi-transparent media. The model also showed that the synergy in increasing the thermal conductivity, together with the use of carbon black, could lead to even greater efficiency and a much shorter melting/solidifying time.

6. Recommendations

Different carbon blacks (especially those from real recycled tyres) need to be tested to see what the effects of different particle sizes, manufacturing techniques, surface areas, etc. are on the solar absorption, dispersion and energy storage. The potential of extra agitation or surfactants to keep the particles well dispersed could also be tested with the different carbon black particles, if needed.

CSP usually work at high temperatures. It is therefore recommended that other PCMs, especially those used in higher temperature applications be tested to see if carbon black provides the same benefits as those observed when using organic eutectic mixtures at low temperatures.

The carbon black did not increase the thermal conductivity of the PCM and for efficient use in an integrated system heat transfer enhancements are necessary. The use of carbon black together with other heat transfer enhancements (like graphite) needs to be investigated. This novel material could then be an effective PCM with enhanced thermal conductivity and enhanced optical properties (due to the carbon black).

The final goal should be to test the carbon black on a pilot scale plant, where it is used in an integrated system (used as the HTF, solar absorber and TES system), preferably on high temperature CSP. PCMs have not combined in such a way and if it is possible could drastically reduce costs and improve the efficiency of solar power plants. The effect of carbon black on the long term use (over many cycles), different heat exchange methods, PCM storage, and the pumping/moving of the PCM need to be investigated (fouling, clogging, erosion, pressure drop, etc.).

The modelling of the overall system, including the heat transfer and the Stefan problem part is very complex and cannot be done with usual finite

methods. An improved model also needs to be made, one that can take into account the complexities of the different methods of heat transfer, radiative properties of the semi-transparent media, phase change and the various transient properties connected to it.

7. References

Agyenim, F (2016) "The use of enhanced heat transfer phase change materials (PCM) to improve the coefficient of performance (COP) of solar powered LiBr/H_2O absorption cooling systems" *Renewable Energy,* 87**,** 229-239.

Agyenim, F, Hewitt, N, Eames, P and Smyth, M (2010) "A review of materials, heat transfer and phase change problem formulation for latent heat thermal energy storage systems (LHTESS)" *Renewable and sustainable energy reviews,* 14**,** 615-628.

Al-Abidi, AA, Mat, S, Sopian, K, Sulaiman, MY and Mohammad, AT (2013) "Internal and external fin heat transfer enhancement technique for latent heat thermal energy storage in triplex tube heat exchangers" *Applied thermal engineering,* 53**,** 147-156.

Baby, R and Balaji, C (2013) "Experimental investigations on thermal performance enhancement and effect of orientation on porous matrix filled PCM based heat sink" *International Communications in Heat and Mass Transfer,* 46**,** 27-30.

Baran, G and Sari, A (2003) "Phase change and heat transfer characteristics of a eutectic mixture of palmitic and stearic acids as PCM in a latent heat storage system" *Energy Conversion and Management,* 44**,** 3227-3246.

Brooks, MJ, Du Clou, S, Van Niekerk, WL, Gauché, P, Leonard, C, Mouzouris, MJ, Meyer, R, Van Der Westhuizen, N, Van Dyk, EE and Vorster, FJ (2015) "SAURAN: A new resource for solar radiometric data in Southern Africa" *Journal of Energy in Southern Africa,* 26**,** 2-10.

Cabeza, LF, Barreneche, C, Martorell, I, Miró, L, Sari-Bey, S, Fois, M, Paksoy, HO, Sahan, N, Weber, R and Constantinescu, M (2015) "Unconventional experimental technologies available for phase change materials (PCM) characterization. Part 1. Thermophysical properties" *Renewable and Sustainable Energy Reviews,* 43**,** 1399-1414.

Chen, CJ (2011) *Physics of solar energy*, John Wiley & Sons*,* Hoboken, N.J. :.

Choi, DH, Lee, J, Hong, H and Kang, YT (2014) "Thermal conductivity and heat transfer performance enhancement of phase change materials (PCM) containing carbon additives for heat storage application" *International Journal of Refrigeration,* 42**,** 112-120.

Churchill, SW and Chu, HH (1975) "Correlating equations for laminar and turbulent free convection from a vertical plate" *International journal of heat and mass transfer,* 18**,** 1323-1329.

Crawley, GM (2013) *The World Scientific handbook of energy*, World Scientific, Singapore.

Date, A (1992) "Novel strongly implicit enthalpy formulation for multidimensional Stefan problems" *Numerical Heat Transfer, Part B Fundamentals,* 21**,** 231-251.

Desideri, U and Campana, PE (2014) "Analysis and comparison between a concentrating solar and a photovoltaic power plant" *Applied Energy,* 113**,** 422-433.

Djefel, D, Makhlouf, S, Khedache, S, Lamrous, N, Lefebvre, G and Royan, L (2014) "Experimental study of the thermal properties of composite stearic acid/coffee grounds/graphite for thermal energy storage", paper presented at *The 5th International Symposium on Aircraft Materials,* 23-26 April, 2014, Marrakesh, Morocco.

Duffie, JA and Beckman, WA (2013) *Solar engineering of thermal processes*, Wiley, Hoboken.

Esapour, M, Hosseini, M, Ranjbar, A, Pahamli, Y and Bahrampoury, R (2016) "Phase change in multi-tube heat exchangers" *Renewable Energy,* 85**,** 1017-1025.

Fan, L-W, Fang, X, Wang, X, Zeng, Y, Xiao, Y-Q, Yu, Z-T, Xu, X, Hu, Y-C and Cen, K-F (2013) "Effects of various carbon nanofillers on the thermal conductivity and energy storage properties of paraffin-based nanocomposite phase change materials" *Applied energy,* 110**,** 163-172.

Fan, L-W, Zhu, Z-Q, Zeng, Y, Lu, Q and Yu, Z-T (2014) "Heat transfer during melting of graphene-based composite phase change materials heated from below" *International Journal of Heat and Mass Transfer,* 79**,** 94-104.

Gil, A, Medrano, M, Martorell, I, Lázaro, A, Dolado, P, Zalba, B and Cabeza, LF (2010) "State of the art on high temperature thermal energy storage for power generation. Part 1—Concepts, materials and modellization" *Renewable and Sustainable Energy Reviews,* 14**,** 31-55.

Han, D, Meng, Z, Wu, D, Zhang, C and Zhu, H (2011) "Thermal properties of carbon black aqueous nanofluids for solar absorption" *Nanoscale research letters,* 6**,** 1.

Harmim, A, Merzouk, M, Boukar, M and Amar, M (2012) "Mathematical modeling of a box-type solar cooker employing an asymmetric compound parabolic concentrator" *Solar Energy,* 86**,** 1673-1682.

Hasnain, S (1998) "Review on sustainable thermal energy storage technologies, Part I: heat storage materials and techniques" *Energy Conversion and Management,* 39**,** 1127-1138.

Hita, I, Arabiourrutia, M, Olazar, M, Bilbao, J, Arandes, JM and Sánchez, PC (2016) "Opportunities and barriers for producing high quality fuels from the pyrolysis of scrap tires" *Renewable and Sustainable Energy Reviews,* 56**,** 745-759.

Karaipekli, A, Sarı, A and Kaygusuz, K (2007) "Thermal conductivity improvement of stearic acid using expanded graphite and carbon fiber for energy storage applications" *Renewable Energy,* 32**,** 2201-2210.

Kibria, M, Anisur, M, Mahfuz, M, Saidur, R and Metselaar, I (2015) "A review on thermophysical properties of nanoparticle dispersed phase change materials" *Energy Conversion and Management,* 95**,** 69-89.

Kumar, V, Shrivastava, R and Untawale, S (2015) "Fresnel lens: a promising alternative of reflectors in concentrated solar power" *Renewable and Sustainable Energy Reviews,* 44**,** 376-390.

Li, M (2013) "A nano-graphite/paraffin phase change material with high thermal conductivity" *Applied energy,* 106**,** 25-30.

Li, M, Chen, M and Wu, Z (2014a) "Enhancement in thermal property and mechanical property of phase change microcapsule with modified carbon nanotube" *Applied Energy,* 127**,** 166-171.

Li, T, Lee, J-H, Wang, R and Kang, YT (2014b) "Heat transfer characteristics of phase change nanocomposite materials for thermal energy storage application" *International Journal of Heat and Mass Transfer,* 75**,** 1-11.

Long, CM, Nascarella, MA and Valberg, PA (2013) "Carbon black vs. black carbon and other airborne materials containing elemental carbon: Physical and chemical distinctions" *Environmental pollution,* 181**,** 271-286.

Magasinski, A, Dixon, P, Hertzberg, B, Kvit, A, Ayala, J and Yushin, G (2010) "High-performance lithium-ion anodes using a hierarchical bottom-up approach" *Nature materials,* 9**,** 353-358.

Mahian, O, Kianifar, A, Kalogirou, SA, Pop, I and Wongwises, S (2013) "A review of the applications of nanofluids in solar energy" *International Journal of Heat and Mass Transfer,* 57**,** 582-594.

Maquin, B, Goyhénèche, J-M, Derré, A, Trinquecoste, M, Chadeyron, P and Delhaès, P (2000) "Thermal conductivity of submicrometre particles: carbon blacks and solid solutions containing C, B and N" *Journal of Physics D: Applied Physics,* 33**,** 8.

Martínez, J, Murillo, R and García, T (2013) "Production of carbon black from the waste tires pyrolysis".

Mills, A, Farid, M, Selman, J and Al-Hallaj, S (2006) "Thermal conductivity enhancement of phase change materials using a graphite matrix" *Applied Thermal Engineering,* 26**,** 1652-1661.

Motahar, S, Nikkam, N, Alemrajabi, AA, Khodabandeh, R, Toprak, MS and Muhammed, M (2014) "A novel phase change material containing mesoporous silica nanoparticles for thermal storage: a study on thermal conductivity and viscosity" *International Communications in Heat and Mass Transfer,* 56**,** 114-120.

Nkwetta, DN and Haghighat, F (2014) "Thermal energy storage with phase change material—a state-of-the art review" *Sustainable Cities and Society,* 10**,** 87-100.

Pierson, HO 1993. Handbook of carbon, graphite, diamond, and fullerenes : properties, processing, and applications. Park Ridge, N.J. :: Noyes Publications.

Pincemin, S, Olives, R, Py, X and Christ, M (2008) "Highly conductive composites made of phase change materials and graphite for thermal storage" *Solar Energy Materials and Solar Cells,* 92**,** 603-613.

Pritchard, G (1998) *Plastics additives : an A-Z reference*, Chapman & Hall*,* London.

Quaschning, V and Muriel, MB (2002) "Solar power-photovoltaics or solar thermal power plants?" *VGB POWERTECH-INTERNATIONAL EDITION-,* 82**,** 48-52.

Rohsenow, WM, Hartnett, JP and Cho, YI (1998) *Handbook of Heat Transfer*, McGraw-Hill Education*,* New York.

Royal Philips (2013) "MASTER MHN-SE 2000W/956 GX22 400V HO Product Data Sheet".

Şahan, N, Fois, M and Paksoy, H (2015) "Improving thermal conductivity phase change materials—a study of paraffin nanomagnetite composites" *Solar Energy Materials and Solar Cells,* 137**,** 61-67.

Saidur, R, Meng, T, Said, Z, Hasanuzzaman, M and Kamyar, A (2012) "Evaluation of the effect of nanofluid-based absorbers on direct solar collector" *International Journal of Heat and Mass Transfer,* 55**,** 5899-5907.

Salunkhe, PB and Shembekar, PS (2012) "A review on effect of phase change material encapsulation on the thermal performance of a system" *Renewable and Sustainable Energy Reviews,* 16**,** 5603-5616.

Sarı, A and Karaipekli, A (2007) "Thermal conductivity and latent heat thermal energy storage characteristics of paraffin/expanded graphite composite as phase change material" *Applied Thermal Engineering,* 27**,** 1271-1277.

Sari, A and Kaygusuz, K (2001) "Thermal energy storage system using stearic acid as a phase change material" *Solar Energy,* 71**,** 365-376.

Sarı, A, Sarı, H and Önal, A (2004) "Thermal properties and thermal reliability of eutectic mixtures of some fatty acids as latent heat storage materials" *Energy conversion and management,* 45**,** 365-376.

Sciacovelli, A, Guelpa, E and Verda, V (2014) "Second law optimization of a PCM based latent heat thermal energy storage system with tree shaped fins" *International Journal of Thermodynamics,* 17**,** 145-154.

Sharma, R, Ganesan, P, Tyagi, V, Metselaar, H and Sandaran, S (2015) "Developments in organic solid–liquid phase change materials and their applications in thermal energy storage" *Energy Conversion and Management,* 95**,** 193-228.

Sigma-Aldrich (2017) "Nanomaterials", http://www.sigmaaldrich.com/materials-science/nanomaterials/nanomaterials-products.html [2017, January 12].

Sircar, AK and Wells, JL (1982) "Thermal conductivity of elastomer vulcanizates by differential scanning calorimetry" *Rubber Chemistry and Technology,* 55**,** 191-207.

Smith, YR, Bhattacharyya, D, Willhard, T and Misra, M (2016) "Adsorption of aqueous rare earth elements using carbon black derived from recycled tires" *Chemical Engineering Journal,* 296**,** 102-111.

Suri, M, Cebecauer, T, Meyer, A and Van Niekerk, J. Accuracy-enhanced solar resource maps of South Africa. 2015. 3rd Southern African Solar Energy Conference, South Africa, 11-13 May, 2015.

Taylor, RA, Phelan, PE, Otanicar, TP, Adrian, R and Prasher, R (2011) "Nanofluid optical property characterization: towards efficient direct absorption solar collectors" *Nanoscale research letters,* 6**,** 1-11.

Trelles, JP and Dufly, JJ (2003) "Numerical simulation of porous latent heat thermal energy storage for thermoelectric cooling" *Applied Thermal Engineering,* 23**,** 1647-1664.

Trieb, F, Schillings, C, O'sullivan, M, Pregger, T and Hoyer-Klick, C (2009) "Global potential of concentrating solar power", paper presented at *SolarPACES,* 15-18 September, 2009, Berlin, Germany.

Velraj, R, Seeniraj, R, Hafner, B, Faber, C and Schwarzer, K (1997) "Experimental analysis and numerical modelling of inward solidification on a finned vertical tube for a latent heat storage unit" *Solar Energy,* 60**,** 281-290.

Yi, H-L, Wang, C-H, Tan, H-P and Zhou, Y (2012) "Radiative heat transfer in semitransparent solidifying slab considering space–time dependent refractive index" *International Journal of Heat and Mass Transfer,* 55**,** 1724-1731.

Zhang, Z and Fang, X (2006) "Study on paraffin/expanded graphite composite phase change thermal energy storage material" *Energy Conversion and Management,* 47**,** 303-310.

8. Appendix A

Thomas algorithm:

The system of equations gives a tridiagonal matrix as represented below:

$$\begin{bmatrix} b_1 & c_1 & 0 & 0 & 0 & 0 \\ a_2 & b_2 & c_2 & 0 & 0 & 0 \\ 0 & a_3 & b_3 & c_3 & 0 & 0 \\ 0 & 0 & a_4 & b_4 & c_4 & 0 \\ 0 & 0 & 0 & a_5 & b_5 & c_5 \\ 0 & 0 & 0 & 0 & a_6 & b_6 \end{bmatrix} \begin{bmatrix} x_1 \\ x_2 \\ x_3 \\ x_4 \\ x_5 \\ x_6 \end{bmatrix} = \begin{bmatrix} r_1 \\ r_2 \\ r_3 \\ r_4 \\ r_5 \\ r_6 \end{bmatrix}$$

The tridiagonal matrix is then converted to the form as shown below, by starting at the first row and moving downwards.

$$\begin{bmatrix} 1 & \gamma_1 & 0 & 0 & 0 & 0 \\ 0 & 1 & \gamma_2 & 0 & 0 & 0 \\ 0 & 0 & 1 & \gamma_3 & 0 & 0 \\ 0 & 0 & 0 & 1 & \gamma_4 & 0 \\ 0 & 0 & 0 & 0 & 1 & \gamma_5 \\ 0 & 0 & 0 & 0 & 0 & 1 \end{bmatrix} \begin{bmatrix} x_1 \\ x_2 \\ x_3 \\ x_4 \\ x_5 \\ x_6 \end{bmatrix} = \begin{bmatrix} \rho_1 \\ \rho_2 \\ \rho_3 \\ \rho_4 \\ \rho_5 \\ \rho_6 \end{bmatrix}$$

This new matrix is then trivial to solve, starting from the bottom row and moving up.

This process of solving tridiagonal matrices is known as the Thomas algorithm.

9. Appendix B

All of the data for the novel UV-vis solar simulator experiments are given in Table 9-1.

Table 9-1: Radiation (W/m^2) passing through a certain depth of liquid at certain carbon black concentrations

	Height (mm)			
Run	6.5 mm	14 mm	26 mm	39mm
0 % CB	882	882	1065	1160
0.01 % CB	345	196	62	24
0.03 % CB	99	38	14	12
0.05 % CB	37	18	12	11
0.1 % CB	17	12	10	10
0.5 % CB	15	13	12	12
1 % CB	12	10	10	10
3 % CB	13	11	11	11
5 % CB	10	9	10	10

Figure 9-1 shows that the amount of radiation passing through a certain length of liquid PCM composite. The amount of radiation passing through the liquid sample decreased substantially for an increase in carbon black percentages. For all of the concentrations tested the maximum length that the radiation can still go through was less than 40 mm. Almost no radiation passes through the PCM composite with carbon black percentages of more than 0.05 %, even at a liquid layer depth of only 6.5 mm.

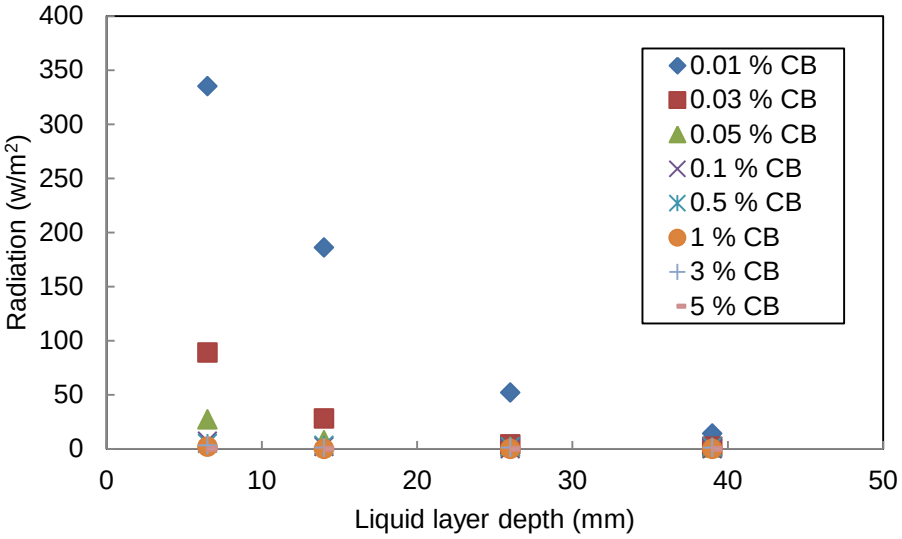

Figure 9-1: Radiation passing through a certain depth of PCM composites.

10. Appendix C

Figure 10-1 shows that the latent heat of melting decreased with an increase in carbon black concentration up to a certain concentration, followed by an increase in the latent heat before eventually showing a constant linear decrease in the latent heat.

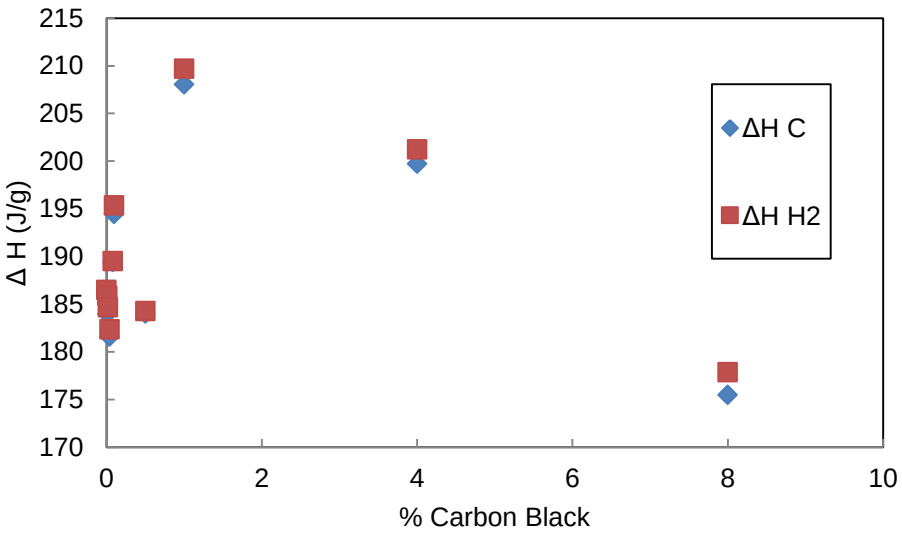

Figure 10-1: Latent heat of cooling and the latent heat of the second melting cycle.

Figure 10-2 shows a closer look at the lower concentration carbon black experiments from Figure 10-1, showing the decrease and eventual increase in latent heat of the composite.

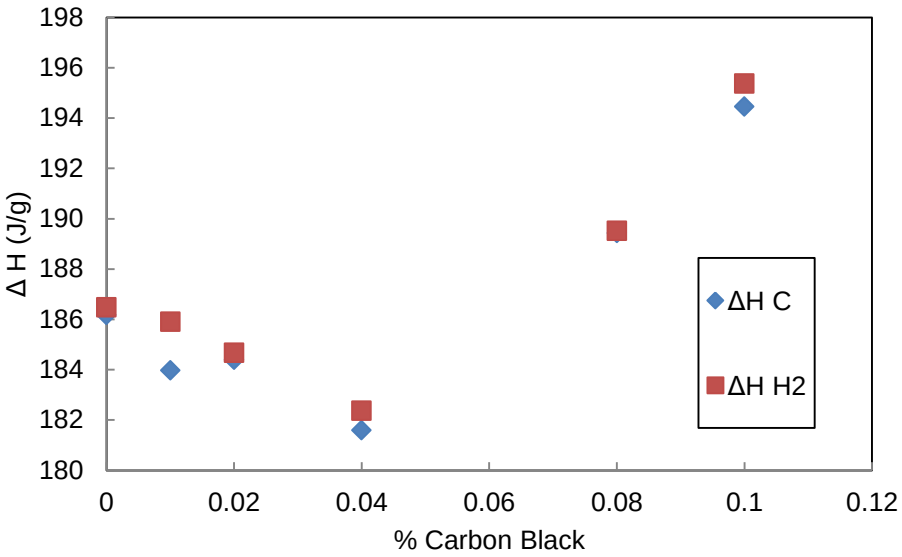

Figure 10-2 Latent heat of cooling and the latent heat of the second melting cycle of the low carbon black concentrations.

Figure 10-3 and Figure 10-4 show that the increase in carbon black had no significant effect on the melting/solidifying onset temperature or the peak temperature of the PCM/PCM composite.

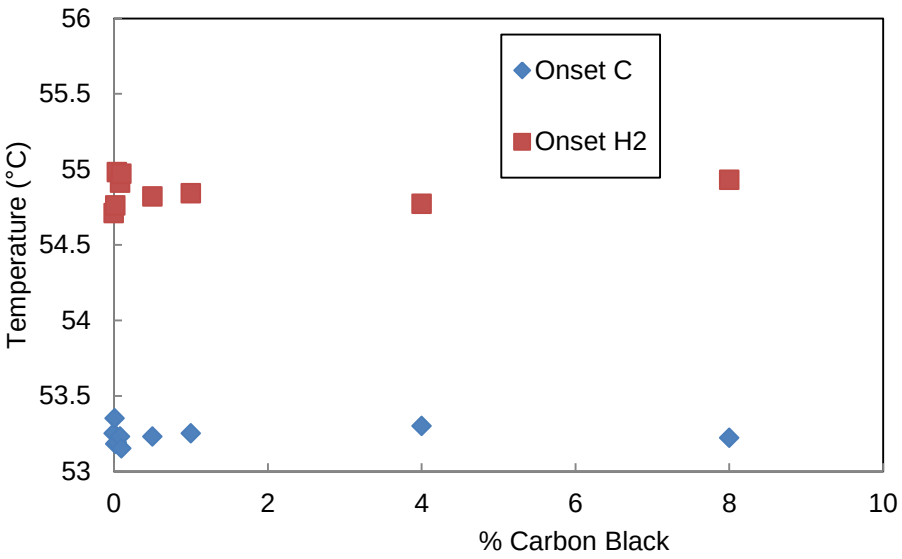

Figure 10-3: Onset temperature of cooling and the onset temperature of the second melting cycle.

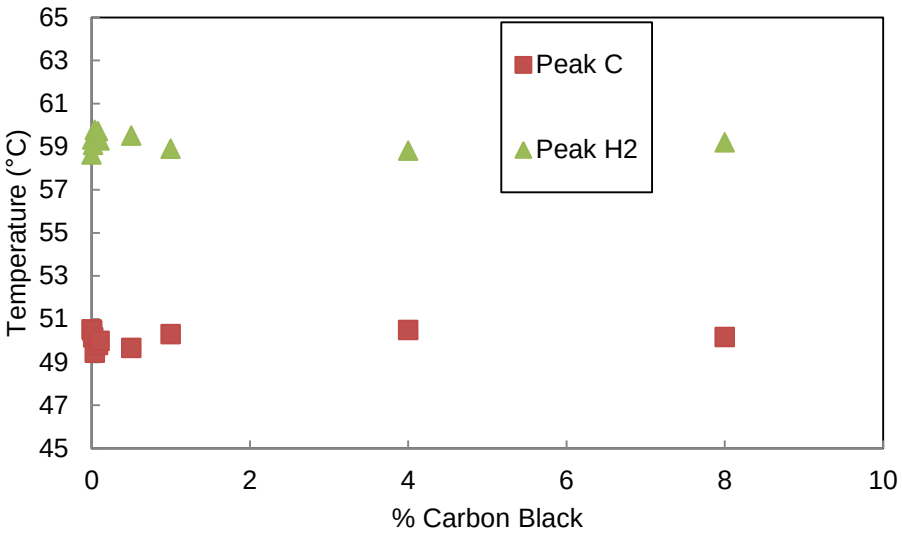

Figure 10-4: Peak temperature of cooling and the peak temperature of the second melting cycle.

The DSC curves can be seen in Figure 10-5 to Figure 10-13

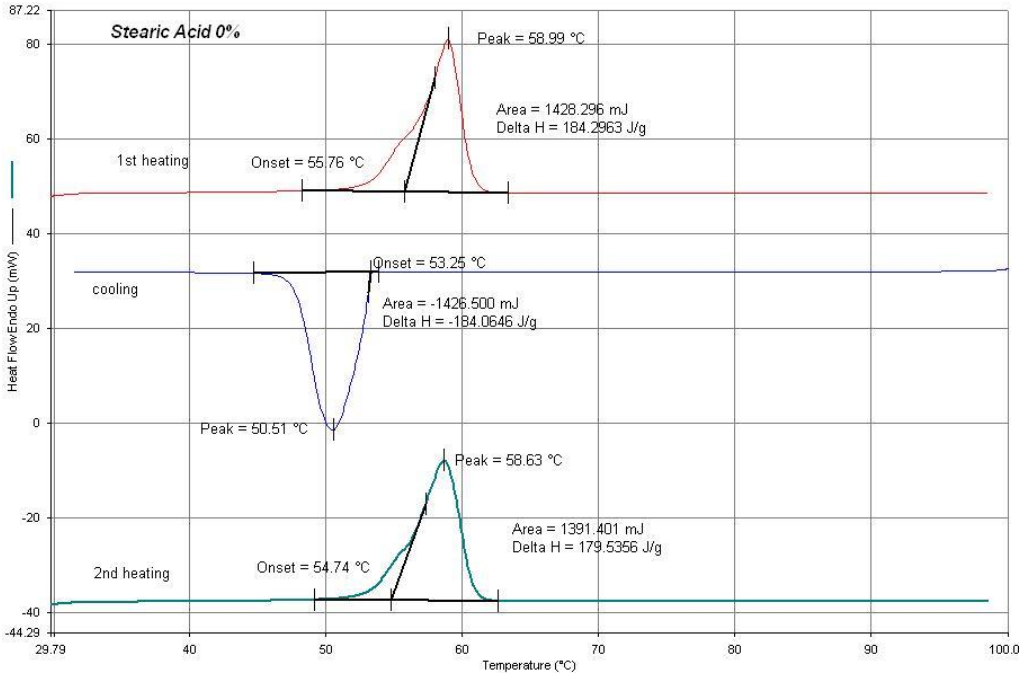

Figure 10-5: Stearic acid with 0 % Carbon black added.

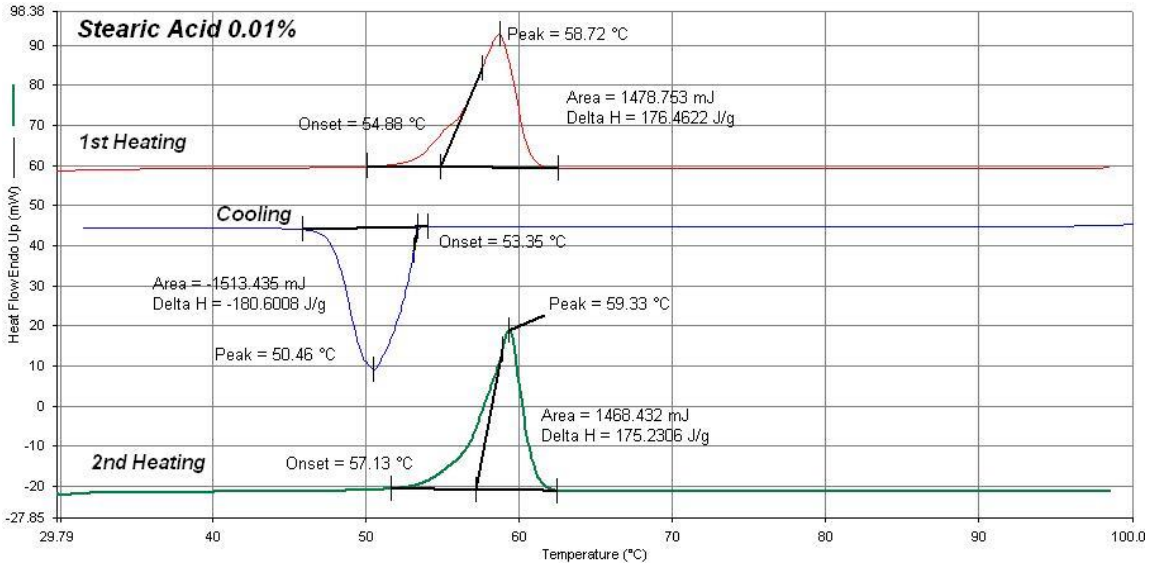

Figure 10-6: Stearic acid with 0.01 % Carbon black added.

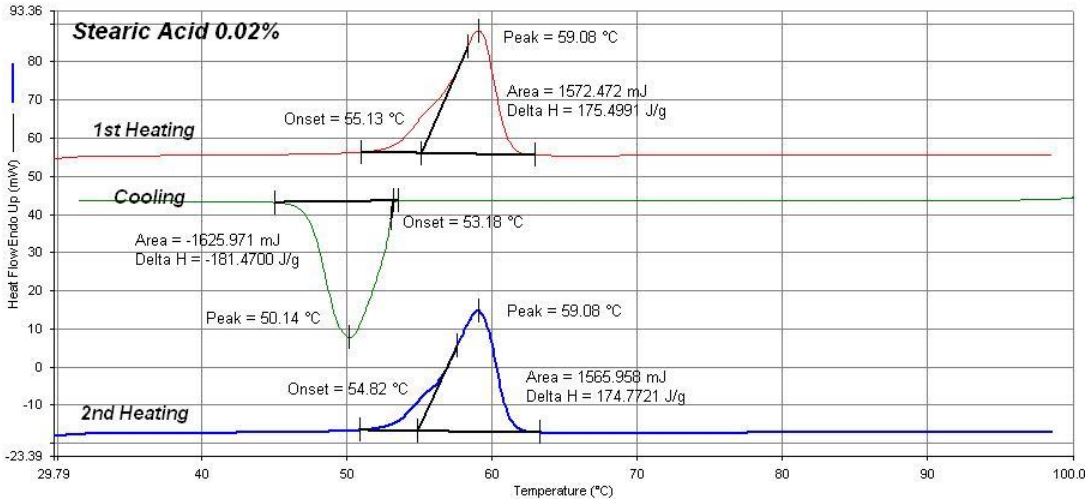

Figure 10-7: Stearic acid with 0.02 % Carbon black added.

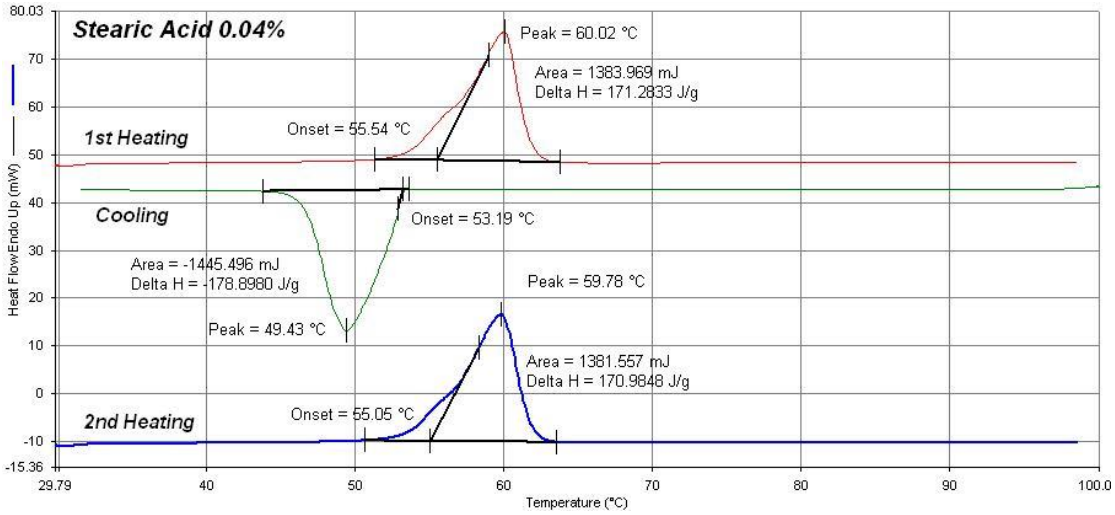

Figure 10-8: Stearic acid with 0.04 % Carbon black added.

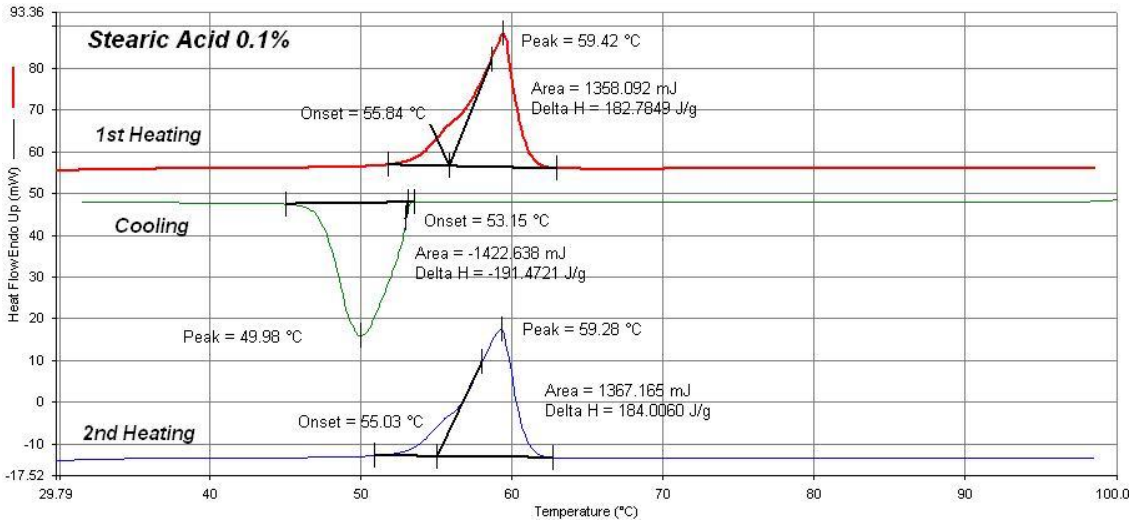

Figure 10-9: Stearic acid with 0.1 % Carbon black added.

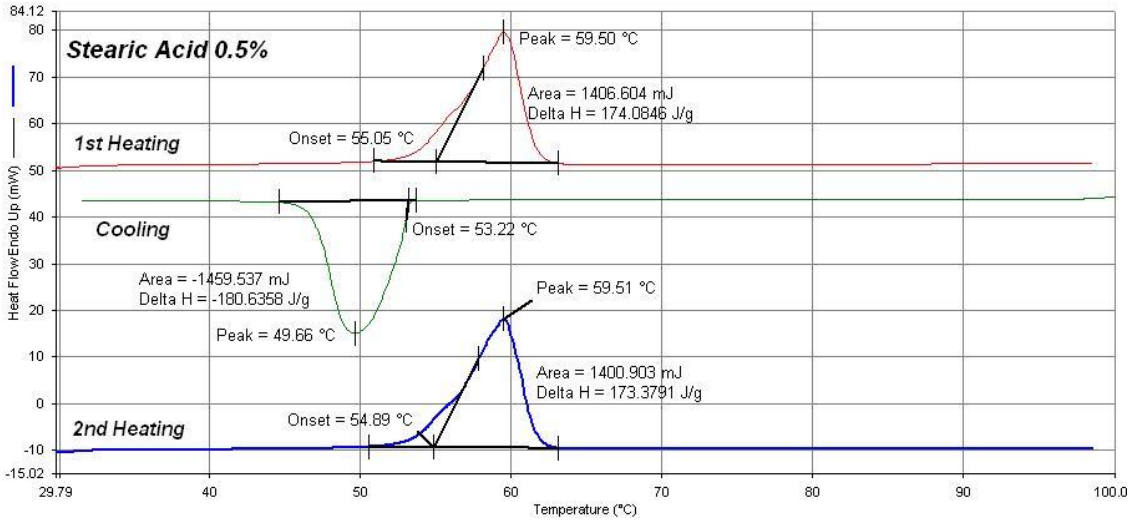

Figure 10-10: Stearic acid with 0.5 % Carbon black added.

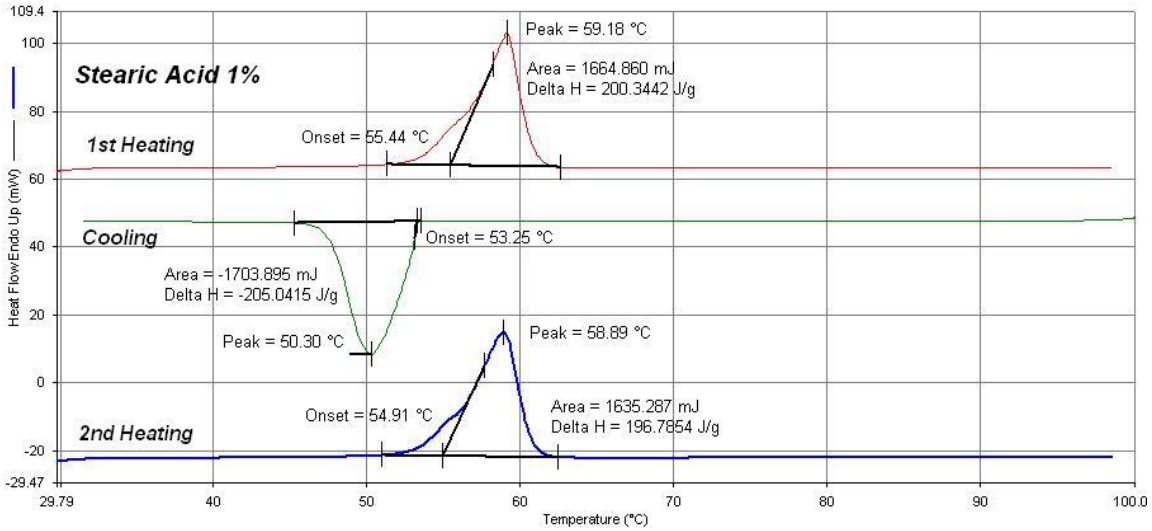

Figure 10-11: Stearic acid with 1 % Carbon black added.

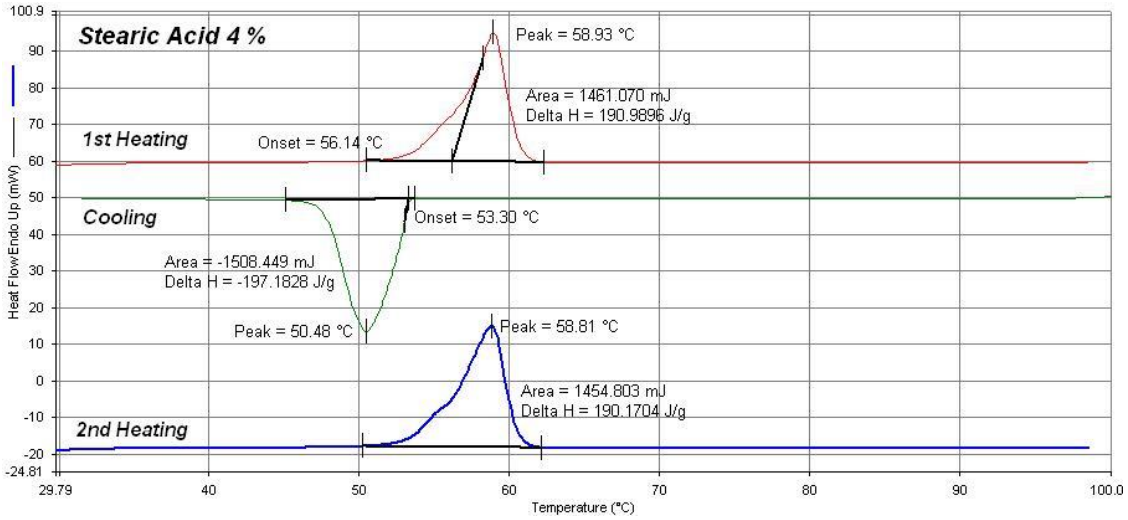

Figure 10-12: Stearic acid with 4 % Carbon black added.

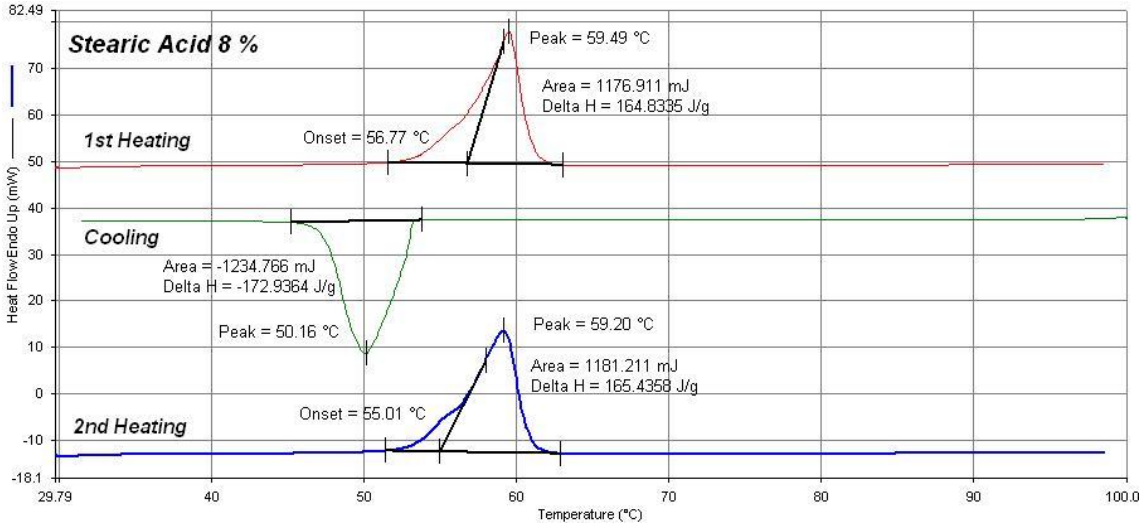

Figure 10-13: Stearic acid with 8 % Carbon black added.

Figure 10-14 shows the effect of 100 freezing/melting cycles on the stability of the PCM/PCM-composite. The data from the 100 heating/cooling cycles for each PCM composite were superimposed on each other and show good stability.

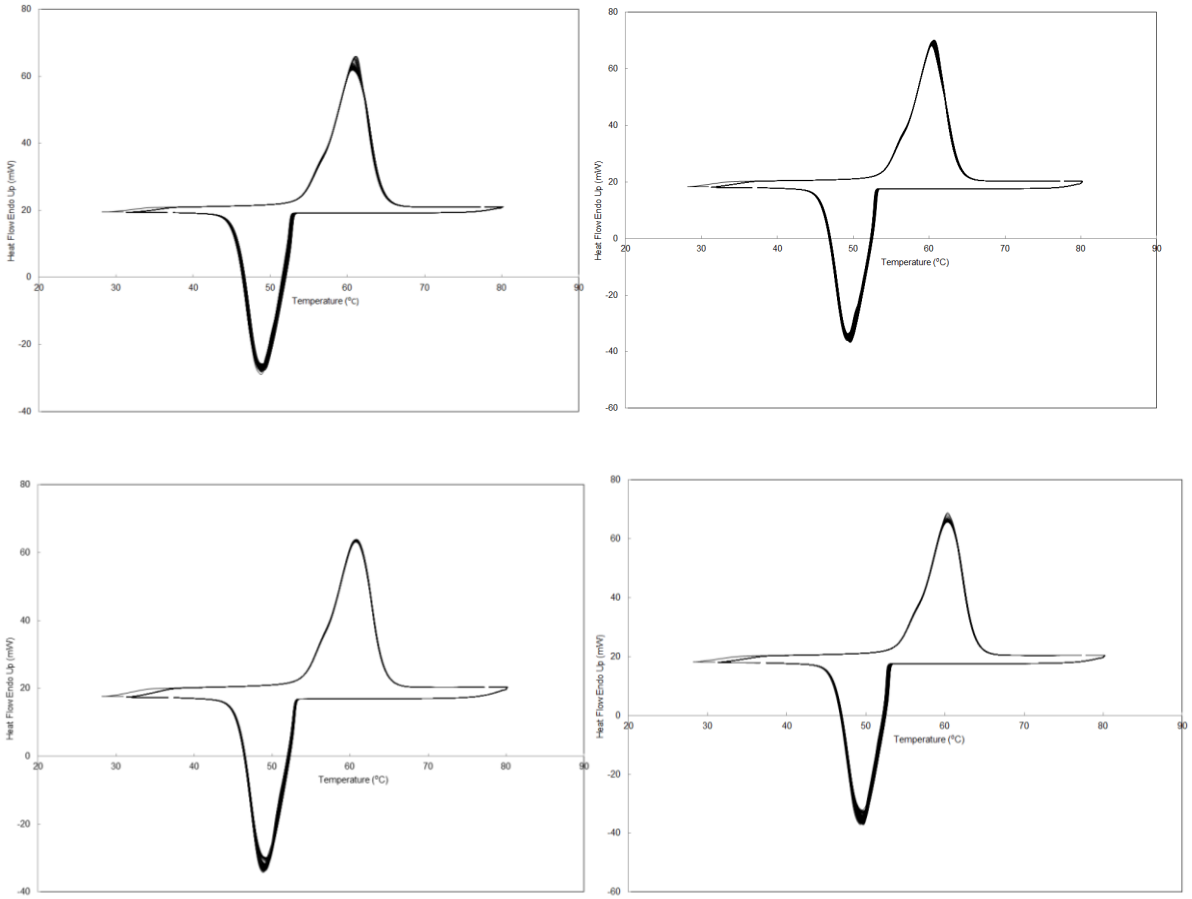

Figure 10-14: 100 consecutive heating and cooling cycles of: the PCM and 0 % carbon black (top left), 0.08 % carbon black (top right), 0.5 % carbon black (bottom left) and 1 % carbon black (bottom right).

11. Appendix D

The complete small scale experimental run for all of the carbon black concentrations can be seen in Figure 11-1.

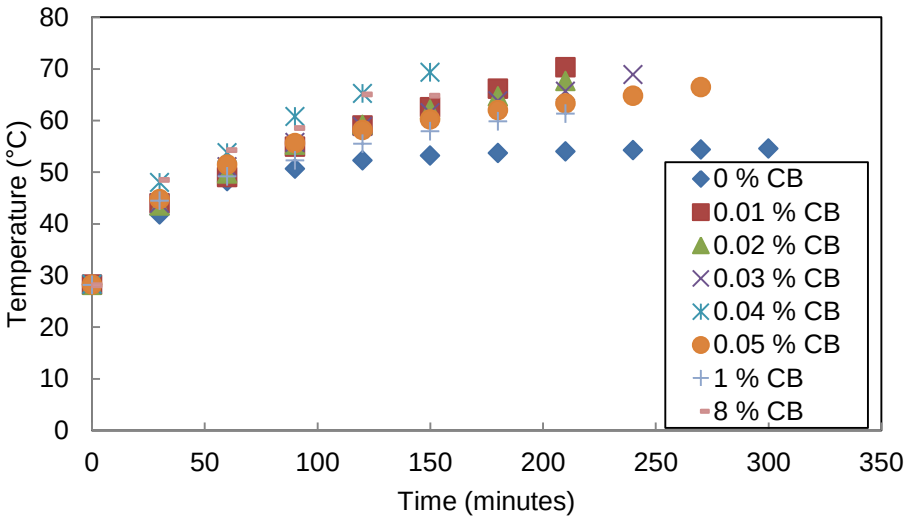

Figure 11-1: Temperature profile of the small scale experimental run.

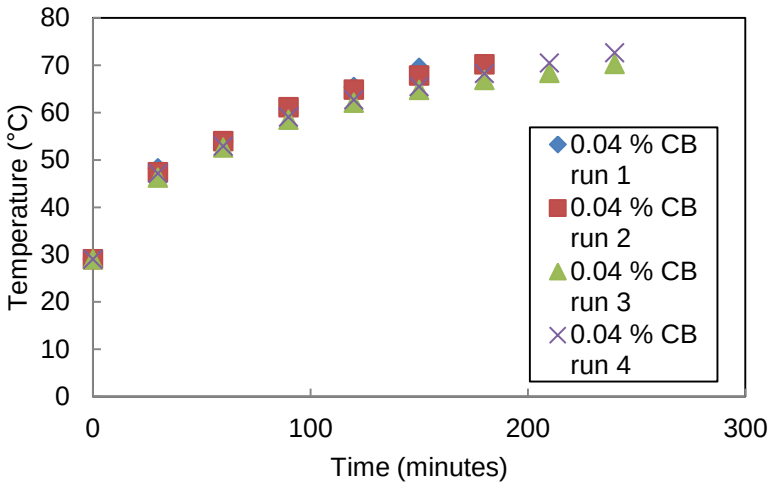

Figure 11-2: small scale experiment with 0.04 % carbon black showed good repeatability over multiple runs.

A summary of the experiments are shown in Figure 11-3. All of the runs with carbon black added performed better than the pure PCM run, with the 0.04 % carbon black loading providing the fastest temperature increase. After 150 minutes the temperature of the 0.04 % carbon black composite was around 30 % higher than that of the pure PCM, while the other low concentrations carbon black were around 20 % higher than that of the pure PCM.

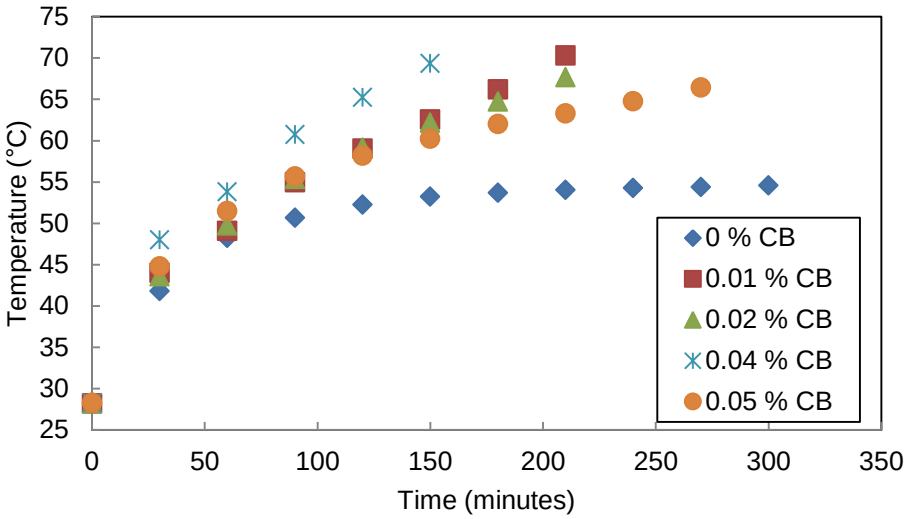

Figure 11-3: The four experiments with the fastest temperature increase are plotted together with the pure PCM run for the small scale experiment.

Figure 11-4 shows the temperature of each experiment at 30 minute intervals. The temperature of the PCM composites increases quickly at the start and then slows down, with the 0.04 % carbon black composite clearly showing the fastest temperature increase.

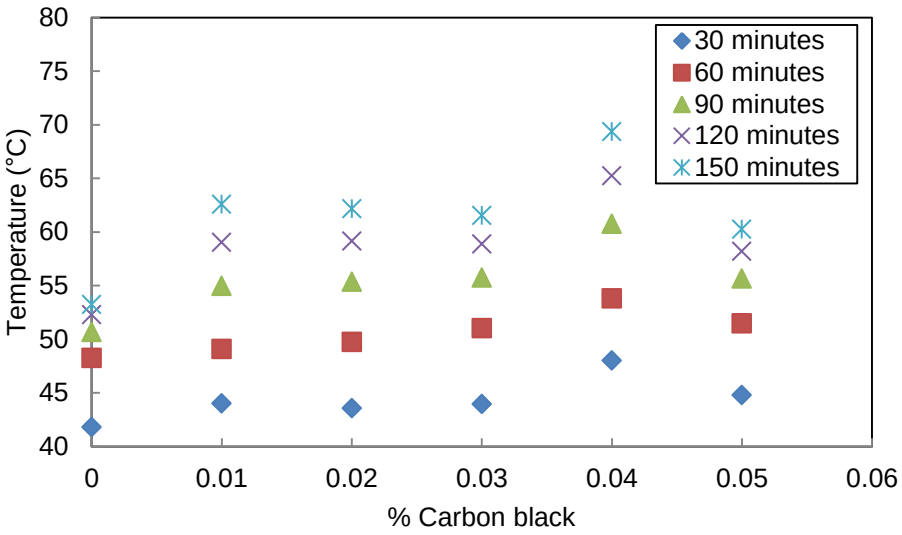

Figure 11-4: The temperature of the carbon black composites are shown after 30 minute intervals.

12. Appendix E

The complete large scale experimental run for all of the carbon black concentrations and all of the thermocouples can be seen in Figure 12-1 to Figure 12-4.

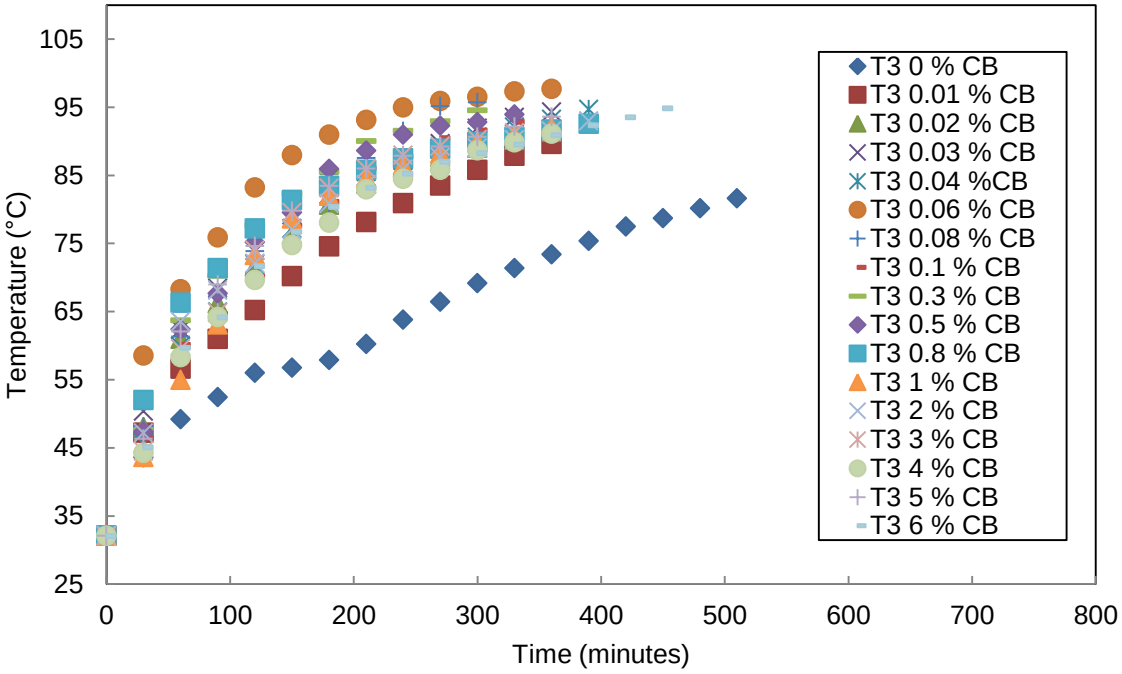

Figure 12-1: Large scale experimental run as measured by Thermocouple 3.

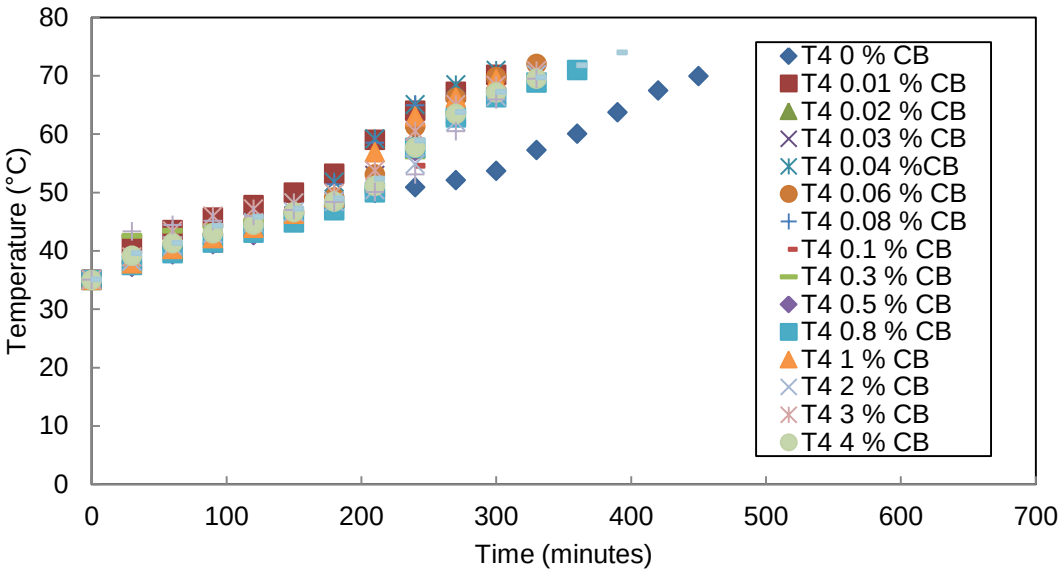

Figure 12-2: Large scale experimental run as measured by Thermocouple 4.

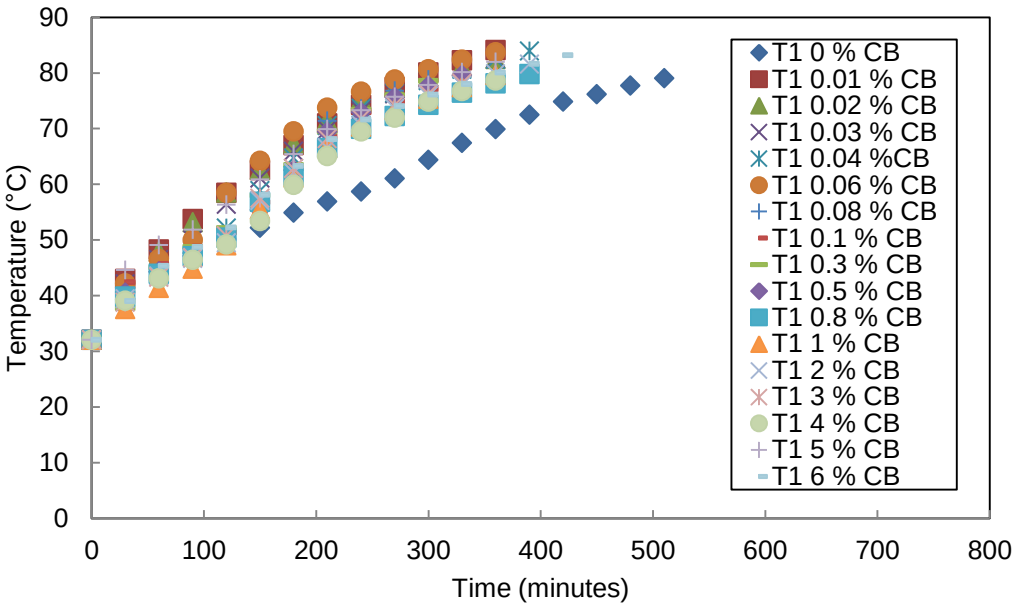

Figure 12-3: Large scale experimental run as measured by Thermocouple 1.

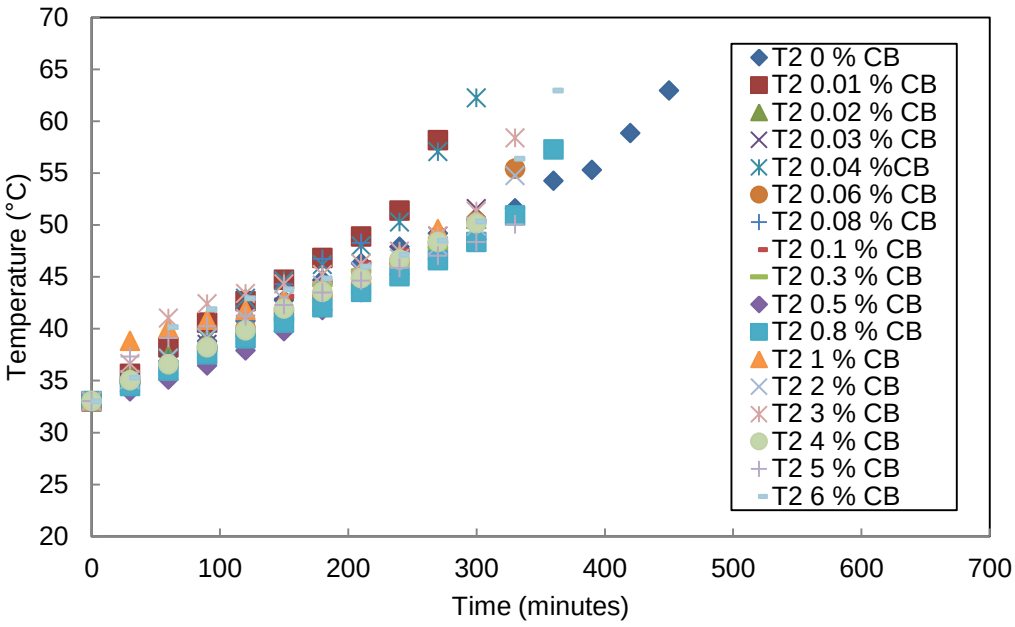

Figure 12-4: Large scale experimental run as measured by Thermocouple 2.

The colour of the solid and liquid phase of the 0.03 % composite is similar to that of the 0.02 % carbon black composite and has good dispersion, as seen in Figure 12-5. Multiple runs also showed small deviations and good repeatability as seen in Figure 12-6 and Figure 12-7.

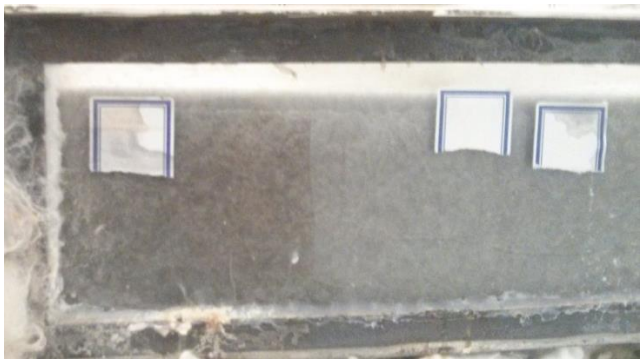

Figure 12-5: 0.03 % carbon black showing the top view of the liquid phase (top left), top view of the solid phase (top right) and side view of the solid phase (bottom).

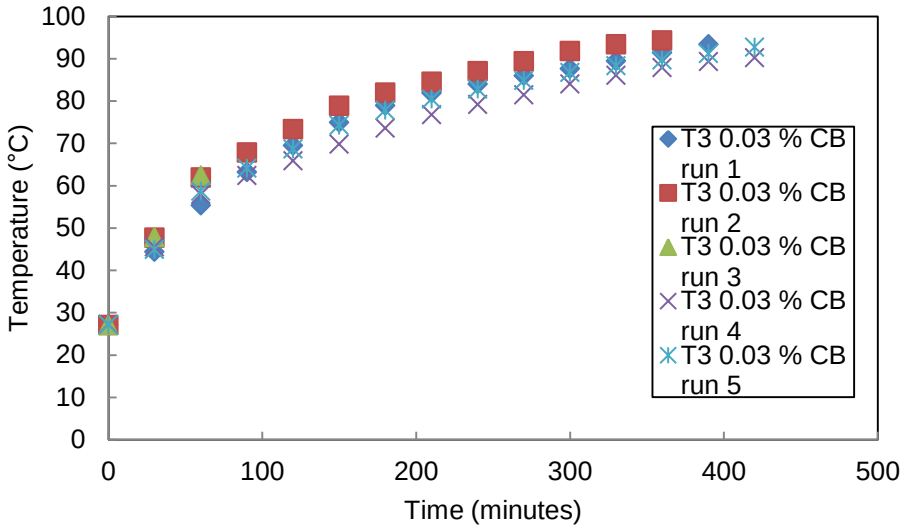

Figure 12-6: Temperature change over time of the 0.03 % carbon black composite, measured at Thermocouple 3.

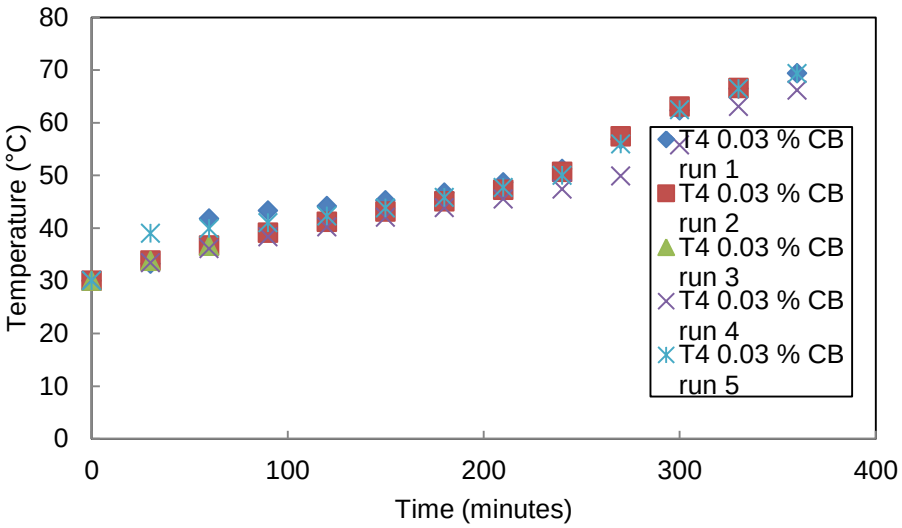

Figure 12-7: Temperature change over time of the 0.03 % carbon black composite, measured at Thermocouple 4.

Multiple runs also showed small deviations and good repeatability as seen in Figure 12-8 and Figure 12-9. Figure 12-8 also shows that the carbon black made the PCM black enough that the thermocouples are no longer visible and the liquid appears opaque

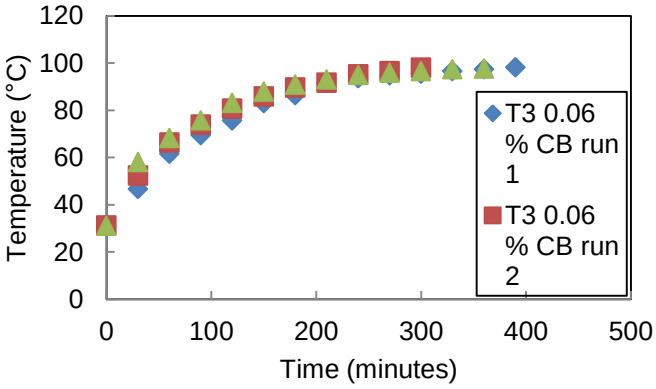

Figure 12-8: Temperature change over time of the 0.06 % carbon black composite, measured at Thermocouple 3 (left) and a photo showing the colour of the 0.06 % carbon black composite (right).

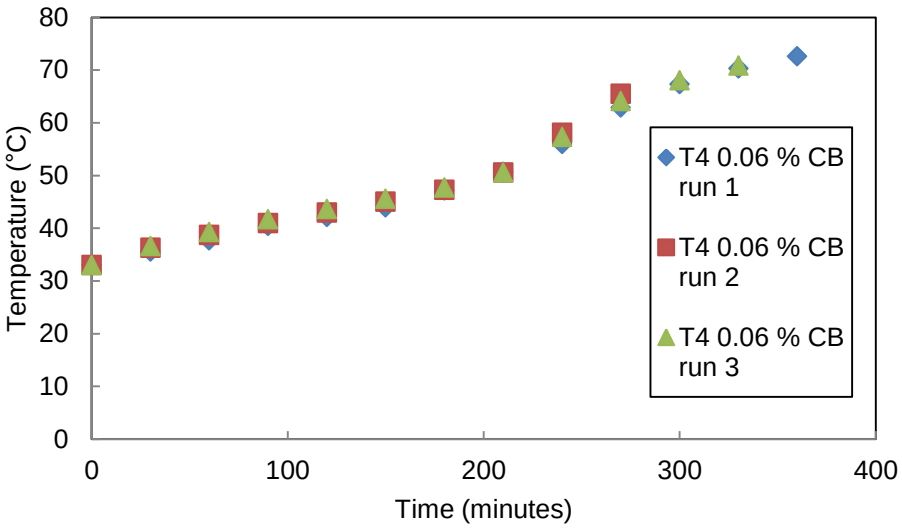

Figure 12-9: Temperature change over time of the 0.06 % carbon black composite, measured at Thermocouple 4.

Multiple runs also showed small deviations and good repeatability, even at higher concentrations as seen in Figure 12-10 and Figure 12-11.

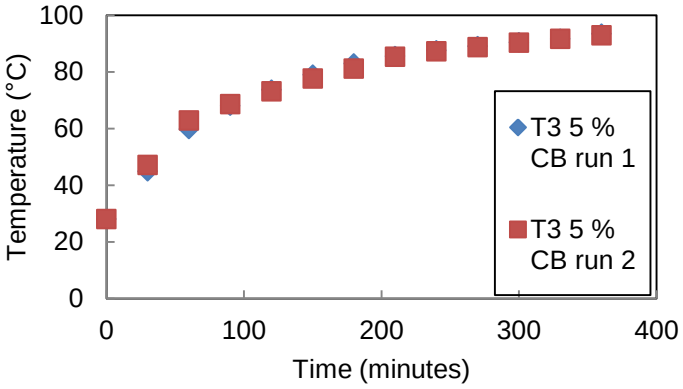

Figure 12-10: Temperature change over time of the 5 % carbon black composite, measured at Thermocouple 3.

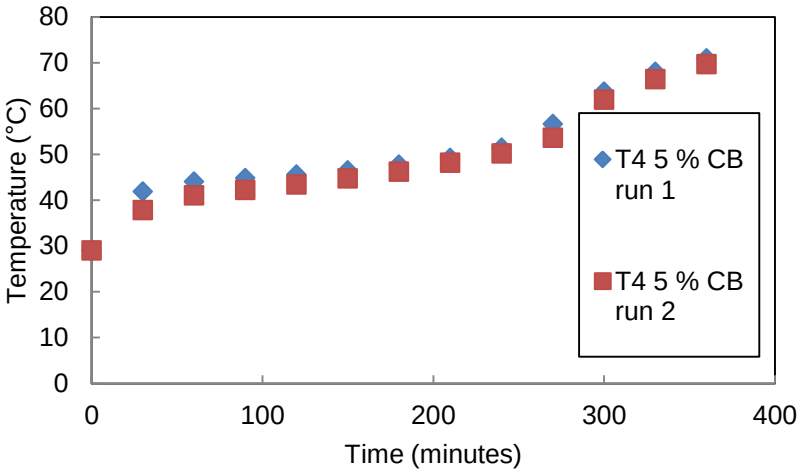

Figure 12-11: Temperature change over time of the 5 % carbon black composite, measured at Thermocouple 4.

Figure 12-12 show that fastest increase in temperature was achieved with very low carbon black concentrations (0.01 % to 0.06 %).

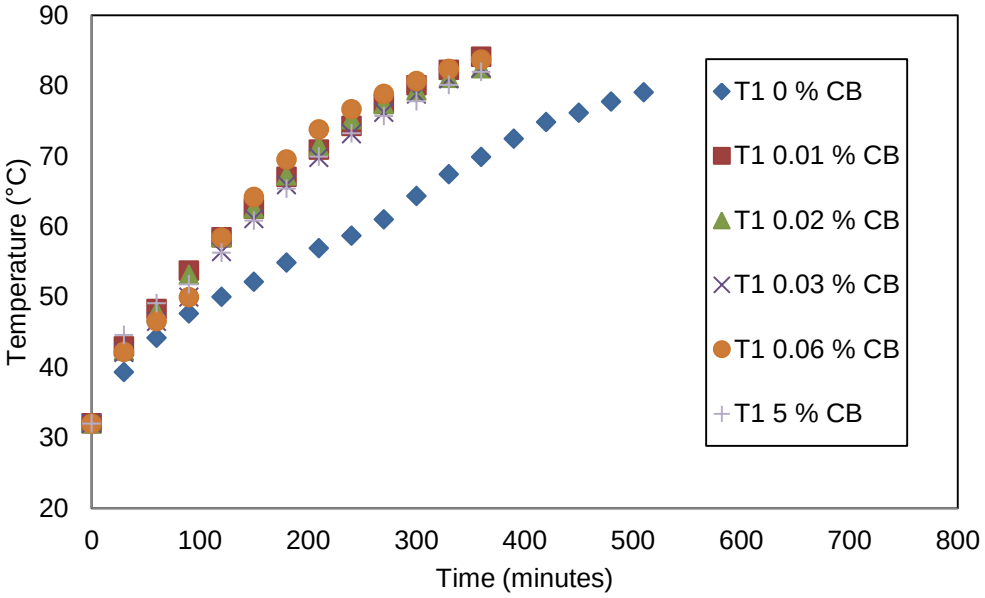

Figure 12-12: Temperature change over time of the PCM and PCM composites as measured by thermocouple 1.

Temperature 2 is measured slightly lower than Temperature 4 (both significantly lower than Temperature 1 and Temperature 3). Temperature 2 showed the slowest temperature increase and the smallest improvement from the pure PCM run. Figure 12-13 shows the 0.01 % and 0.04 % carbon black runs, which had a much larger improvement compared to any other run.

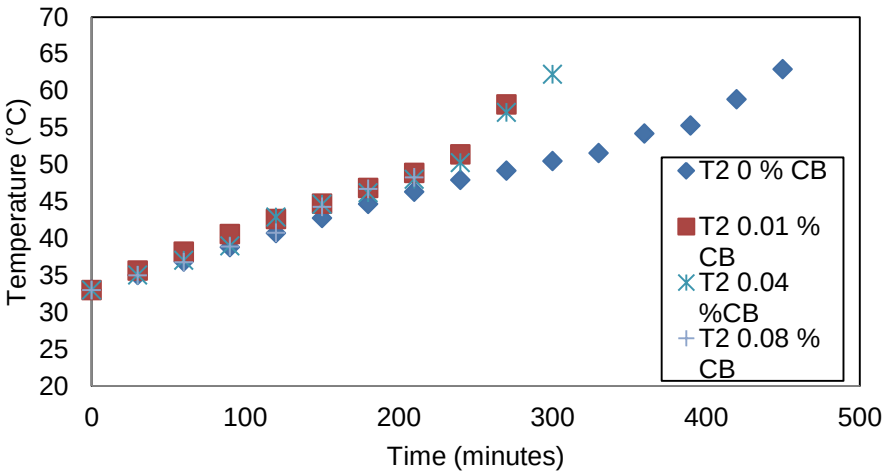

Figure 12-13: Temperature change over time of the PCM and PCM composites as measured by thermocouple 2.

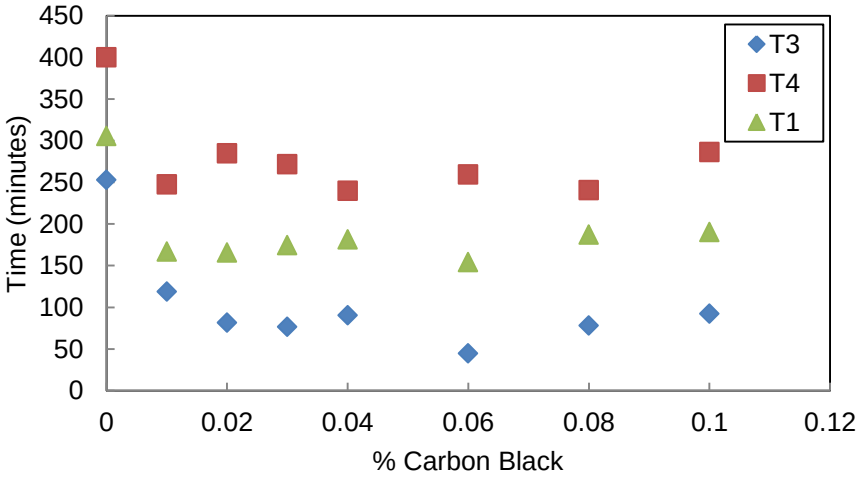

Figure 12-14: Time it took different thermocouple readings (and therefore different depths) to reach 65 ^{0}C at specific carbon black loadings.

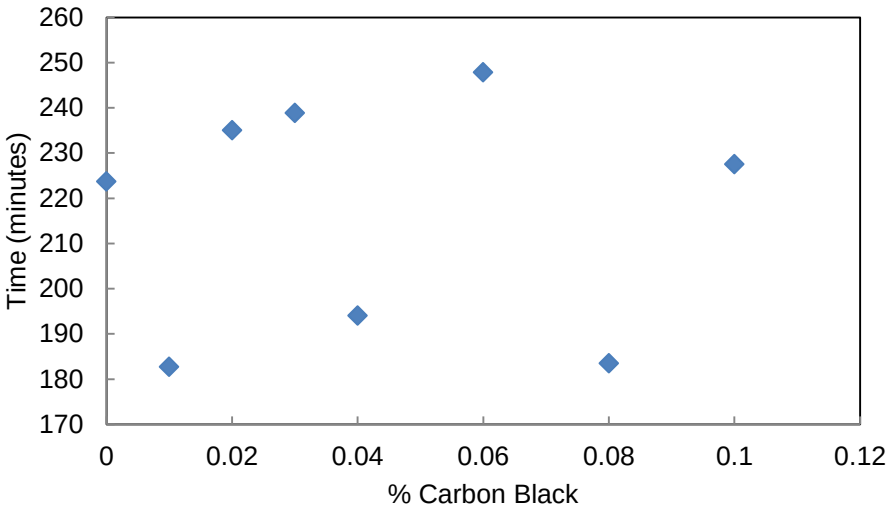

Figure 12-15: Time it took for Temperature 2 to reach 47 ^{0}C at specific carbon black loadings.

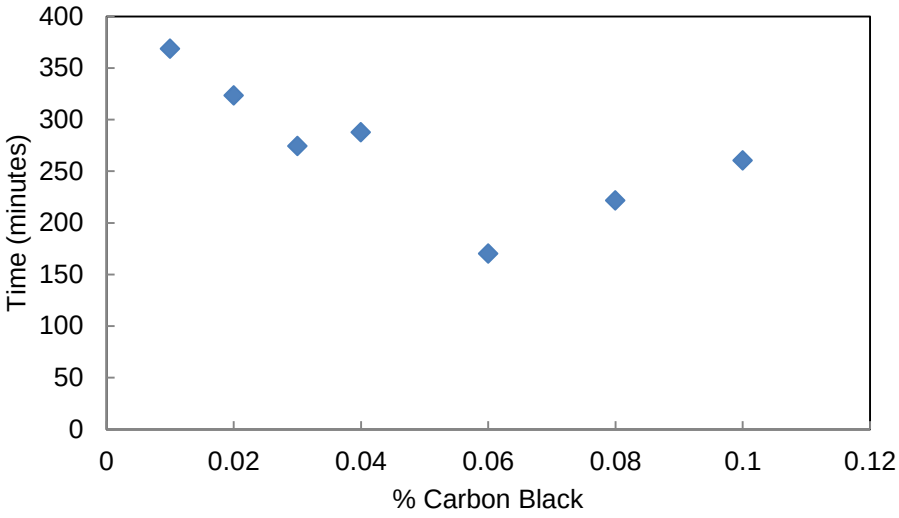

Figure 12-16: Time it took for Temperature 3 to reach 90 ^{0}C at specific carbon black loadings.

The temperature difference between each run and the pure PCM is shown in Figure 12-17, the difference in temperature increases, reaches a peak and then decreases.

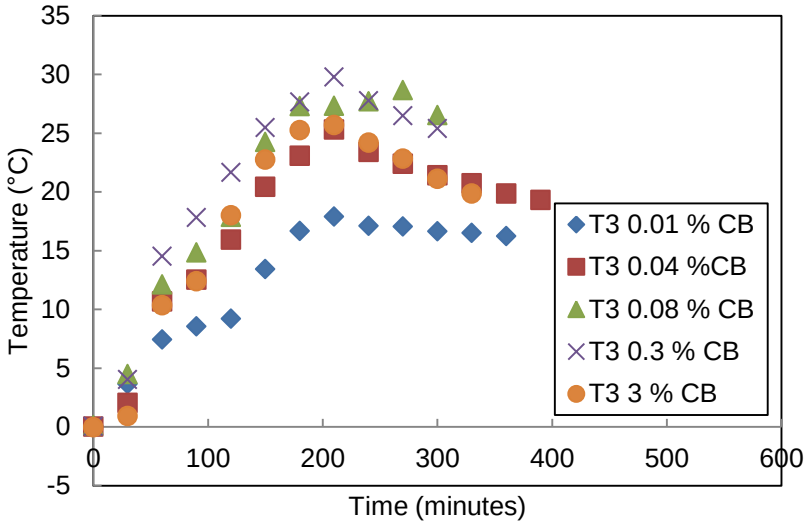

Figure 12-17: Temperature difference between the carbon black composite and the pure PCM, with a peak at 200 minutes.

The time it takes to reach the peak temperature changes with each thermocouple reading.

The largest temperature difference for temperature 3 is after 200 minutes, for temperature 1 after 250 minutes, for temperature 4 after 300 minutes, and for temperature 2 after more than 300 minutes. The time it takes to reach this peak temperature takes longer the further down the temperature measurement is. This shows that the time it took the PCM to reach its most effective point differs depending on the size/depth of the PCM.

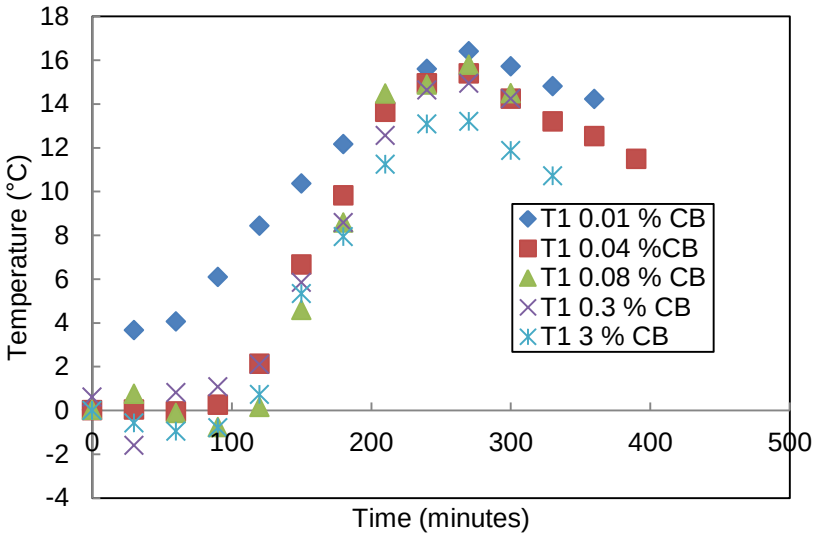

Figure 12-18: Temperature difference between the carbon black composite and the pure PCM, with a peak at 250 minutes.

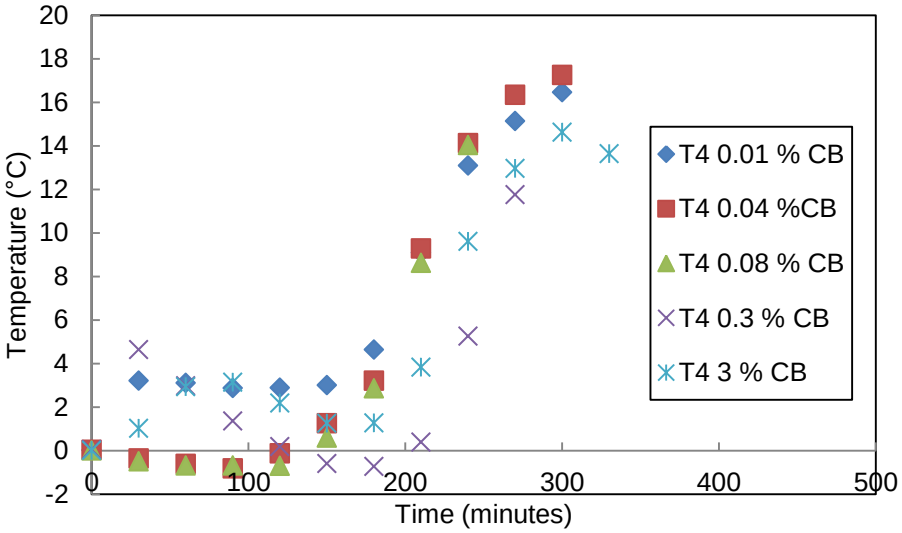

Figure 12-19: Temperature difference between the carbon black composite and the pure PCM, with a peak at 300 minutes.

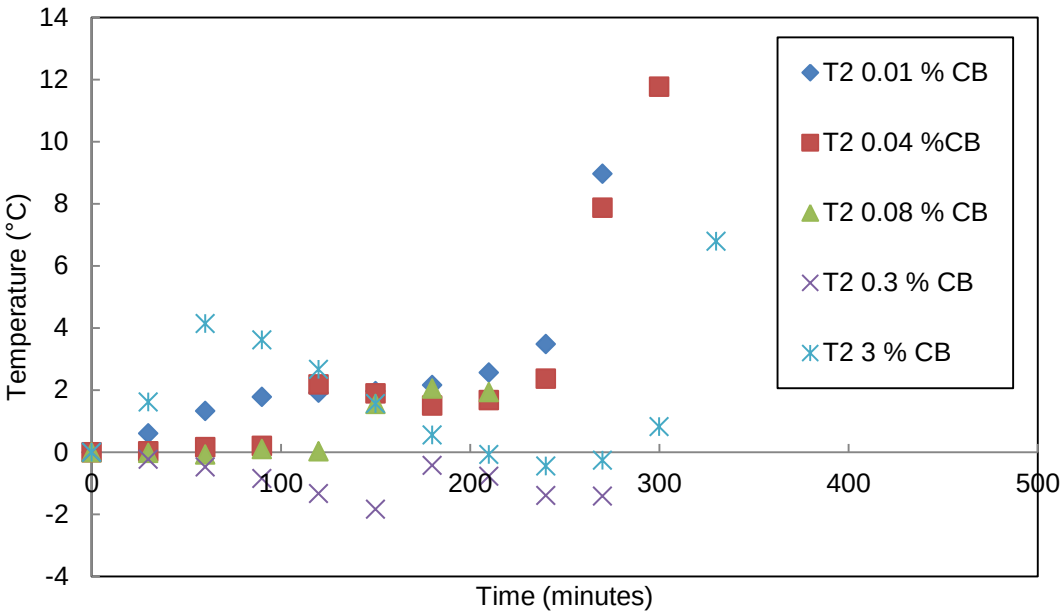

Figure 12-20: Temperature difference between the carbon black composite and the pure PCM, with a peak at more than 300 minutes.

The temperatures of various carbon black concentrations at 1 hour intervals are plotted for Thermocouple 3 on Figure 12-21 and Figure 12-22. Similarly the temperatures of various runs for Thermocouple 4 are shown in Figure 12-23 and Figure 12-25.

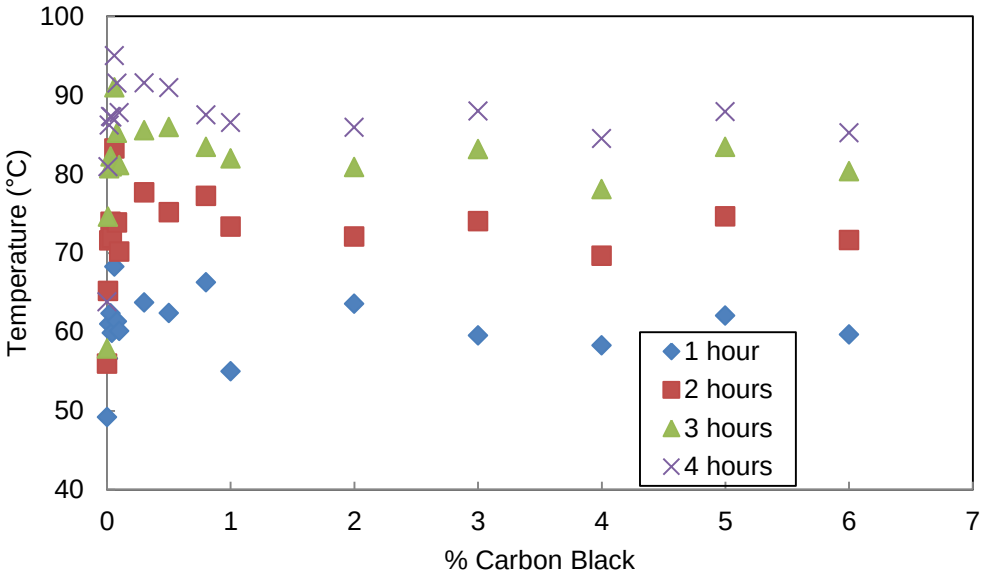

Figure 12-21: Temperatures measured by Thermocouple 3 of various PCM composites after certain time intervals.

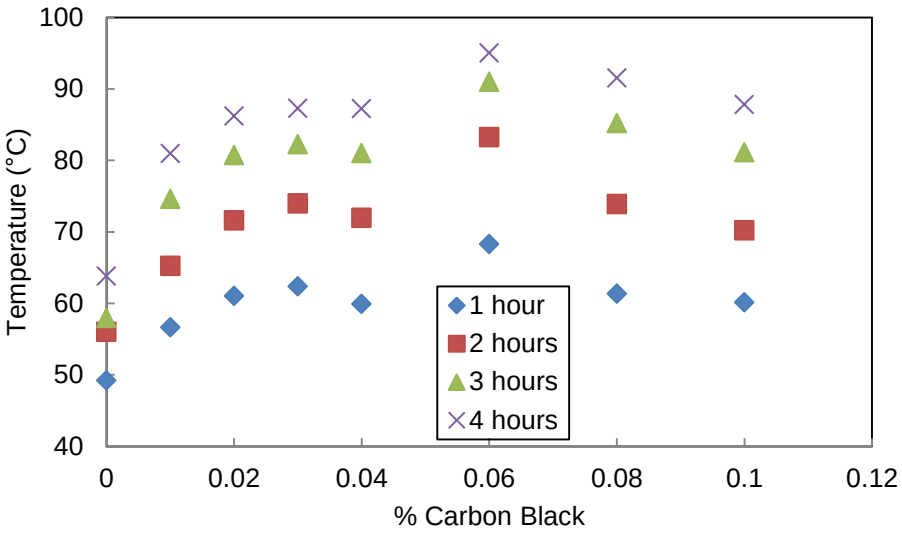

Figure 12-22: Temperatures measured by Thermocouple 3 of the low carbon black concentration PCM composites after certain time intervals.

Temperature 4 has much more variability without a clear trend, this is because of its position so far down in the PCM which increases the effect of all of the smaller influences (while masking the big, overwhelming influences like the large amount of radiation hitting the top part of the PCM).

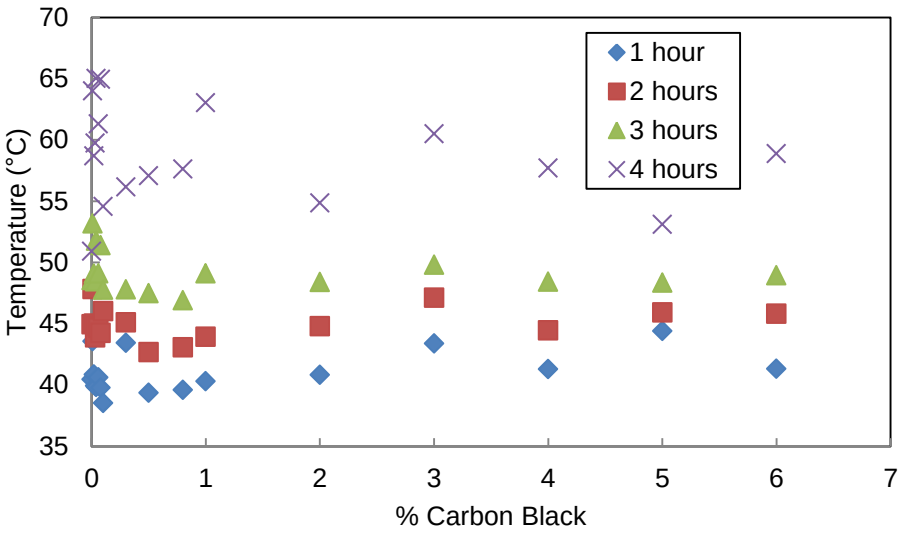

Figure 12-23: Temperatures measured by Thermocouple 4 of various PCM composites after certain time intervals.

The time for Temp 3 to reach 90 ^{0}C is shown in Figure 12-24. Figure 12-24 is similar to those showing the time it took to reach 75 ^{0}C as shown earlier; the differences between each run are just more pronounced.

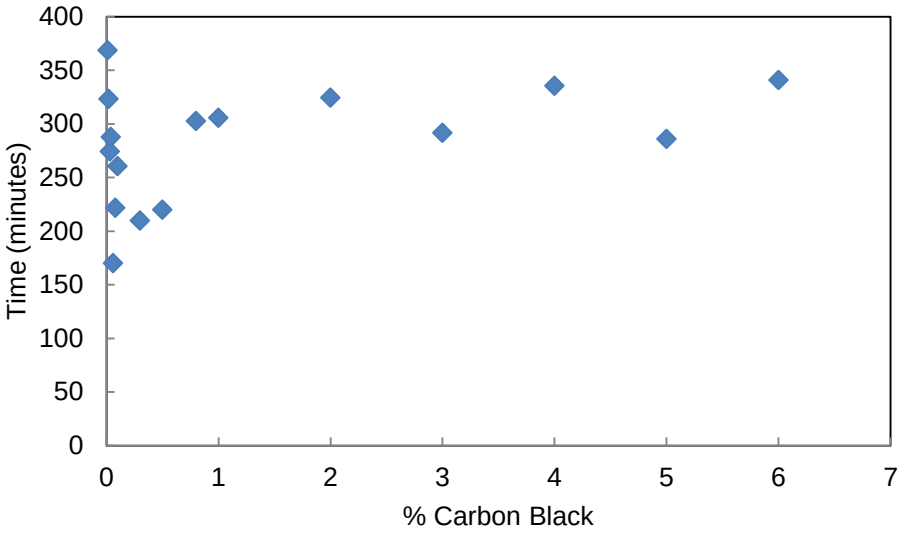

Figure 12-24: Time it took for Temperature 3 to reach 90 ^{0}C at specific carbon black loadings.

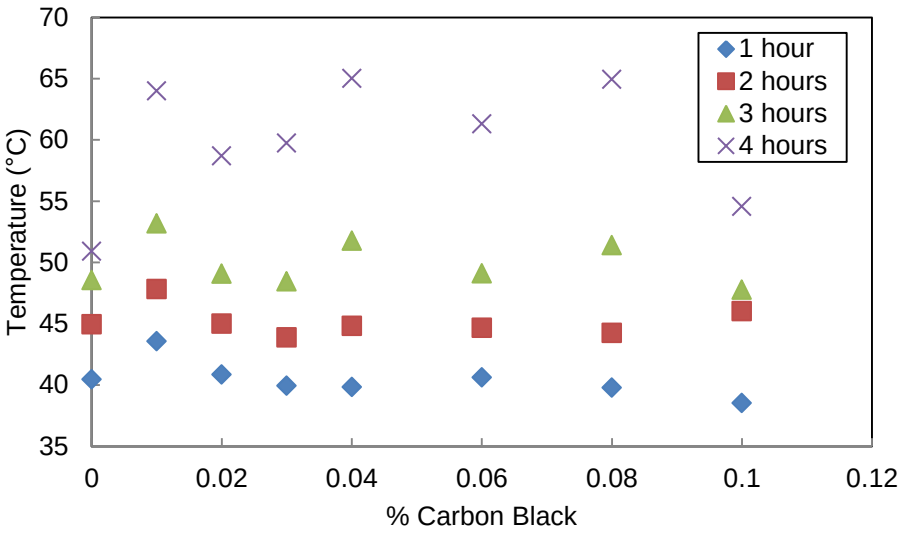

Figure 12-25: Temperatures measured by Thermocouple 4 of the low carbon black concentration PCM composites after certain time intervals.

Temperature 4 has much more variability without a clear trend, this is because of its position so far down in the PCM which increases the effect of all of the smaller influences (while masking the big, overwhelming influences like the large amount of radiation hitting the top part of the PCM).

The temperature increase for the first 3 hours is also much less pronounced for most of the experiments measured at Thermocouple 4. At the 4 hour mark the difference in the temperature between the pure PCM and most of the carbon black composites become very large. This is because this temperature reading is so far down the PCM, where the temperature change is dominated by conduction heat transfer. After 4 hours the slow conductive heat transfer (of the first 3 hours) is overtaken by the faster natural convection and the temperature increases faster (the amount of solid PCM that the heat needs to get through by conduction gets smaller until the liquid layer reaches the spot where the temperature is measured)

13. Appendix F

The complete novel UV-vis experimental run for all of the carbon black concentrations can be seen in Figure 13-1.

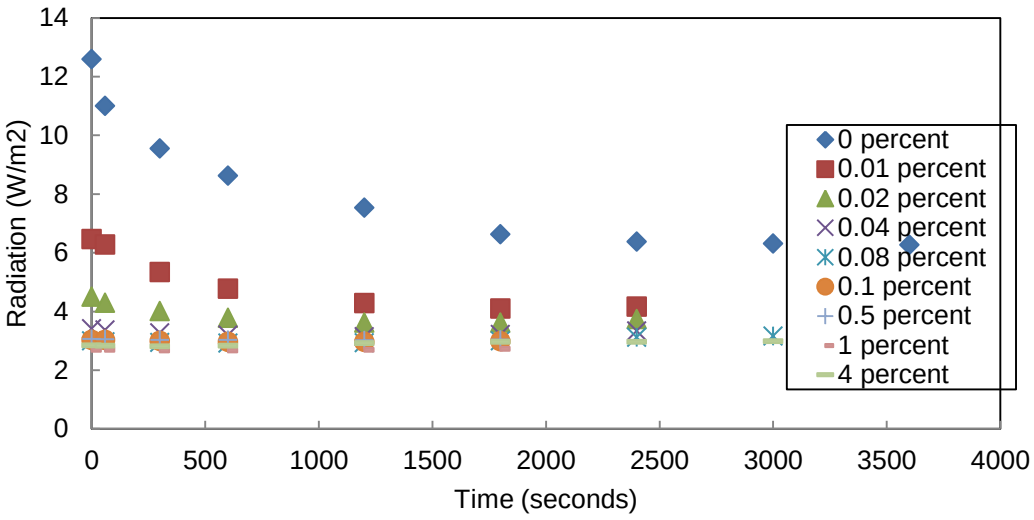

Figure 13-1: The amount of radiation passing through 1 cm path length cuvettes as they cool from a liquid to a solid.

The Beer-Lambert law is only applicable to very dilute solutions. As seen in Figure 13-2 and Figure 13-3, the strength of the light passing through the sample dropped very quickly before levelling out. This strong absorption of the carbon black as well as “high” carbon black concentrations means that the Beer-Lambert law might not hold.

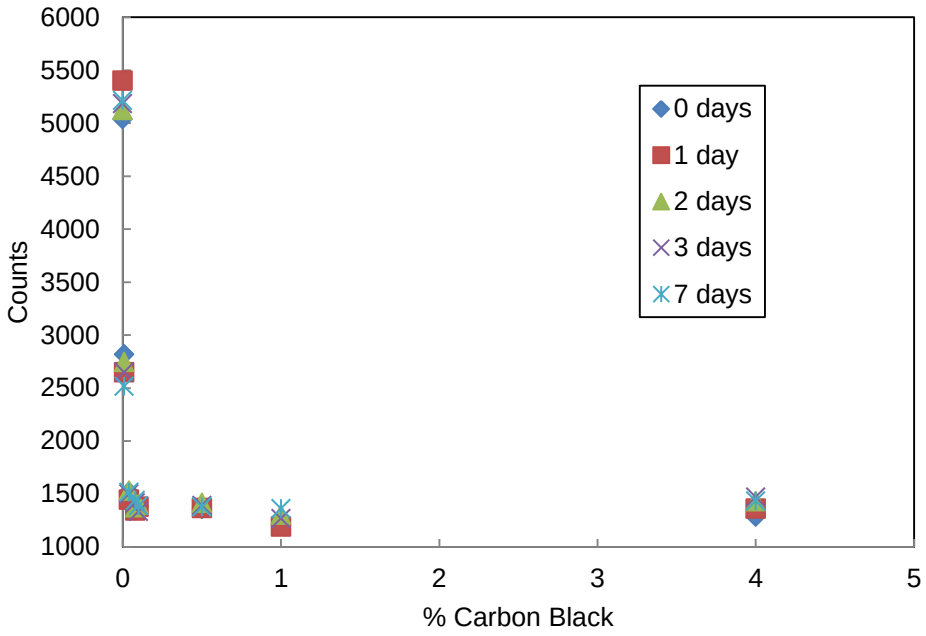

Figure 13-2: Relative strength of the 450 nm wavelength light passing through a liquid PCM sample with a certain carbon black loading

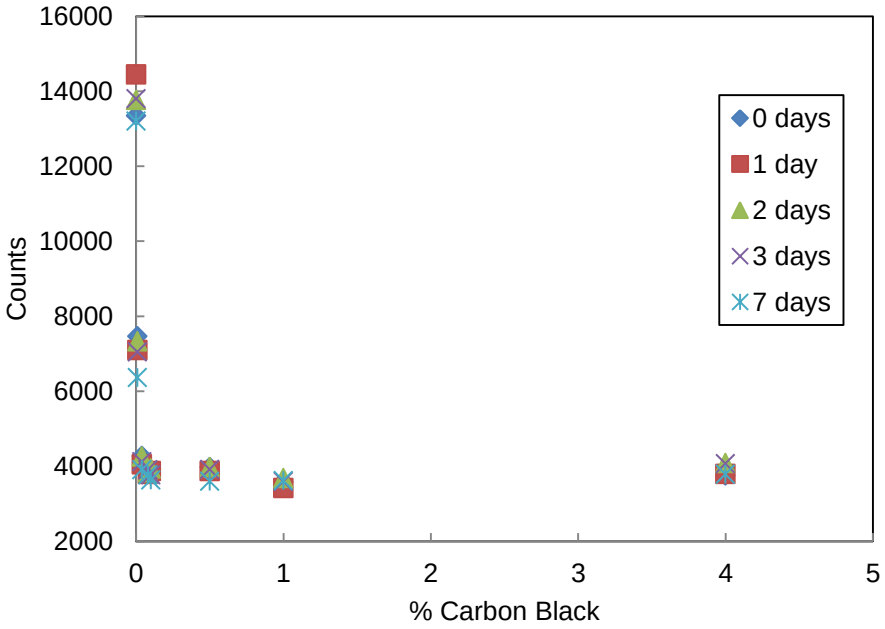

Figure 13-3: Relative strength of the 550 nm wavelength light passing through a liquid PCM sample with a certain carbon black loading.

The absorptivity of the samples at the higher carbon black concentrations were slightly lower every day as seen in Figure 13-4 to Figure 13-7. This is

because some of the carbon black started to settle out, leading to more radiation passing through the sample and a lower absorptivity. The dispersion at the lower concentrations was much more stable, showing very small or hardly any reduction in absorptivity.

Similar to that of the transmittance, the absorptivity increased sharply at very low carbon black concentrations before levelling out at around 0.1 %.

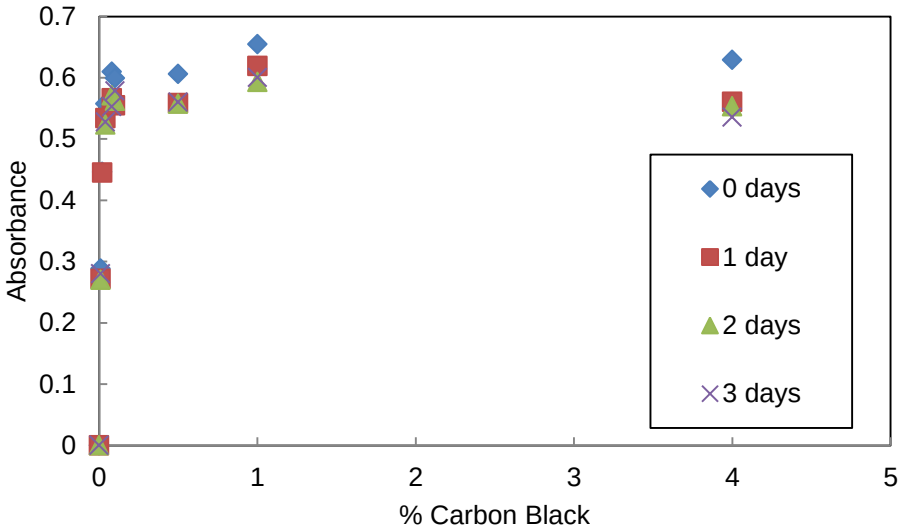

Figure 13-4: Absorptivity of the PCM composites at a wavelength of 450 nm.

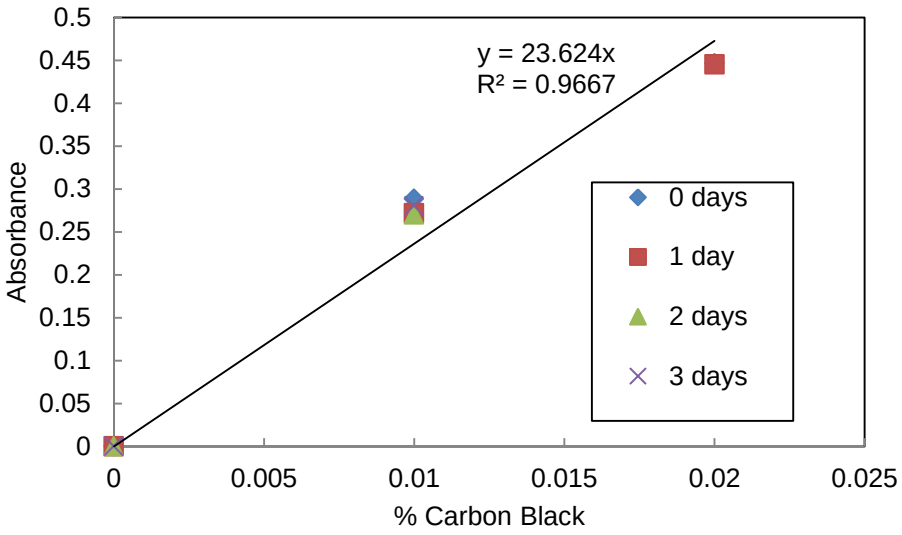

Figure 13-5: Absorptivity of the PCM composites at a wavelength of 450 nm, for the lower carbon black concentrations with a linear trendline.

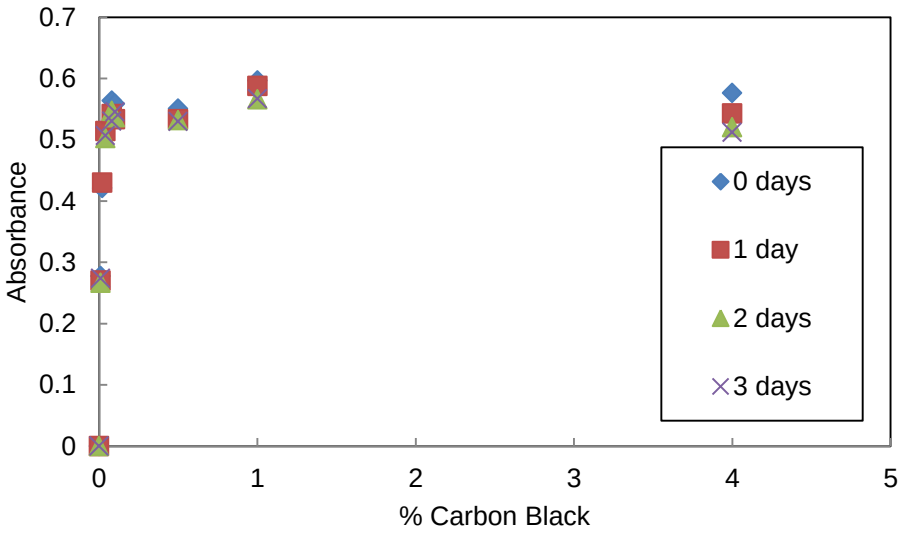

Figure 13-6: Absorptivity of the PCM composites at a wavelength of 550 nm.

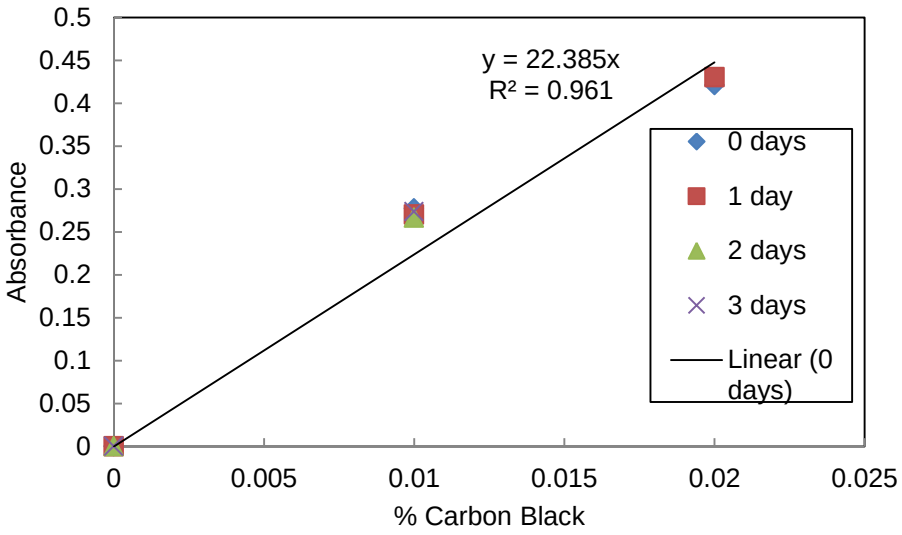

Figure 13-7: Absorptivity of the PCM composites at a wavelength of 550 nm, for the lower carbon black concentrations with a linear trendline.

14. Appendix G

Thermal energy storage charge/discharge rate for higher concentration carbon blacks.

Figure 14-1 and Figure 14-2 show the charge and discharge rate of higher concentrations carbon black composites. A larger increase in carbon black loading does not show any significant changes in the charge and discharge rate.

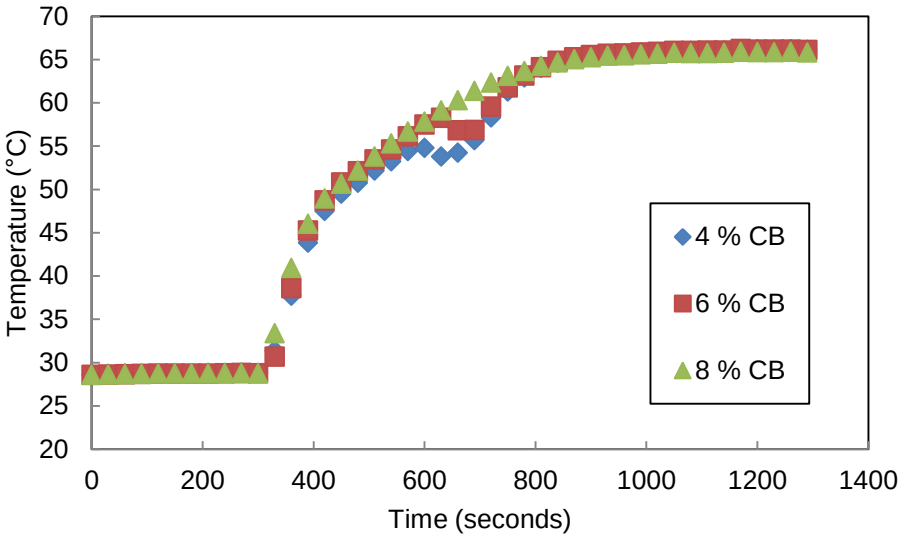

Figure 14-1: The energy storage charge of the pure PCM and high concentration carbon black composites.

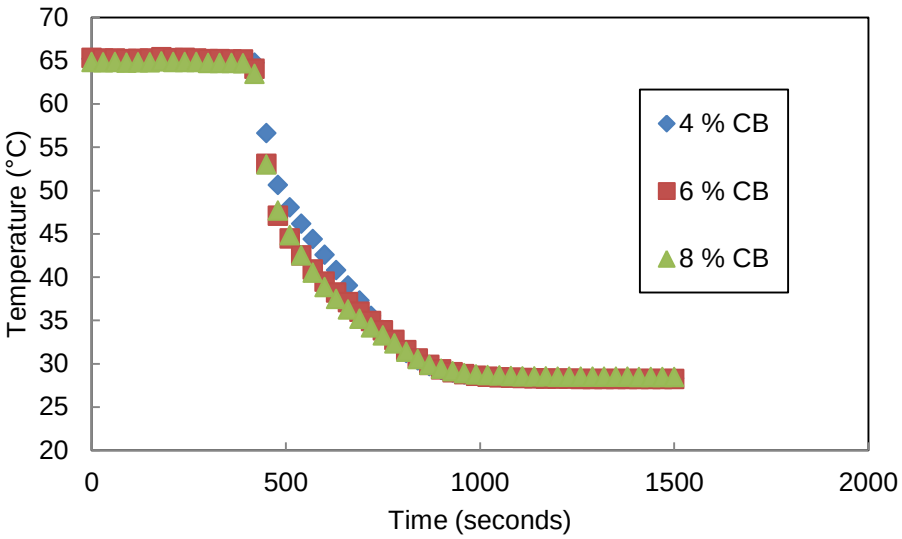

Figure 14-2: The energy storage charge of the pure PCM and high concentration carbon black composites.

15. Appendix H

Figure 15-1 to Figure 15-8 show extra SEM micrographs, illustrating the surface of the carbon black:

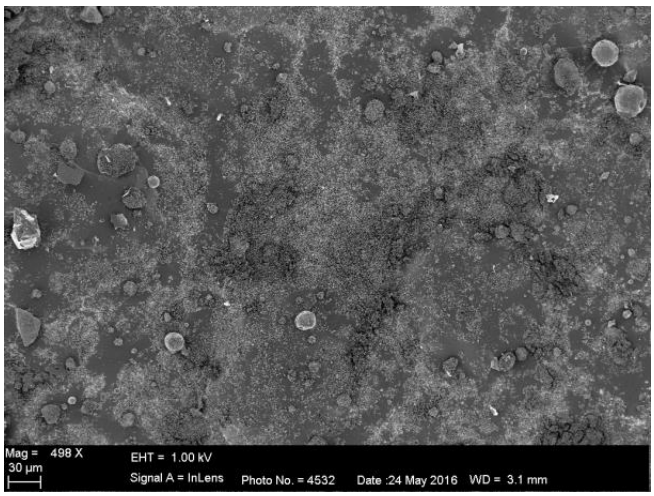

Figure 15-1: Micrograph of the carbon black, showing large globular carbon black structures.

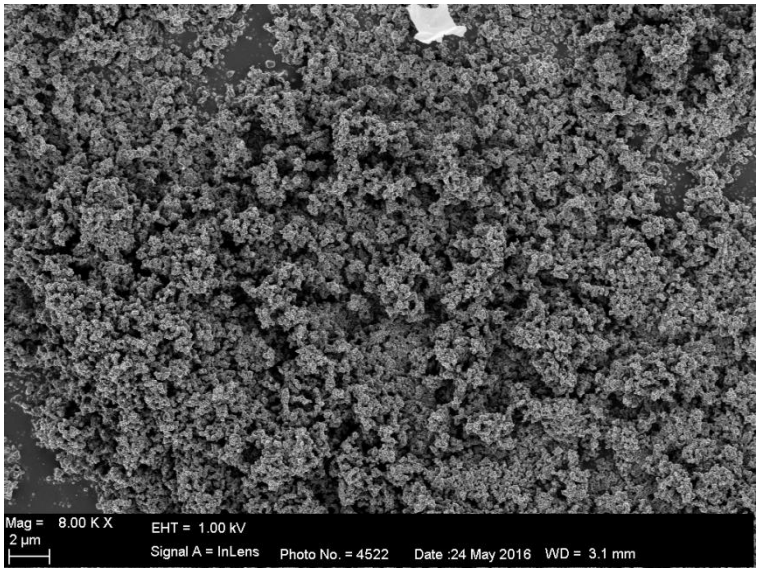

Figure 15-2: Large grape like carbon black agglomerates.

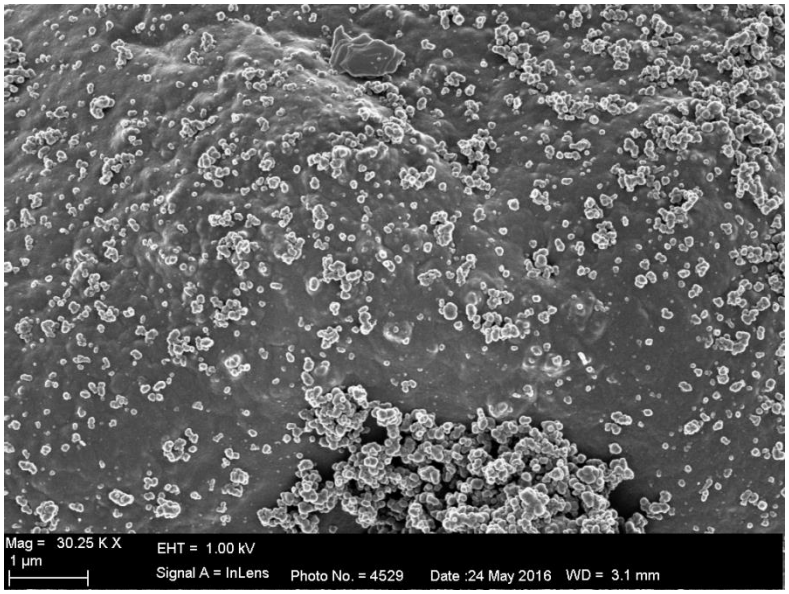

Figure 15-3: Closer look at the surface of the globular structure, with separate carbon black particles on its surface.

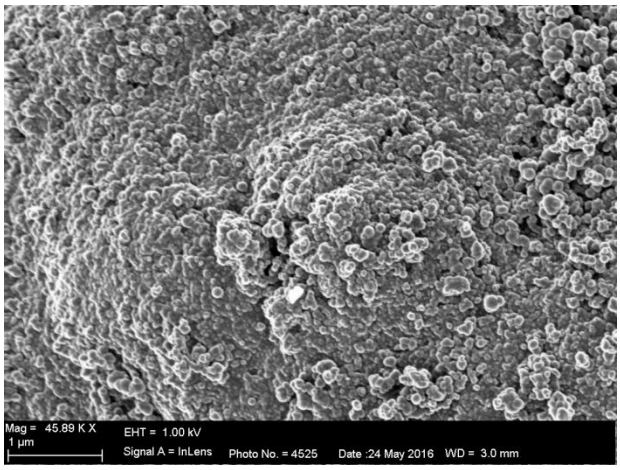

Figure 15-4: Closer look at the surface of the globular structure, showing mostly spherical particles.

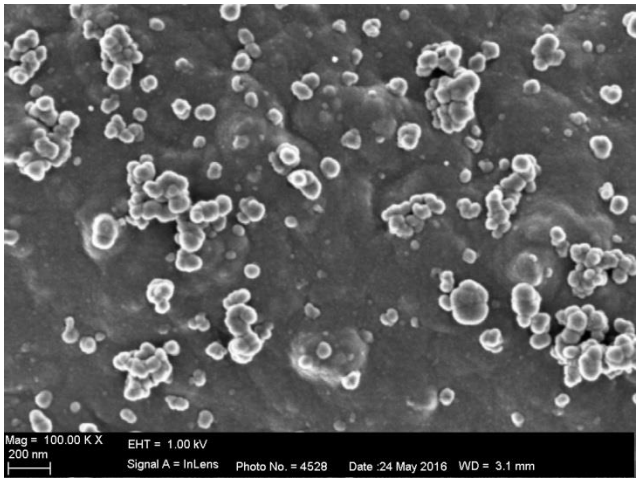

Figure 15-5: Surface are showing some separate carbon black nodules.

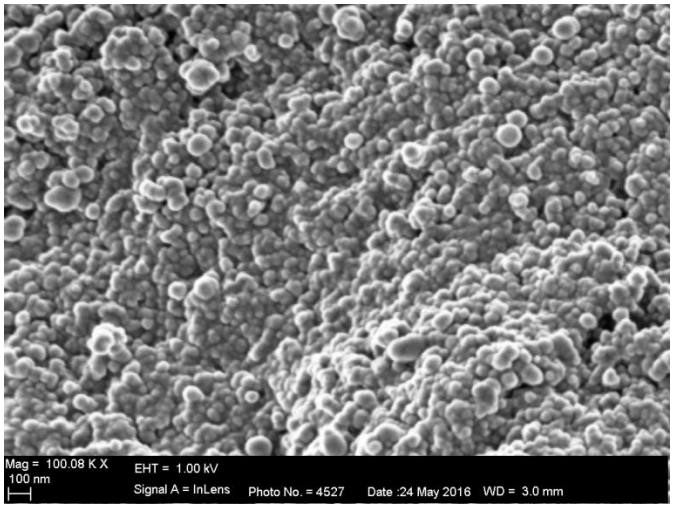

Figure 15-6: surface of the globular structure.

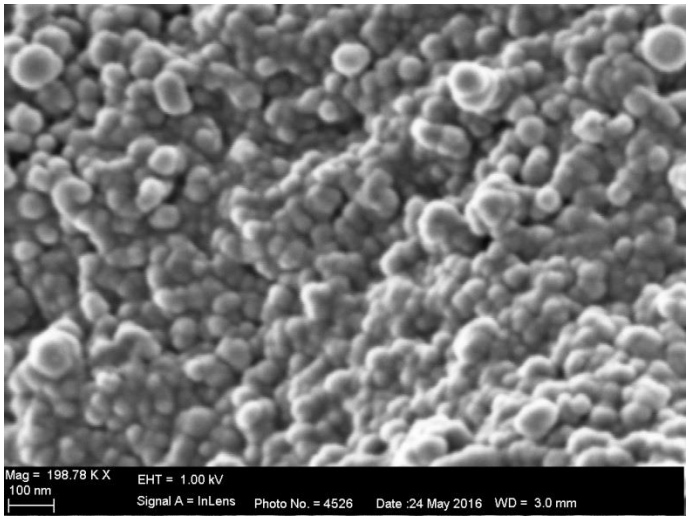

Figure 15-7: Closer look at the surface area.

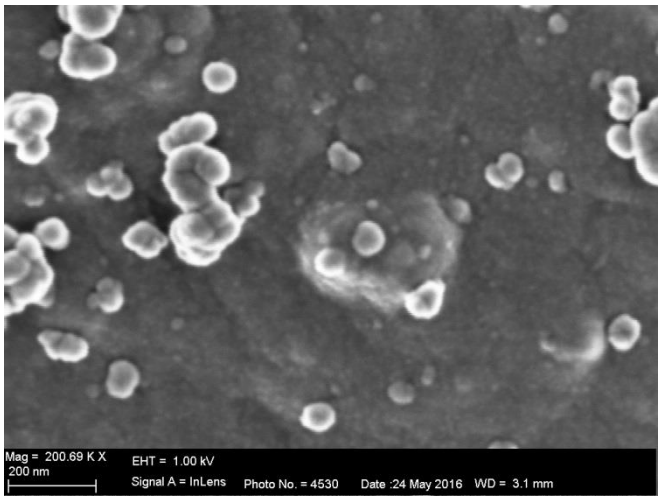

Figure 15-8: Carbon black particles on the surface.